CONTROL OF CHARGE TRANSPORTS IN SEMICONDUCTOR SUPERLATTICES USING AN ACOUSTIC WAVE

A Doctoral Thesis submitted in partial fulfilment of the requirements for the award of
Doctor of Philosophy of

LOUGHBOROUGH UNIVERSITY

Mojoyinola Kofoworola Awodele

2014

Abstract

In this work, we describe the electron dynamics in semiconductor superlattices (SLs) when driven by an acoustic wave.

First, we discuss the physical features and structure of SLs. Then we describe semiclassical transport in periodic potential driven by a plane wave, and the dynamics of ultracold atoms in the periodic potentials.

Secondly, we explore single electron dynamics in superlattices driven by an acoustic wave, then present and analyse the types of electron trajectories according to the strength of the acoustic wave amplitude. The two dynamical regimes obtained depend on the wave amplitude strength and the initial position of electrons in the acoustic wave. The frequency range of the oscillation produced can be as large as terahertz.

Lastly, we discuss the effect of applying a static electric field to the acoustically driven SLs. When the acoustic wave and electric fields were applied together along the axis of SLs, we obtained a higher peak drift velocity than when the acoustic wave or electric fields were applied alone. We use the phase portrait to explain the electron trajectory and the path of the electrons. The global state associated with the drastic change in the drift velocity of the electrons depends on the varied parameters in the dynamical systems. We numerically calculate the electron trajectories while we varied the strength of electric field and wave amplitude to investigate the role of interactions in the system. When very high electric field and very high wave amplitude are applied together along the axis of SL, global catastrophe occurs. This is the discontinuous bifurcation in dynamical system.

Acknowledgements

Firstly, I would like to thank GOD almighty for giving me the fortitude and health to carry on throughout the years to complete this work. In addition, my special thanks go to my research supervisors Professor Feo Kusmartsev and Dr. Alexandro Balanov for believing in me, and for their helpful guidance, advice, support and encouragement throughout the course of my study at Loughborough University.

During the course of my studies at the University, I worked with several academic and non-academic members of staff directly and indirectly, most especially in the Department of Physics and the postgraduate coordinator in the department, Dr. Binoy Sobnack. Without their support and assistance at various times, completing this research work and thesis would have been impossible. Therefore, I thank them all.

When things became difficult, confusing and complicated, different family members and friends gave words of encouragement. I therefore express my appreciation for their support.

Also my appreciation goes to all my in-laws for their love and care, especially to my children in my absence while on this work. My sincere thanks go to all my siblings, nephews and nieces for their support throughout my studies.

Lastly, I would like to give a warm thank you to my husband, Oladayo, and my children, Omoyosola, Ayoyiwaka and Olufoyinsola for their understanding and support throughout the years of my absence.

Kofo Awodele

2014

Contents

Chapter 1

Semi-classical transport in periodic potentials driven by a plane wave.

1.1 Motivation

Understanding the effect of periodic potential on the motion of quantum particles is very important in solid-state physics [1]. Unique dynamical effects like complex spatio-temporal patterns including chaos have interested scientists for many years [2, 3]. There are two important systems in which quantum particles experience periodic potentials: electrons in SLs and cold atoms in optical lattices. Ultra cold atoms inside light-induced periodic potential (optical lattices) share many features with electrons in solids [4].

Interest in SLs has steadily grown over the years; this can be seen in different on-going studies seeking to understand the electronic properties of these novel structures [5-7]. Esaki and Tsu initiated synthesized SLs of a one-dimensional periodic structure of alternating layers with its period less than the electron mean free path [1, 8-9]. SLs are

nanostructures that consist of two or more different semiconductor materials that have similar lattice constants. The materials are deposited alternatively on one another to form a periodic structure in the direction of growth. Consequently, SLs have a large effective lattice period of ~ 1-10 nanometres that can be structured at will during its formation for different applications; for example, it can be used as a light source or photodetectors [10, 11]. SLs are also used as logic and light modulators, as well as infrared detectors [12, 13]. Some important novel quantum phenomena are observed when an external field is applied to the device. SLs are used as terahertz source generators and for quantum cascade lasers [14]. The lattice period of SLs is larger than that of conventional crystals; therefore the electrons in the former are allowed to traverse a whole miniband before scattering.

Optical lattices are formed when two laser beams interfere with each other creating standing wave potentials, which is a periodic intensity pattern seen as a periodic potential by the atom [15]. The atom in the optical lattice is an analogue to an electron in a solid; therefore the two share many of the same properties [16]. Like the SL, the lattice parameter can be altered by changing the wavelengths and the intensity of the laser beams. Unlike the SL, however, there are no defects or lattice vibrations, so there is no consideration for scattering. The lattice periods are also longer, which makes the measurement of the dynamics easy and the time scale longer than that of electron dynamics (milliseconds to picoseconds). The atoms in the lattice can be imaged and the optical lattice can be turn off, which allows for an extra degree of control over the system, and the momenta of the atoms can be measured directly [17]. Optical lattices are used in atomic physics in the area of atom diffraction with applications in atom optics and atom interferometry to trap and cool atoms [18-20].

The analysis of the dynamics of conducting electrons in this unique structure predicted the occurrence of THz Bloch oscillations [21], dynamical electron confinement, negative differential conductance [7, 22], cyclotron-Bloch resonances and chaotic transport [23]. These interesting phenomena have led to various studies on SLs over the years [24-27]. For example, research has recently been conducted on intersubband transitions in SLs and quantum wells [28] and optoelectronic devices [29, 30]. The unique dynamical effects were observed when electric or magnetic fields were applied to the axes of SLs. When a constant electric field is applied to the axis of a SL the electrons perform a periodic motion both in the Brillouin zone and in the real space,

which is referred to as a Bloch oscillation, and the accelerating charges emit radiation [8]. Electrons in the periodic potential of a SL experience chaotic behaviour when both electric field and magnetic field are applied together [31, 32]. A recent study was conducted on effect of applying an acoustic wave along the axis of a SL [33].

An acoustic strain pulse, when applied along the axis of a SL, induces current in the device [33], even when the electric field is not applied to the SL. The charge is used to study ultrafast carrier dynamics in SLs. The strain pulses applied to the axis of SLs is generated by ultrafast optical excitation of an Al film [25, 34] and this strain pulse propagates through the material at the speed of sound over large distances [35]. SLs exhibit non-KAM chaos (Kolmogorov-Arnold-Moser Theorem) when in an electric field and a tilted magnetic field, which have effect on its electrical conductivity, revealing vital information on quantum effects, nonlinear effects and scatterings [35-38]. The oscillation produced when external fields are applied emits terahertz radiation [39].

1.2   Aims

The aim of this research was to study electron transport in SLs induced by the applied acoustic wave. To do this, we investigated the dynamics and paths of the electrons in SLs using an acoustic wave.

The electron dynamics in SLs were also investigated when both the electric field and acoustic wave were applied together along the axes of SLs and when an acoustic wave alone was applied [40]. In this case, the electron transport by the static electric field interacted with the electrons that were being dragged through the lattices and produced high-frequency current oscillations. The oscillations emitted terahertz radiation that has useful applications in the ultrafast electronics industry. The intense THz radiation has been exploited to engineer transient states of matter, to control matter and light resonantly and nonresonantly [41]. The SL is used as a terahertz source generator and it is applicable in quantum cascade lasers [14, 39]. Many of the optoelectronic devices are designed using SLs [42].

 In order to understand the electron dynamics in the SLs, we looked at some fundamental theories of electrons in solids [43-46], the crystal structure of SLs and some quantum mechanics tools used in this work. Atom dynamics in optical lattices are

closely related to electron dynamics in solid-state crystals, but optical lattices have favourable characteristics such as an absence of defects and a high degree of experimental control [47-48]. The work consisted of the theoretical analysis of the behaviour of electron transport in the SLs when a static electric field and acoustic wave were applied. The results of this thesis were obtained by the numerical solutions of differential equations.

1.3   Scope of the work

Chapter 1 has explained the system under consideration in detail, as well as some applications of this system. Chapter 2 looks at the general theory of some of the quantum mechanics tools that were used in this work.

In Chapter 3, we explore the effect of applying an acoustic wave to a SL. A coherent acoustic wave applied along the axis of a SL will generate a deformation potential given by the electron-phonon interaction. An acoustic wave propagating in a SL is an example of a moving lattice propagating through a stationary lattice. The dynamics of electron and drift velocity depend critically on the wave amplitude.

Chapter 4 examines the effect of the static electric field on the acoustically driven SL, when the static electric field and acoustic wave are applied simultaneously along the axes of SLs. We investigate the effect at values less than the critical values of both electric field and acoustic wave. The critical values depend on the parameters of the SL. Finally, Chapter 5 summarizes the overall results of the work.

Chapter 2

Semi-classical theory of periodic potentials

2.1 Band theory

Energy-band theory is a quantum mechanical theory of the motion of electrons in a solid. The electronic band structures explain the ranges of energy an electron in the solid can have and may not have, these are referred to as "allowed" or "forbidden" bands respectively. The band structure of a solid describes those ranges of energy in which an electron is forbidden or allowed to thrive, and the band gap is the energy range in the crystal where no electron state exists. The free electron model of metal does not explain the distinction between metals, semiconductors and insulators [49]; it only answers qualitative questions like how an electron behaves in metals [50].

Band theory explains distinctly how metals, semiconductors and insulators differ from each other. In insulators, there is a big gap between the highest occupied state and the lowest unoccupied state. The electrons in the valence band are separated by a large gap from the conduction band, and this makes it difficult for electron to migrate to it. Therefore, an insulator cannot conduct electricity even if the temperature of the material is increased to cause excitation of the electrons. In metals or conductors, the valence band and the conduction band overlap, so the electron can easily move into the conduction band. The electron can move randomly in the conductors or metals even when no external fields are applied. In the conduction band the electron can move freely through the material and when an external field is applied the electron will move in the direction of the applied force.

In the case of semiconductors, there is a small gap between the valence and conduction bands. This gap is close to $k_B T$, where k_B is the Boltzmann constant and T is the temperature. This gap can be bridged by thermal or other excitations and cause the electrons to move in the direction of the applied field. The pure semiconductor is a poor electrical conductor but, doping these materials can increase their conductivity greatly [51-54]. When a significant number of electrons are excited thermally into the conduction band, the crystal is enabled to carry current. The semiconductor interaction with an electric field or light makes it useful for the construction of a device that can switch, amplify and convert an energy input. The band structures of semiconductors can be engineered, and this provides opportunity to tailor their electronic properties for specific needs. There are two types of semiconductor, n-type and p-type, depending on the doping nature. The p-type semiconductors are doped with acceptor impurities which are trivalent impurities such as boron, aluminium or gallium. They create deficiencies of valence electrons called hole. The n-type semiconductors are doped with donor impurities which are pentvalent element such as antimony, arsenic or phosphorous to contribute free electrons. When two types of semiconductor are brought together to form an artificial crystal, the mismatch in the band levels causes the band to "bend" across the device junction. This is as shown in Fig. 2.1 when p-type and n-type semiconductors are brought together. This study examines the electron transport in the artificial crystal and the effect of an applied electric field and acoustic wave.
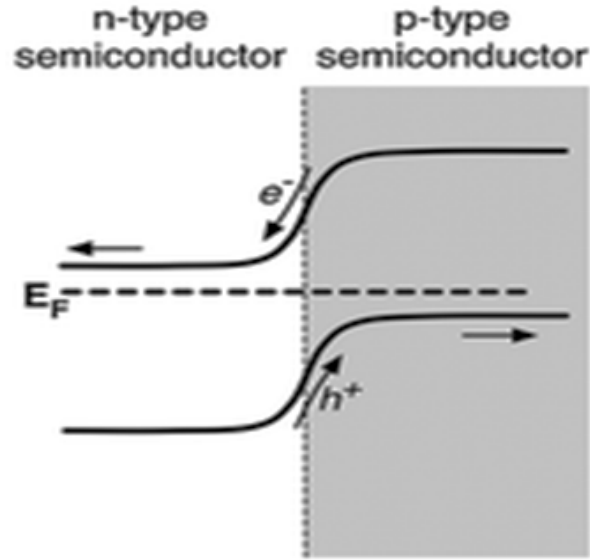
Figure 2.1: The two types of semiconductor (n-type and p-type) brought together to form an artificial crystal, showing bend at the junction. E_F is the Fermi energy level. The figure is adapted from reference [55].

Band theory is important for understanding the dynamics of particles in the crystal. The energy bands in solids are the fundamental electronic structure of a crystal. For simplicity, we consider the electron behaviour in a one-dimensional periodic lattice which can be explained by the Schrödinger equation. Therefore, for a particle with energy E moving in the periodic potential $V(x)$, the crystal lattice will have an eigenstate $\psi(x)$ that satisfies

$$\hat{H}\psi = \left(-\frac{\hbar^2}{2m}\nabla^2 + V(x)\right)\psi(x) = E\psi(x) \qquad (2.1)$$

The Bloch theorem states that 'the eigen-functions of the wave equation for a periodic potential are the product of a plane wave $exp(ikx)$ and a wave function $u_k(x)$ with periodicity of the crystal lattice' [56]. Therefore, the above eigenstate can be written as

$$\psi_k(x) = u_k(x)exp(ikx) , \qquad (2.2)$$

where $u_k(x)$ is a periodic function, and also the translational symmetry of the lattice. A periodic potential $V(x)$ will create a spatial lattice generated by the atoms in a solid or by counter propagating lasers in an optical lattice [57]. The Bloch wave functions for a

particular system can be determined by solving Schrödinger's equation, where E is the energy of the system and ψ is the wavefunction

$$\hat{H}\psi = E\psi ,$$

(2.3)

where the Hamiltonian operator $\hat{H}$ of a periodic system of infinite extent that is a large periodic potential is

$$\hat{H} = -\frac{\hbar^2}{2m}\nabla^2 + V(x)$$

(2.4)

where $V(x)$ is the potential energy of the system and has the periodicity of the lattice, m is the mass of the quantum particles and ∇^2 is the Laplacian [34, 53]. In the above equation, $\hbar = h/2\pi$ where $h = 1.054 \times 10^{-34} Js^{-1}$, the Planck constant [58-59]. *Equation* 2.2 can be solved using different techniques, analytical and numerical. So the dynamics of electrons in the SLs can be determined by solving the time-independent Schrödinger equation [60].

The solution of the Schrödinger *equation* (2.3) shows that there is an unlimited number of solutions for a given value of k. Therefore, each wave function with a particular wavevector k is assigned a quantum number, n and has a corresponding energy $E^n(k)$; this function is known as the dispersion relation. The Bloch theorem then physically means that the wavefunction at position $x + X$ and x are the same, except for the phase factor e^{ikx}, a plane wave. X is any translation vector of the lattice under consideration. Since, the wave function $u(x)$ must be periodic

$$u(x) = u(x + X)$$

(2.5)

the periodicity induced properties of the single-electron Schrödinger equation will then be

$$\left(-\frac{\hbar^2}{2m}\nabla^2 + V(x)\right)\psi(x) = E\psi(x)$$

(2.6)

if we substitute *equation* (2.2) into *equation* (2.6), the solution of Schrödinger equation will then be

$$\left[\frac{-\hbar^2\nabla^2}{2m} + V(x)\right]e^{ikx}u(x) = Ee^{ikx}u(x)$$

(2.7)

and the function $u(x)$ satisfies the condition, for all vectors of lattice X; therefore the potential is periodic.

To obtain the dispersion relation energy $E^n(k)$ for the electron, we solve the Schrödinger equation for a single primitive cell of the SL. We use the Kronig-Penney model, which represents the one-dimensional periodic potential for the energy band. Fig. 2.2 shows an infinite periodic array of potential barriers, V_0 and an electron moving in the x-direction. Regions I and II represent well and barrier respectively. The potential function is approximately equal to the square potential.
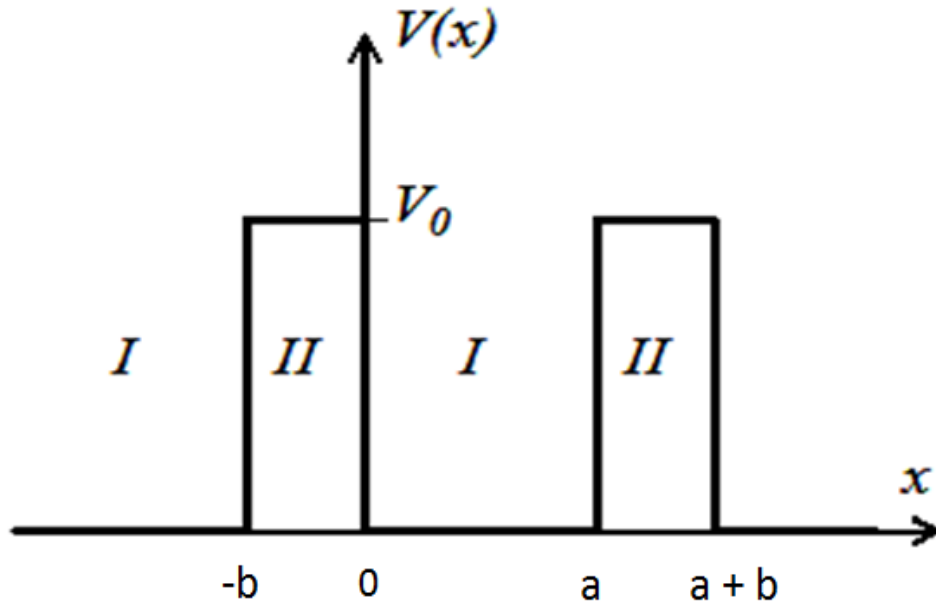

Figure 2.2: The square well periodic potential, showing an electron moving in the x-direction against the Kronig-Penney potential, $V(x)$. Region I is the well and region II is the barrier.

In the region, $0 < x < a$, the potential, $V = 0$ and the eigenfunction is

$$\psi = Ae^{iKx} + Be^{-iKx} \tag{2.8}$$

with the energy in the region described as

$$E = \frac{\hbar^2 K^2}{2m}$$

Similarly in the region, $-b < x < 0$, the solution will be

$$\psi = Ce^{Qx} + De^{-Qx} \tag{2.9}$$

we described the energy in the region as

$$V - E = \frac{\hbar^2 Q^2}{2m}$$

Using the Bloch theorem, the wavefunction would satisfy

13

$$\psi(a < x < a + b) = \psi(-b < x < 0)e^{ik(a+b)} \tag{2.10}$$

and the boundary conditions at $x = 0$ and $x = a$ for ψ and $\frac{d\psi}{dx}$ to be continuous [45].

Let $\qquad \beta = \frac{Q}{K} \qquad$ and $\qquad d = a + b$

therefore, we obtain

$$\cos kd = \cos Qb \cos ka + \frac{1}{2}\left(\beta - \frac{1}{\beta}\right) \sinh Qb \sin ka \tag{2.11}$$

This equation can be solved numerically for the dispersion relation in the miniband. Let represent the right hand of the *equation* (2.11) as $f(\varepsilon)$ and expand it around the energy eigenvalue ε_j of an isolated well (that allows for narrow minibands), then *equation* (2.11) will become

$$\cos kd = f(\varepsilon_j) + f'(\varepsilon_j)(\varepsilon - \varepsilon_j) \tag{2.12}$$

Solving for ε, gives

$$\varepsilon = \varepsilon_j - f(\varepsilon_j)/f'(\varepsilon_j) + 1/f'(\varepsilon_j)\cos kd \tag{2.13}$$

The cosine dispersion is a good approximation for narrow minibands. The miniband dispersion is approximated by the cosine function with bandwidth, Δ and band edge ε_0 which can be derived from the dispersion relation in the *equation* (2.11). Therefore, for the electron band, we write

$$\varepsilon(k) \approx \varepsilon_0 - \frac{\Delta}{2}(1 - \cos(kd)) \tag{2.14}$$

2.2   Effective mass

Particles in a Bloch state will respond to an external field differently than a free particle. An important concept that describes this difference is the idea of an effective mass [52]. The effective mass is the mass that a free particle would have if it responded to applied forces in the same way as a particle in a Bloch state [61]. An electron with the effective mass of m^* in the semiclassical model, will respond to an external electric field and the velocity associated with the centre of mass of the particle as

$$v = \frac{1}{\hbar}\frac{\partial E(k)}{\partial k} \tag{2.15}$$

This can be differentiated to give an expression for the acceleration as

$$\frac{dv}{dt} = \frac{1}{\hbar}\frac{d}{dt}\left(\frac{dE}{dk}\right) = \frac{1}{\hbar}\frac{d^2E}{dk^2}\frac{dk}{dt} \tag{2.16}$$

Let *equation* (2.16) be equal to force, F as

$$F = \left(\frac{1}{\hbar^2}\frac{d^2E}{dk^2}\right)^{-1}\frac{dv}{dt} \tag{2.17}$$

If this is compared to the Newton's second law, it shows that the effective mass of the Bloch particle is

$$m^* = \left(\frac{1}{\hbar^2}\frac{d^2E}{dk^2}\right)^{-1} = \hbar^2\left(\frac{d^2E}{dk^2}\right)^{-1} \tag{2.18}$$

Therefore, the electron in a lattice behaves like a particle with an effective mass. This is the force exerted on the particle by a periodic potential, and it has negative values when the particle is demonstrating a negative acceleration due to the force in the positive direction. Fig. 2.3 shows a typical variation of the effective mass with the wave vector of the electron. We can see that the effective mass, m^* in the principal material of the structure is effectively constant around $k_x = 0$, and also that, due to scattering, the electron will remain near the centre of the Brillouin zone of the crystal lattice.
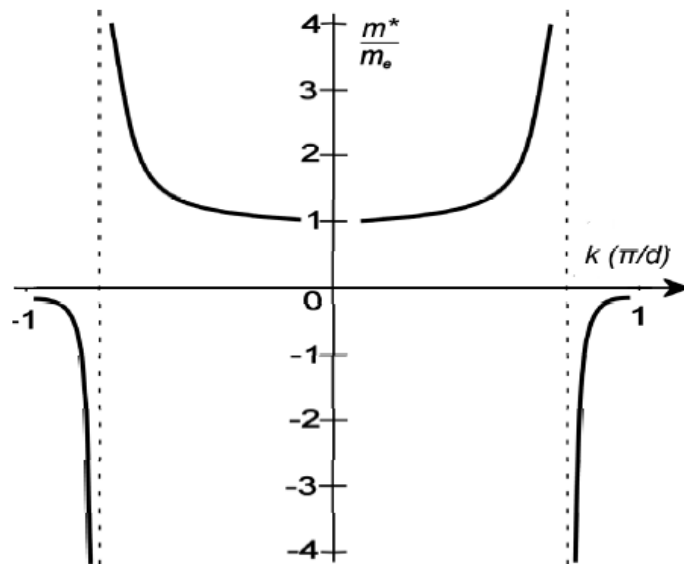

Figure 2.3: The plot of ratio of the effective electron mass m^* to the bare electron mass m_e against the wave vector in the k-space. In the lowest energy band, the ratio of effective mass to the bare electron mass within the k-space where the dispersion relation is $d^2E/dk^2 = 0$ is shown in the figure.

We then assume that the effective mass is constant with varying wave vector k_x. Therefore, the mass of the electron in the SL was replaced with the effective mass to include the effect of the principal crystal lattice. The electron in SL is subjected to two different types of periodic potentials: the rapidly varying potential due to the crystal structure, and the slow variation of the conduction band edge in the layers of the SL, called the superlattice potential, V_{SL}. The mass of the electron in the SL is replaced with the effective mass to incorporate the effect of the crystal lattice. That is, the crystal potential is taking into account without including it explicitly in the calculations. Therefore, for an electron in one-dimensional superlattice potential, V_{SL} with the influence of an effective mass approximation, the time-independent Schrödinger equation will be

$$\left(-\frac{\hbar^2}{2m^*}\frac{\partial^2}{\partial x^2} + V_{SL}\right)\psi(x) = E\psi(x) \qquad (2.19)$$

2.3   Bloch oscillations

Electrons in the crystal behave like free particles under some conditions. We can therefore calculate the velocity of the particle in the state $|k>$. In elementary wave mechanics, the dispersion relation or energy, $E(k)$ is associated with a time-varying factor, so the electron energy is related to the frequency of the electron wave as

$$\omega = \frac{1}{\hbar}E(k) \qquad (2.20)$$

$\hbar$ is the reduced Planck constant, and the energy depends on the wave vector k. In a dispersive medium the group velocity of a wave packet near this frequency will be described as

$$v_g = \frac{d\omega}{dk} = \frac{1}{\hbar}\frac{\partial E(k)}{\partial k} \qquad (2.21)$$

Therefore, the velocity of an electron in the Bloch state is the gradient of $E(k)$ in k-space. For free electrons, the energy is described as

$$E(k) = \frac{\hbar^2 k^2}{2m} \tag{2.22}$$

The gradient of $E(k)$ in k-space for free electrons will then be described as

$$\therefore v_g = \frac{1}{\hbar} \frac{\partial}{\partial k} \left(\frac{\hbar^2 k^2}{2m} \right) = \frac{p}{m} \tag{2.23}$$

where p is the momentum, m is the effective mass and v_g is the velocity of an electron considered as a wave packet moving freely in space with a momentum ($\hbar k$), which makes the momentum $p = \hbar k$. This is not the case in the semiclassical model; for Bloch electrons, the quantity $\hbar k$ is known as the crystal momentum. The rate of change of the actual momentum depends upon the total force acting on the particle, including the force experienced due to periodic potential. In the Newtonian law, "The rate of change of crystal momentum is therefore equal to force" [51, 62].

Bloch's work on the dynamics of electron wave packets in the periodic potentials led to the prediction that an electron in a uniform electric field performs Bloch oscillations instead of linear acceleration if there is no scattering. Bloch oscillations are the coherent motion of quantum particles in periodic structures when they are subjected to an external force [63, 64]. These oscillations are caused by Bragg reflections of ballistically accelerated electrons at the Brillouin zone boundary. They are the motions of electrons in a real space due to evolution through the Brillouin zone when an external field such as a static electric field is applied and they describe the oscillation of particles that are confined in a periodic potential when a constant force is acting on them. In natural crystals this phenomenon is extremely hard to observe due to the scattering of electrons by lattice defects, but it has been observed in SLs. A SL has an artificial periodic constant that is larger than the period of natural crystals. The dynamics of a particle are affected by the band gap structure of its energy spectrum in a periodic potential, like a SL. Such a particle does not follow the direction of the driving force or linear acceleration but rather performs an oscillatory motion called Bloch oscillation, which is one of the predictions of the semi-classical model of electron dynamics [56, 65]. Maxime, et al., in the experiment where they prepared ultracold caesium in the ground energy band of the potential induced by an optical standing wave, observed the Bloch oscillations of atoms which are driven by a constant inertial force [66].

When force is applied to SLs, the electrons will gain momentum since the band structure is periodic. The initial field distribution will be recovered after one cross of the Brillouin zone. Therefore, an oscillatory motion is observed and there will be no net shift of the particle in a real space as shown in Fig 2.4. For a constant electric field applied along the x-direction of a lattice to a particle in the lowest energy band, the wave vector k_x will increase linearly with time but at constant rate and the energy applied is equal to

$$F_x = \hbar \frac{dk}{dt} \tag{2.24}$$

Initially $k_x = 0$ with the applied force, k_x increasing towards the Brillouin zone boundary to $k_x = \pi/d$ with time. So, the gradient of the dispersion curve becomes increasingly positive and the particle accelerates and increases its velocity in the real space in the x-direction. As the velocity is increasing, the particle approaches the first Brillouin zone boundary, gaining energy. When the electron passes the zone edge at π/d it reappears at $-\pi/d$, then descends again. This motion in k-space is periodic and the particle repeats the motion. The particle reaching the edge of the Brillouin zone at $k_x = \pi/d$ and reappearing at the opposite boundary $k_x = -\pi/d$, and the wave vector value k_x increasing at a constant rate, is referred to as Bragg reflection. This is illustrated well in Fig. 2.4 for the energy-wave vector relation of a quantum particle in a one-dimensional lattice of constant d.

At one point the gradient of dispersion curve is negative and the particle will be moving in the negative direction in real space. It will continue to accelerate in the negative direction attaining a maximum negative speed when $d\varepsilon/dk$ is maximal. The velocity, v is maximal when $d\varepsilon/dk$ is maximal; and when $d\varepsilon/dk = 0$ the particle comes to a standstill. Thereafter the particle slows until $k_x = 0$ where it reaches a standstill at its starting position in a real space. The rate of change of k is constant

$$\frac{dk}{dt} = \left| \frac{e}{\hbar} F \right|$$

Therefore, the frequency of oscillation will be $dt = 2\pi\hbar/eFd$, where e is electron, d is the lattice constant and F is the electric field applied. The process is known as Bloch oscillation, and it repeats over and over [67, 68]. Fig. 2.4 shows the wave vector tracing the dispersion relation, the electron moving up and down and repeating indefinitely while the wave vector changes steadily.
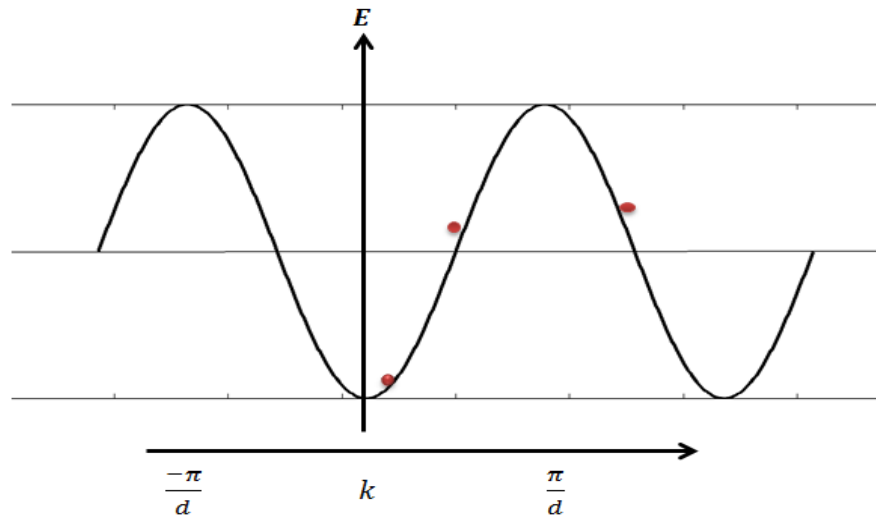

Figure 2.4: The motion of electron (*electron coloured red on line*) changing at a constant rate, It is relating the applied energy, E to the wave vector, k.

Bloch oscillation can then be described as an electron returning repeatedly to its original position in momentum space, causing a periodic motion both in momentum and real space leading to the reduction and eventual disappearance of transport as external fields' increase [69, 70]. The critical field therefore drives the electrons through the Brillouin zone before they are scattered.

2.4   Semiconductor superlattices

Esaki and Tsu in 1969 [7, 71] considered the idea of a one-dimensional SL which is a periodic structure of layers of two or more materials. The materials have a similar lattice constant but a different bandgap. The structure is formed by a periodic variation of alloy composition or impurity density introduced during epitaxial growth. These nanostructures consist of two or more different (typically two) semiconducting materials of similar lattice constants. The materials are deposited alternatively on each

other to form a periodic structure in the growth direction [72, 73]. Nowadays the fabrication of these structures has been made possible by the development of epitaxial growth techniques such as molecular beam epitaxy. The process involves heating the pure element so that it sublimates. The resulting gaseous elements are allowed to condense on a substrate to form a layer of the constituent atoms of that element. The process, crucially, is slow (around a monolayer per second) so that it is possible to precisely control the constituent atomic layers of the device, allow for the crystal to be tailored for specific experiments and applications [33, 43]. However, it is hard to grow materials with high vapour pressure using this process. Other types of epitaxial growth techniques are metal-organic chemical vapour deposition (MOCVD) and nanoscale lithography techniques (electron beam lithography) [74].

In the presence of external electric and magnetic fields the transport of electrons in minibands is a complex behaviour which results in a number of interesting phenomena that have useful applications in the ultrafast electronics like THz Bloch oscillations [71, 75], dynamical electron confinement, negative differential velocity [63], cyclotron-Bloch resonances and dynamical chaos [62]. These properties of SLs derive from a number of periodic layers that can be structured and controlled as desired. The chemical composition of SLs varies periodically in space at distances of (1-10nm) which is greater than the periods of its constituent materials. This man-made structure is made to investigate a fundamental quantum mechanical phenomenon that forms quantised energy states [17, 76-77], since the thickness of the layers, the number of periods and periodic potential strength can be controlled [43]. The motion of electrons in the SLs is modified by the arrangement of the atoms in a periodic way; it has been assumed in this research that there was no interaction between the electrons. The magnitude of the band gap of the SLs can be tuned and the parameters of the materials can be varied, which optimises and widens its applications. The arrangement shown in Fig. 2.5, is describing the SL used in this study. The SL consisted of two layers of different semiconductors of similar lattice constants and had a lattice period, d. The figure illustrates the vertical axis as the energy, E or the potential, and the horizontal axis indicates the direction, in which the particle was moving, x.
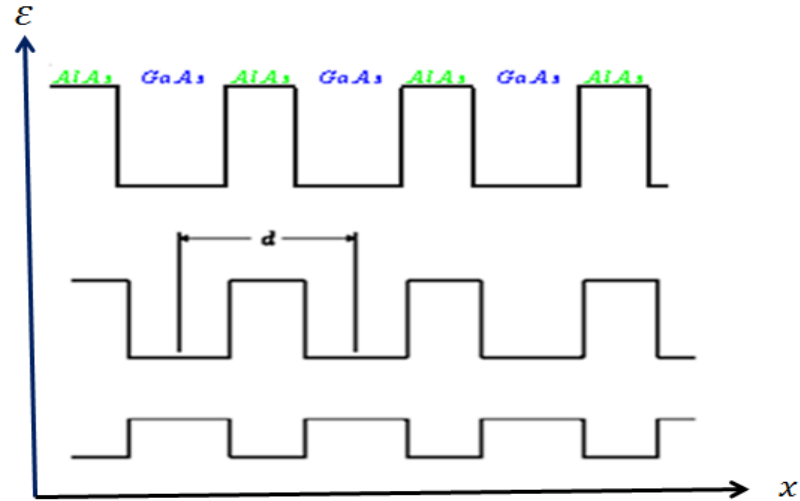
Figure 2.5: Schematic illustration of alternating structure of semiconductor with the lattice period, d for the SL formed. The superlattice unit cell consists of a quantum well (GaAs) enclosed by barriers (AlAs).

The difference in the width of the energy gap in different semiconductors forms the boundary of the conductivity band for perfect SLs which is modulated periodically and leads to the formation of energy minibands [14, 78]. The doping and controlled lattice strain in the SL structure can be combined to achieve a maximum tuneable state. SLs can be categorised as a weakly or strongly coupled based on the thickness of the barriers separating the quantum wells [8]. The weakly coupled have relatively thick barriers between the quantum wells, which makes the decay length of the electron wavefunction small and resonant, like the emission of acoustic phonons that occurs in the vertical hopping transport regime [79].

In this work, the SL structure consisted of two layers and was strongly coupled, since the barriers were thin. The electron wave functions of such a structure can extend over several periods of the SL. A diagram explaining the structure of the SL is shown in Fig. 2.6. The first layer is AlAs with a relatively large bandgap that serves as a barrier region controlling the position of the new quantum states that will be generated in the well, and GaAs is the quantum well. So the lattice period, d_{sl} of the device will be the addition of each of the lattice periods. That is $d_{Al} + d_{Ga}$ which is $12.5nm$ for this sample and the first miniband width, is $7meV$.
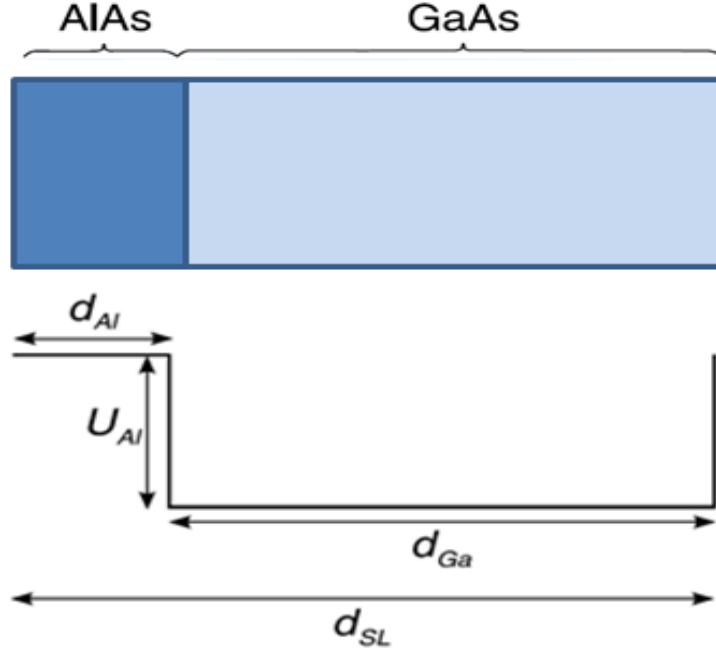
Figure 2.6: The physical structure of one period of the SL sample and the potential of the SL in the unit cell, which is due to the variation in the conduction band edge, $U_{Al} = 409\ meV$ and $d_{Al} = 2.5nm$, $d_{Ga} = 10nm$. Therefore, $d_{sl} = 12.5nm$.

2.5 Electron scattering and drift velocity

When considering the dynamics of electrons in a SL it is realistic to consider the effect of scattering on transport. As was shown in the discussion of the Bloch oscillation, without scattering there would be no electrical conduction in solids. The ions that form a solid influence the electrons in the solid. The effects of these ions on electron transport are included in Bloch theory [8]. We do not have perfect lattice ions in reality, and the effect of imperfect lattices on electron transport needs to be considered. A scattering event occurs from two major sources, one of which is the imperfections in the structure of the semiconductor crystal [80]. This imperfection includes impurities in the structure and deformations in the lattice structure and both disrupt the periodicity of the lattice. When fabricating the nanostructure of SLs by molecular beam epitaxy, the likelihood of defects forming in the structure can be minimised by controlling the deposition process. Another lattice defect is associated with the interface between two types of semiconductor materials. The interface roughness can occur in the deposition

process, but can also arise if the adjoining semiconductor materials have a different lattice constant that stretches or compresses the two layers when they are in contact, and this can lead to electron scattering events [33]. The second type of imperfection occurs as a result of external factors such as mechanical deformations or thermal vibrations of the lattices; this again disrupts the periodicity of the crystal and leads to electron-phonon scattering events. This vibration occurs at all temperatures of the lattice, but the impact decreases as the temperature decreases.

The scattering mechanics can be categorised as inelastic and elastic scattering. Inelastic scattering arises from electron-phonon interactions, and the electron trajectory deviations are due to scattering events in which both the energy and momentum can change. Only the momentum of the electrons is allowed to change during elastic scattering and the energy remains constant. For the model of transport in SLs the concept of scattering time, τ is introduced, and we define the probability of a scattering event to occur in small time dt ($\ll \tau$) as dt/τ.

Drift velocity is the average velocity a particle will have when an external field is applied to the device. It is the actual velocity that the electrons have due to the applied field. Electron drift velocity is calculated to determine the measured transport characteristics of electron in SLs because of the scattering effect. The electron drift velocity can therefore be described using the Esaki-Tsu formula as

$$v_d = \frac{1}{\tau} \int_0^\infty \dot{x}(t) \, e^{-t/\tau} dt \tag{2.25}$$

τ is the scattering time and takes the value $\tau = 2.5 \times 10^{-13}$s.

The electron drift velocity analysis takes into account scattering, which is why we have a relaxation time approximation in the model of the drift velocity. The electron in the SL is affected by scattering events and, by the approximation; the scattered electrons do not remember their behaviour before the scattering event. The scattering time does not depend on the position and the dispersion relation, therefore it could be considered as a constant [7, 51].

So, the drift velocity of an electron in a SL can be estimated if we assume that the number of electrons that are not scattered at time, t is $N(t)$. We take the probability of an electron that will scatter in time dt to be dt/τ as discussed and τ is the scattering time. So therefore the number of electrons scattered in time dt will be

$$N(t) \frac{dt}{\tau} \tag{2.26}$$

The probability of an electron scattering in time, dt is therefore the number of electrons that will scatter in time, dt divided by the total number of electrons that is

$$P(t)dt = \frac{N(t)dt}{\tau} \frac{1}{N_0} \tag{2.27}$$

The number of unscattered electrons at time t is $N(t) = N_0 e^{-t/\tau}$ where N_0 is the number of electrons is at time, $t = 0$. Therefore, substituting for $N(t)$ in the *equation* (2.27) will get the probability as $N(t)$

$$P(t)dt = \frac{N_0 e^{-t/\tau}}{\tau} \frac{1}{N_0} \tag{2.28}$$

Only the behaviour of the electrons after the scattering event at time t will contribute to the average electron velocity at time, t. Therefore the total electron drift velocity at time, t over the entire system will be given as

$$v_d(t) = \int_0^\infty v_x(t)P(t)dt \tag{2.29}$$

Substituting *equation* (2.28) into the above equation will give a general form for the drift velocity of an electron in a SL.

$$v_d(t) = \frac{1}{\tau} \int_0^\infty v_x(t)e^{-t/\tau}dt \tag{2.30}$$

When there is no magnetic field, the velocity of the electron will be as stated in *equation* (2.15),

$$v_x = \frac{1}{\hbar} \frac{\partial E(k)}{\partial k_x}$$

The dispersion relation can be described as the relationship between energy and the wave vector for a miniband that has inversion symmetry about the centre of the Brillouin zone to give,

$$E(p_x) = \frac{\Delta_{SL}}{2} \left(a_0 - \sum_{n=1}^\infty a_n \cos\left(\frac{np_x d_{SL}}{\hbar}\right) \right) \tag{2.31}$$

Δ_{SL} is the width of the first energy band. The SL period is d_{SL} and n is an integer, while a_n are the Fourier coefficients that can be determined. If we substitute *equations* (2.15) and (2.31) into *equation* (2.30), we obtain

$$v_d(t) = \frac{\Delta_{SL}}{2\hbar} \sum_{n=1}^\infty na_n \int_0^\infty \sin\left(\frac{np_x d_{SL}}{\hbar}\right) e^{-t/\tau} \, dt/\tau \tag{2.32}$$

At $t = 0$, the electron will initially be at the bottom of the miniband and when the electric field is applied such that $p_x = eFx$ and by integrating *equation* (2.25) by parts we have the drift velocity as

$$v_d = \frac{\Delta_{SL}}{2\hbar} \sum_{n=1}^{\infty} n a_n \left(\frac{n\omega_B \tau}{1+(n\omega_B \tau)^2} \right) \tag{2.33}$$

We define $eF\, d_{SL}/\hbar = \omega_B$; ω_B is known as the Bloch frequency. For the first miniband in a given SL and a simple miniband approximation of $a_0 = a_1 = 1, a_{n>1} = 0$ [81] we obtain using *equation* (2.31)

$$E(p_x) = \frac{\Delta_{SL}}{2} \left(1 - \cos\left(\frac{p_x d_{SL}}{\hbar} \right) \right)$$

And, with the same miniband approximation, the drift velocity will be

$$v_d = \frac{\Delta_{SL} d_{SL}}{2\hbar} \left(\frac{\omega_B \tau}{1+(\omega_B \tau)^2} \right) \tag{2.34}$$

Relating the drift velocity to the applied electric field gives an expression known as the Esaki-Tsu curve, Fig.2.7 and we observed a maximum drift velocity at $\omega_B = 1/\tau$. When $\omega_B \ll 1/\tau$ the relation is ohmic, due to a long Bloch period that allows for scattering to take place before a Bloch oscillation can be completed, therefore electron localisation is suppressed. At $\omega_B > 1/\tau$ a phenomenon is predicted called a negative differential velocity, which occurs when the Bloch oscillations increase rapidly with increasing electric fields; this allows for a demonstration of localisation effects before scattering.
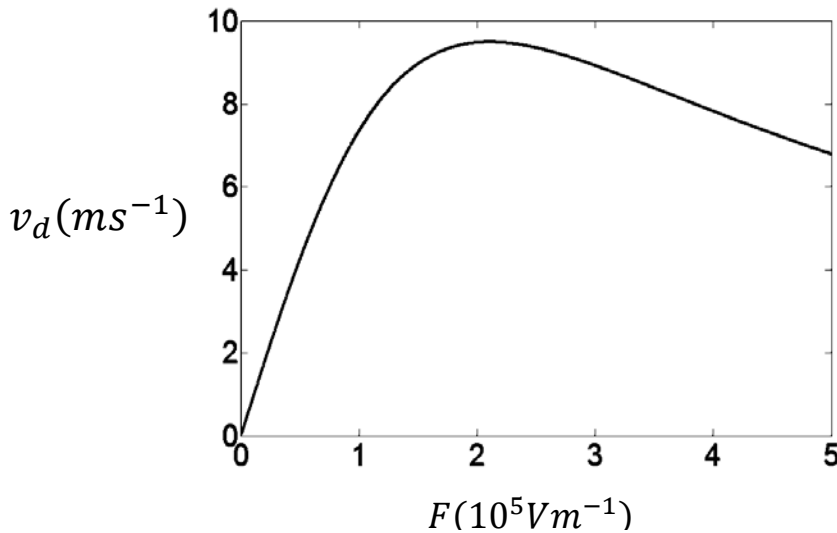

Figure: 2.7: Plot showing the form of the Esaki-Tsu curve, $v_d(F)$. The drift velocity varied with the electric field.

The maximum drift velocity is reached when $\omega_B \tau = 1$, where ω_B is the frequency of the Bloch oscillations when electric field is applied to the SL, defined as $\omega_B = eFd/\hbar$. τ is the scattering time, d is the lattice constant, e is the electron charge, $\hbar$ is Planck's constant, and F is the electric field. Therefore, the electric field applied to the SL at that frequency of Bloch oscillations will be

$$F = \frac{\hbar}{ed\tau}$$

2.6 Optical lattices

The energy band transport is realised not only in the crystal structure but also in optical lattices [51, 82]. Optical lattices are usually formed when two laser beams interfere with each other creating standing wave potentials, which is a periodic intensity pattern seen as a periodic potential by the atom.. The atom in the optical lattice can be considered as an analogue to an electron in a solid; therefore the two share many of the same properties [83 - 84]. Like the SL, the lattice parameter can be altered by changing the wavelengths and the intensity of the laser beams [83]. Unlike the SL, there are no defects or lattice vibrations so there is no consideration for scattering. The lattice periods are also longer which makes the measurement of the dynamics easy; and the time scale is longer than that of electron dynamics (milliseconds to picoseconds). The atom in the lattice can be imaged and the optical lattice can be turned off, which allows an extra degree of control over the system and the momenta of the atoms can be measured directly [85 - 86]. In the Fig. 2.8, the electron is trapped in the potential wells that are created by the standing-wave laser beam; X indicates the position of the atom and V_0 is the potential.
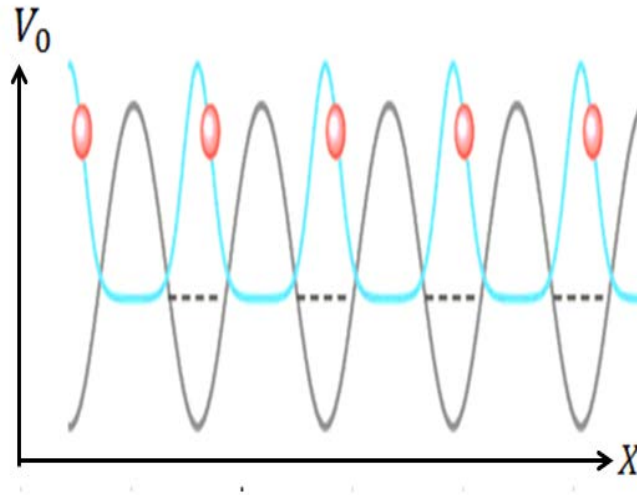
Figure 2.8: Atoms (*red colour on line*) in an optical lattice trapped in a sinusoidal potential well created by a standing-wave laser beam [87].

Optical lattices provide a way of exploring a quantum system which is analogous to electrons in a crystal but with complete control over the lattice and the atom. A 2D optical lattice can be used in experiments to produce highly correlated states, such as the Mott-insulator state, or to engineer 1D potentials [88].

A static electric field from the lasers produces a periodic potential energy profile that acts on the ultra-cold alkali atoms. When an electric field F is applied to a single atom, it induces an electric dipole moment d in the atom by shifting the energy levels. We can define the polarisability of the atom, denoted as α, as the measure of the tendency of the electron to be distorted by the external field. But the expectation value of the dipole moment is proportional to the applied field, therefore

$$\langle d \rangle = \alpha F \qquad (2.35)$$

A small change in the energy of the atom's state in the electric field then will be

$$dV = -\langle d \rangle . dF \qquad 2.36)$$

Integrating the *equation* (2.36) gives,

$$\Delta V = -\int \alpha F . d F = -\frac{1}{2} \alpha F^2 \qquad (2.37)$$

For an electric field oscillating with a frequency ω, we can say $F(t) = F_0 \cos \omega t$, therefore the energy will be a function of the frequency dependent, dynamical polarisability, $\alpha'(\omega)$

$$\Delta V = -\frac{1}{2}\alpha'(\omega)\langle F(\boldsymbol{r},t)^2\rangle_t \tag{2.38}$$

The field is the square of the electric field, averaged over a time much longer than the period of the wave. To have a lattice potential the electric field must be constructed so that it is periodic in space. For a one-dimensional optical lattice, the two counter propagating laser beams of wavelength, λ, will have electric fields as

$$F_1(x,t) = \frac{F_0}{2}e^{i(kx-\omega t)} \tag{2.39}$$

and

$$F_2(x,t) = \frac{F_0}{2}e^{i(-kx-\omega t)} \tag{2.40}$$

where $k = 2\pi/\lambda$. If we sum *equations* (2.39) and (2.40) we have a standing wave equation

$$F(x,t) = F_1(x,t) + F_2(x,t) = F_0\cos(kx)\,e^{(-i\omega t)} \tag{2.41}$$

and the real part of the wave is

$$\Re\{F(x,t)\} = F_0\cos(kx)\cos(\omega t) \tag{2.42}$$

By substituting equation (2.42) into (2.38) we obtained an expression for the effective periodic potential that an atom will experience due to the optical lattice.

$$\Delta V = -\frac{1}{2}\alpha'(\omega)F_0{}^2\cos^2(kx)\langle\cos^2(\omega t)\rangle_t = V_0\cos^2(kx) \tag{2.43}$$

where V_0 is described as

$$V_0 = -\frac{1}{2}\alpha'(\omega)F_0{}^2\langle\cos^2(\omega t)\rangle_t \tag{2.44}$$

With $k = 2\pi/\lambda$, and trigonometric identity, $\cos^2 A = (1 + \cos(2A))/2$ substituting in *equation* (2.43) gives

$$\Delta V = \frac{V_0}{2} + \frac{V_0}{2} \cos\left(2\pi \frac{x}{\lambda/2}\right) \tag{2.45}$$

Therefore, the period of the optical lattice, d_{OL}, is $\lambda/2$.

The cold atoms can be ultracold bosonic, a dilute gas of bosons cooled very close to absolute zero or fermionic condensate: fermionic particles at low temperature. The cold atoms have a temperature very close to zero kelvin, formed by trapping and pre-cooling in a magneto-optical trap through laser cooling. The atom is cooled further by evaporative cooling in a magnetic or optical trap [85, 89].The cold atoms are used to study quantum many-body physics when placed in an optical lattice. They are also used to study superfluid behaviour in the lattices [85, 90].

2.7 Acoustic wave in solid

Acoustic waves are longitudinal waves; they are sound pressure vibrating in an active medium. The mode of vibration in a crystal is particle-like, which means they have energy, and the quantum of lattice vibration is the phonon. Therefore, the energy or frequency of the phonon can be determined as a function of the wave vector, since phonon dispersion is the relationship between frequency and wave vector. The conversion of acoustic energy into electromagnetic radiation was discovered in the mid-1930s [91, 92]. The heat pulse was viewed as a collection of quantized lattice vibrations or phonons, and its propagation through the solids was similar to the propagation of photons through matter. But advancements such as the development of femtosecond laser technology produced some other experimental procedures to generate picosecond acoustic waves [33]. An acoustic wave can be generated by a SASER device, the analogue to LASER. Sound amplification by stimulated emission of radiation, acoustic radiation, the sound wave, is emitted by the process of sound amplification that was based on the stimulated emission of phonons. The coherent strain pulse is generated by the fast thermoelastic deformation of a thin metal film. The strain pulse moves in the material at the speed of sound for the material, and the frequency of range of the strain pulse is between 100 -200 GHz. The pulse was used recently to drive an electric current

29

through SLs with no electric field applied to it [34]. The coherent strain pulse of the acoustic wave when it propagated along the axis of the SL caused an effect on the dynamics of the electron and induced an electric current [93].

A longitudinal coherent acoustic wave propagating along the x-axis of the SLs could generate a deformation potential given by the electron-phonon interaction, and it is assumed that the piezo-electric potential effects are negligible [94]. When an acoustic wave propagates in the SLs, it interacts with electrons: this electron-phonon interaction is due to the phonon existing in a real system. Therefore, the electron dynamics are affected by the electron-phonon interaction, and this changes the property of the dynamical localization of the electron.

When the phonon frequency is equal to the Bloch frequency in a dc field or w in ac field, or one of them is in an ac/dc field, the electron will scatter rapidly. In order to be able to establish the dynamical localization of an electron in an experiment, the resonance between the phonon and external electric field must be controlled [95, 96].

Each miniband electron will gain potential energy due to the longitudinal acoustic wave. The energy is a function of wave vector, k_S and U, the amplitude of the wave which depends on the maximum strain, S_0 and the deformation potential, D.

$$U = S_0 D \qquad (2.46)$$

S_0 is usually $< 0.5\%$, and the deformation potential is usually obtained from the periodic variation of the conduction band edge of the SLs [97, 98]. The stress will lead to deformation in the energy bands caused by the interaction of the electron with acoustic phonons [99,100]. When energy in the form of the acoustic wave is applied to the SL, it interacts with the electron excitations causing a shift in the energy of the band edge per unit of the elastic strain. This is the deformation potential the electron in the crystal will experience. Table 1.0 shows, the deformation potential value for some semiconductors; the energies are in eV. D_d and D_u are constants characteristics of the conduction band valley. D_d relates to pure dilation and is associated with pure shear. a, b and d are positive strains that lower the valence band edge, and these are associated with acoustic strains. d_0 is the optical deformation potential for the valence band. D_0 is an optical deformation potential constant for the electron, and it is energy per unit displacement [74].

Table 1.0

Deformation potentials for some semiconductors

	D_d (eV)	D_u (eV)	a (eV)	b (eV)	d (eV)	d_0 (eV)	D_0 (eV)cm^{-1}
Si	-6.0	7.8		2.1	3.1		(10^9 *intervalley*)
		9.2		2.5	5.3		
Ge	-9.1	15.9	2.6	-2.4	-4.1	6.4	$7\times 10^8 < 111 >$
	-12.3	19.3	3.9	-2.7			
AlSb	+1.8						
	+2.2	6.2		-1.4	4.3		
GaSb		20		-2	-4.6		
		22.6		-3.3	-8.4		
GaAs	+7.0	+7.4	-8.7	-1.8	-4.6		(10^9 *intervalley*)
			-9.2	-2.0	-6.0		
GaP		6.2		-1.3	-4.0		
InSb	+4.5		-88	-0.2	-4.6		
	+16.2			-2.1	-5		
InP		21		-1.6	-4.4		

Table 1.0: The deformation potential for some semiconductors; the energies are in (eV). D_d and D_u are constants characteristics of the conduction band valley. a, b and d are positive strains that lower the valence band edge, and d_0 are associated with acoustic strains. d_0 is the optical deformation potential for the valence band. D_0 is an optical deformation potential constant for the electron [77].

In semiconductors, the attention is near the band extremum and the shift in energy of the band edge per unit of elastic strain is called the deformation potential D. Since u is the displacement of a unit cell, we define the strain tensor as

$$S_{ij} = \frac{1}{2}\left(\frac{\partial u_i}{\partial x_j} + \frac{\partial u_j}{\partial x_i}\right) = S_{ji}$$

The change in energy of a given non-degenerate band edge can be defined by
$$\Delta E = \sum_{ij} D_{ij}\, S_{ij}$$
where D is the deformation potential tensor and S_{ji} is the strain tensor.

2.8 Semi-classical model of acoustic wave

A longitudinal coherent acoustic wave propagating along the x-axis of the SL will generate a deformation potential, resulting in the periodic variation of the conduction band edge of the SL. In this analysis the strain wave is taken to travel along the principle growth axis of the SL, therefore the piezo-electric coupling is zero. This means that any piezo-electric potential effects will be negligible and only the mechanism of electron-phonon interaction exists and is equal to the deformation potential.

The potential energy obtain as a result of strain of the lattice, S in the semi-classical model will be

$$V_S = DS \tag{2.47}$$

The electron-phonon coupling constant is described by D and can be measured experimentally; in previous work it was found to be $\sim 10\ eV$ [27, 31]. The strain, $S(x,t)$ that will be obtained due to the coherent acoustic wave propagating along the x-axis of SLs will be

$$S = -S_0 \sin(k_s x + \omega_s t) \tag{2.48}$$

The maximum strain the wave generates is $S_0 < 0.5\%$; k_s is the wave number of the acoustic wave and takes the value within the first half of the SL minizone. If we assume a linear dispersion relation for the frequency of this acoustic wave, $\omega_S = v_S k_S$ and the speed of sound is $v_S = 5000 \ ms^{-1}$ from the experiment [79], the maximum strain is

$$S_0 = k_S A \tag{2.49}$$

A describes the physical displacement of the lattice obtained from the acoustic wave and is called the mechanical displacement amplitude. Therefore, substituting *equations* (2.48) and (2.49) into *equation* (2.47), we obtain the potential energy generated by the acoustic wave as

$$V_S(x,t) = -U \sin(k_s x - \omega_S t) \tag{2.50}$$

and $U = DS_0$, the wave amplitude.

Chapter 3

Dynamics of electron in semiconductor superlattice driven by acoustic wave

3.1 Introduction

In this chapter, the electron dynamics in the SL will be explained by analysing electron trajectories, and calculating the drift and average velocity of electrons when driven by an acoustic wave. Greenaway in his work [33] and others [35, 40] studied the dynamics of a single electron in SLs using acoustic waves. They showed that an acoustic wave propagating through a SL will induce a charge current, and that there are two dynamical regimes. This hinges on whether the energy amplitude of the acoustic wave is more or less than a critical value which is defined as the value of the wave amplitude where the dynamical change occurred, denoted as U_c. This critical value depends on the parameter of the SLs. When a coherent acoustic wave is applied along the axis of a SL, it generates a deformation potential produced by the electron-phonon interaction. An acoustic wave propagating through a SL can be considered as an example of a moving lattice propagating through a static lattice. A continuous gigahertz acoustic wave will create complex terahertz electron dynamics in a SL, consequently producing high-frequency current oscillations [34]. When the amplitude of the acoustic

wave is less than the critical value, the electron will be dragged through the SL by the velocity of the acoustic wave. This causes a strong resonant enhancement of the electron transport that can be accompanied by a high periodic frequency oscillation of the electron orbits [26]. If the wave amplitude is increased to a value greater than U_c, the electrons will perform Bloch-like oscillations that dramatically suppress electron transport, localising the electrons in a quantum well of the SL. The minibands electrons driven by a gigahertz acoustic wave attain a higher maximal drift velocity due to the scattering and the assumption that the electron start at $x = 0$. When an acoustic wave is applied along the axis of a SL whose electrons are moving randomly, the electrons will move in the direction of the travelling wave.

In this work, we investigated the transport characteristics of electrons depending on the initial conditions. We calculated the average trajectory by averaging across the initial conditions, since the electrons in the device were moving randomly. We assumed the temperature was very close to zero, $T \sim 0$ so that the momentum would start at zero. The velocity of the electron can be determined using the potential energy generated by the acoustic wave and we describe the semiclassical Hamiltonian of the system. The phase portrait will be analysed to understand the electron behaviour in the SL.

3.2   Model of electron dynamics

To describe the single-electron dynamics in the SL, driven by an acoustic wave, we formulated a model from the semiclassical Hamiltonian of the system. In section (2.8) we derived an expression for the potential energy, $V_S(x,t)$, from the acoustic wave. The semi-classical Hamiltonian of the system is the sum of the kinetic and potential energy and is described as

$$\hat{H}(x, p_x, t) = E(p_x) + V_s(x, t) \tag{3.1}$$

The total kinetic energy is the dispersion relation as derived in section (2.5) and is

$$E(p_x) \;\; = \;\; \frac{\Delta_{SL}}{2}\left[1 - cos\left(\frac{p_x d}{\hbar}\right)\right] \tag{3.2}$$

 and the potential energy is described as

$$V_s(x, t) = -U \sin(k_s x - \omega_S t) \tag{3.3}$$

where U is the wave amplitude. We described $U = S_0 D$ as the wave amplitude of the acoustic wave which creates the maximum strain, $S_0 < 0.5\%$ on the deformation potential, D. The wave number, k_s of acoustic waves lies within the inner half of the minizone so the linear dispersion for frequency of the acoustic wave will be $\omega_s = v_s k_s$ where v_s is the speed of the sound wave. Therefore, the Hamiltonian of the system will be

$$\therefore \quad \hat{H} = \frac{\Delta}{2}\left[1 - \cos\frac{p_x d}{\hbar}\right] - U\sin(k_s x - \omega_s t) \tag{3.4}$$

The semi-classical Hamilton's equations of motion can be obtained from the Hamiltonian in the above equation as

$$v_x = \frac{dx}{dt} = \frac{\partial H}{\partial p_x} = \frac{\Delta d}{2\hbar}\sin\frac{p_x d}{\hbar} \tag{3.5}$$

$$\frac{dp_x}{dt} = -\frac{\partial H}{\partial x} = k_s U\cos(k_s x - \omega_s t) \tag{3.6}$$

We solved these *equations* (3.5) and (3.6) numerically using a 4th order Runge-Kutta algorithm [101-102]. Taking initial position and momentum to be $x = p_x = 0$ when $t = 0$, for time independent, the electron trajectories are determined in the absence of scattering. We obtained the electron trajectories for different wave amplitudes and analysed the trajectories to understand the electron transport in the SL.

3.3 Electron driven acoustically in superlattices

When the acoustic wave is applied along the axis of a SL, the electron dynamics depends on the value of the wave amplitude. The wave amplitude will produce a force on the electrons that causes them to experience acceleration and movement, since energy states are available in the bands. The electrons' drift velocity as explained in *equation* (2.25) helps to determine the measured transport characteristics of the electron in a SL in the presence of scattering. Fig. 3.1 shows the relation of the drift velocity against the wave amplitude applied for the miniband electrons. Thus, we have a region of negative differential velocity which is caused by the localisation of the electron trajectories due to Bloch-like oscillations. We obtained a peak value for v_d of about $4.5 \times 10^4 ms^{-1}$ and a high magnitude of the negative differential velocity.
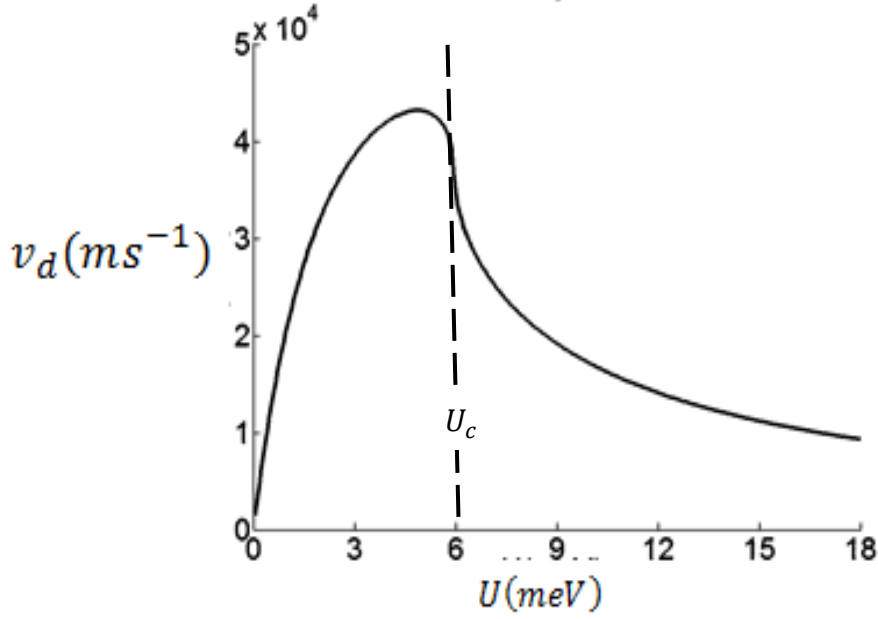
Figure 3.1: The drift velocity, v_d versus wave amplitude, U obtained for the miniband electron been driven by the acoustic wave with initial value of $x = 0$, $p = 0$. The dashed vertical line is the position of U_c, the transition between the two dynamical regimes.

Here, it was assumed that the electron started from $x = 0$ for simplicity, at a temperature very close to zero, $T \sim 0$, where the initial momentum can be considered as $p_x = 0$. It can be observed in Fig. 3.1 that when the values of the wave amplitudes are between $1meV$ and $3meV$, for the single electron dynamics, we have an almost linear curve in the positive direction. Afterward a maximum is reached before a steeper negative drift velocity. This suggests that there must be a transition between the dynamical regimes. The dashed vertical line in Fig. 3.1 is the position of U_c, the critical value. This is the value of wave amplitude at the transition between the two dynamical regimes. At this point the critical value must be equal to the local maximum of $E'(P_x)$, the modified dispersion relation. This is defined as

$$E'(p_x) = E(p_x) - v_s p_x \tag{3.7}$$

p_x is the momentum and v_s is the speed of sound, where $E(p_x)$ is the dispersion energy given in *equation* (3.2) . The local maximum of $E'(p_x)$ will occurs when

$$\frac{dE'(p_x)}{dp_x} = 0 \tag{3.8}$$

Therefore
$$\frac{dE'(p_x)}{dp_x} = \frac{d}{dp_x}\left\{ \frac{\Delta}{2}\left[1 - \cos\frac{p_x d}{\hbar}\right] - v_s p_x \right\} = 0$$

37

$$= \frac{\Delta d}{2\hbar}\sin\frac{p_x d}{\hbar} \; - \; v_s = \quad 0$$

Therefore,

$$\sin\frac{p_x d}{\hbar} \; = \; \frac{2\hbar v_s}{\Delta d}$$

Using Taylor expansion around π for p_x in the first Brillouin zone,

Taylor series: $f(a) + \frac{f'(a)}{1!}(x-a) + \frac{f''(a)}{2!}(x-a)^2 + \frac{f^3(a)}{3!}(x-a)^3 + \cdots \cdots$.

Therefore we now have

$$\sin\frac{p_x d}{\hbar} \; = \; \sin\pi \; + \cos\pi\left(\sin\frac{p_x d}{\hbar} \; - \pi\right)$$

$$\therefore \quad \sin\frac{p_x d}{\hbar} \; = \; \pi - \; \frac{p_x d}{\hbar}$$

So we now have

$$\pi - \; \frac{p_x d}{\hbar} \; = \; \frac{2\hbar v_s}{\Delta d} \; ,$$

therefore maximum momentum is

$$p_x^m \; \approx \; \frac{\pi\hbar}{d} \; - \; \frac{2\hbar^2 v_s}{\Delta d^2}$$

The Hamiltonian of the system in the rest frame is

$$H' = E(p_x) - v_s p_x + V(x') \; = \; E'(p_x) \; + V(x') \tag{3.9}$$

where $H' = 0$, since it does not depend explicitly on time, is a constant of motion and is equal to zero for all time, t. So therefore at maximum

$$E(p_x^m) \; - \; v_s p_x^m \; = - V(x')$$

therefore,

$$\frac{\Delta}{2}\left[1 - \cos\frac{P_x^m d}{\hbar}\right] \; - \; v_s P_x^m \; = \; - V(x') \tag{3.10}$$

Substituting for P_x^m in the above equation, we have

$$\frac{\Delta}{2}\left[1 - \cos\left(\pi - \frac{2\hbar^2 v_s}{\Delta d^2}\right)\right] - v_s\left[\frac{\pi\hbar}{d} - \frac{2\hbar^2 v_s}{\Delta d^2}\right] = \; - V(x')$$

Considering the parameter used [33], $\frac{2\hbar v_s}{\Delta d} \approx 0.08$ and consequently $\frac{2\hbar^2 v_s}{\Delta d^2}$ will be negligible. Therefore

$$\Delta - v_s\frac{\pi\hbar}{d} = - V(x') \tag{3.11}$$

This is the potential, which is $E'(p_x) = \Delta - v_s \frac{\pi\hbar}{d}$ and can only take values between $\pm U$ which are determined by the amplitude $V(x')$

$$\therefore E'(p_x) = U_c$$

This is the critical value of the wave amplitude.

We illustrate the electron trajectories for different values of wave amplitude to see if the dynamical regime can be distinguished. Fig. 3.2 shows the electron trajectory when $U = 1meV$, which was obtained numerically from *equations* (3.5) and (3.6). The $x(t)$ trajectory consists of regular oscillations that are almost sinusoidal, and the electron is being dragged in the SL with the velocity of the acoustic wave.
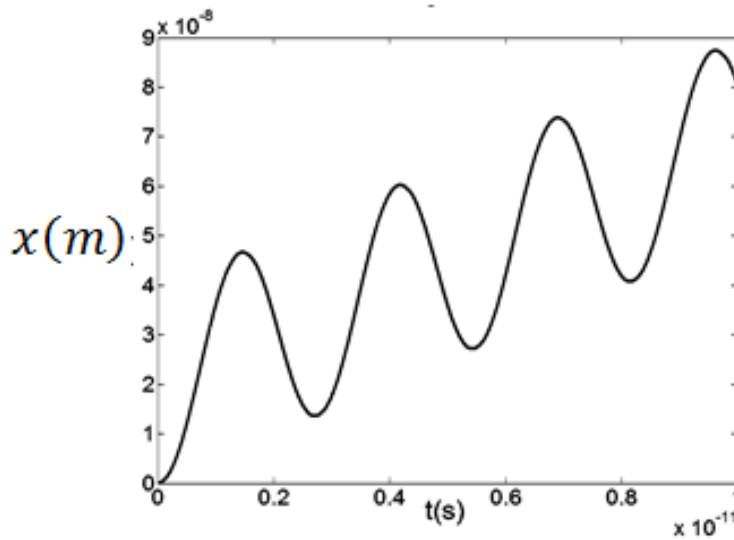
Figure 3.2: The electron trajectory in real space when the wave amplitude, $U = 1meV$, initially at $x = 0 \ and \ p = 0$. The electron is being dragged in the SL with the velocity of the acoustic wave.

In this region, when $U = 1meV$, the electrons are trapped. The electron will be in the parabolic region of the $E'(p_x)$ curve, where the momentum, $p_x = 0$ as shown in Fig. 3.3. The electron is confined within a single potential well in the acoustic wave and oscillates back and forth across the well. $E'(p_x)$ is the modified dispersion relation. When U reaches the critical value, U_c this is equal to the local maximum of $E'(p_x)$, arrowed in Fig.3.3, the electron is no longer trapped within the acoustic wave but traverse since the wave amplitude, $U > 4meV$.
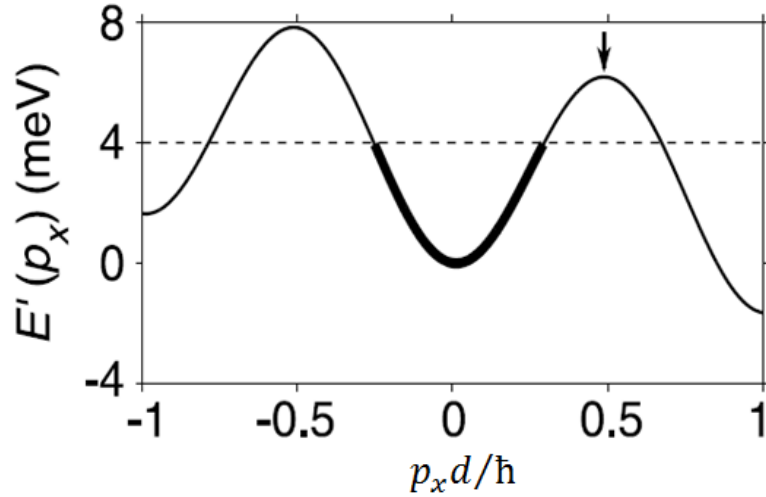
Figure 3.3: The modified dispersion relation is plotted against the momentum showing electron transport in the potential well. The wave amplitude must be greater than the miniband for the electron to traverse over the barrier. At the arrowed peak $E'(p_x) = U_c$ refer to as the critical value. The figure is adapted from reference [33].

As the wave amplitude increases, consequently increasing the drift velocity of the system, the electrons begin to Bloch oscillate. Fig. 3.4 is the electron trajectory when the wave amplitude is increasing; the wave amplitude is $7meV$. At this region, the electron has started Bloch oscillate which causes the electron transport to be suppressed. The electron $x(t)$ trajectory consists of Bloch-like oscillations caused by the acoustic wave.
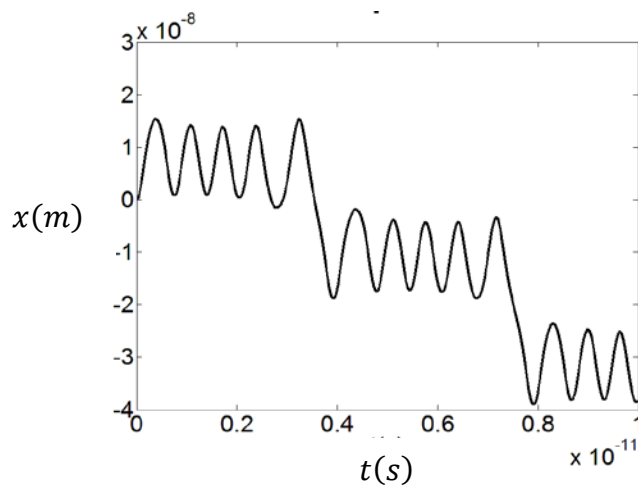
Figure 3.4: Electron trajectory when the wave amplitude, $U = 7meV$. The frequency oscillations are interrupted by jumps in the negative $x - direction$.
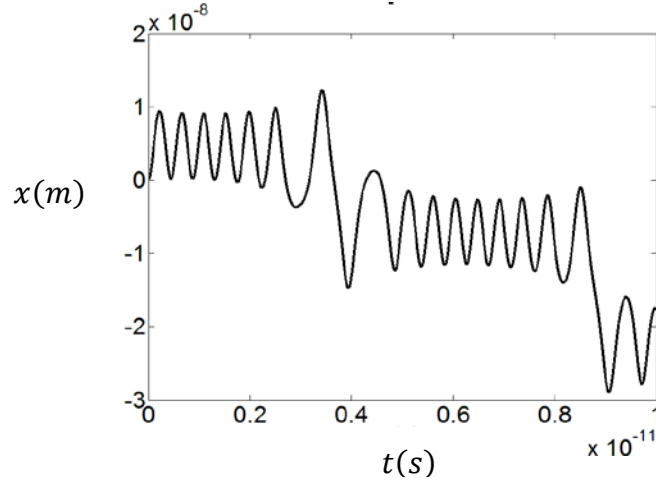
Figure 3.5: Electron trajectory in real space when the wave amplitude is $U = 10meV$ with initial condition $x = 0$ and $p = 0$. The high frequency oscillations are driven by the acoustic wave.

When the wave amplitude is increased further, we have bursts of high-frequency fluctuations in electron trajectory $x(t)$ but they are moving in the negative $x -$direction. The bursts of Bloch-like oscillations are interrupted by jumps in the negative direction as shown in Fig. 3.5. We could observe a change in trajectory at different strengths of wave amplitude but more investigations are still required.

3.3.1   Average drift velocity

The average drift velocity is needed since we are dealing with propagating wave whose wavelength is less than the length of the SL. The average drift velocity measures the actual velocity of the electron and this helps produce a general overview of the dynamics of the electron in the SL. To calculate average drift velocity $\langle v_d \rangle$, we assume that the electron will start at $x = x_0$, and at a low temperature close to zero; then the momentum states as $p_x = 0$. We sum up the electron drift velocity at different initial conditions over many periods of oscillation and average over all the initial conditions. Fig. 3.6 shows the $\langle v_d \rangle$ against the wave amplitude applied. From the graph, when the wave amplitude U is between $1meV$ and $3meV$, we have an almost linear curve that reaches the *arrowed* peak at(1), the curve dropped down sharply to point (2).
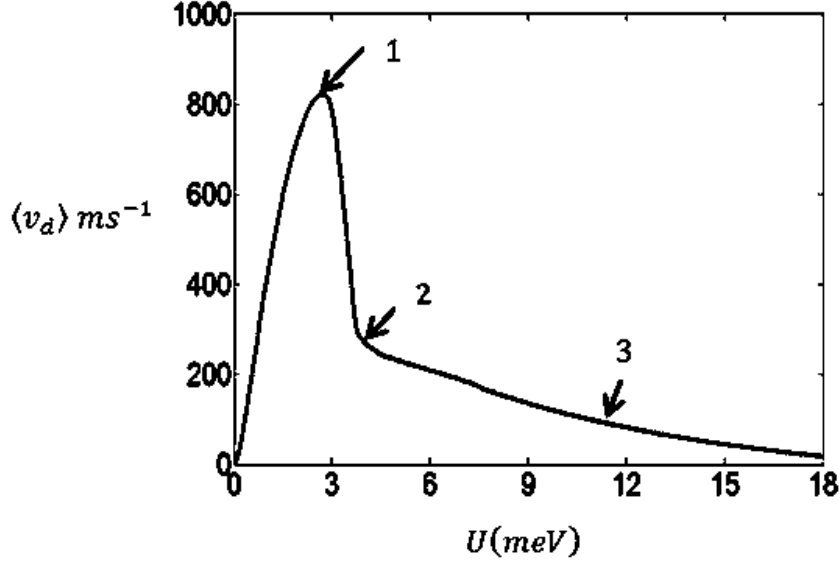
Figure 3.6: Relationship between the average drift velocity, $\langle v_d \rangle$ and the wave amplitude, U when an acoustic wave is applied along the axis of the SL. The arrowed peak of the average drift velocity is observed between $3meV$ and $4meV$.

After the drop, the graph maintains a steady slope, *arrowed* (3) as the wave amplitude is increased further. Therefore, there is dynamical change and the maximum still exists. Thus, we conceivably will observe the dynamics of the electron before the peak when the wave amplitude is very minimal, the dynamics of electron at the peak of $\langle v_d \rangle$ and far away from the peak when the wave amplitude is much higher. This means that we have transitions in the dynamical regimes. We have three distinct regimes: before the peak, the peak or maximum of the drift velocity and far beyond the peak. For further investigation, we calculate average trajectories at each of these phases: before the peak, when $= 1meV$, at the peak we take the wave amplitude to be $U = 4meV$ and after the peak when $U = 10meV$. Fig. 3.7 shows the average electron trajectories calculated for these wave amplitudes. The area marked (1) corresponds to when $U = 1meV$, and the average trajectory is as shown in Fig. 3.7 (a). The graph shows a monotonic behaviour. The area marked (2) relates to $U = 4meV$, and Fig. 3.7(b) of the $\bar{x}(t)$ trajectory is a non-linear function going down. In Fig. 3.7(c), the $\bar{x}(t)$ trajectory for $U = 10meV$ corresponds to an area far away from the peak, marked (3) and the graph is meandering down swiftly.
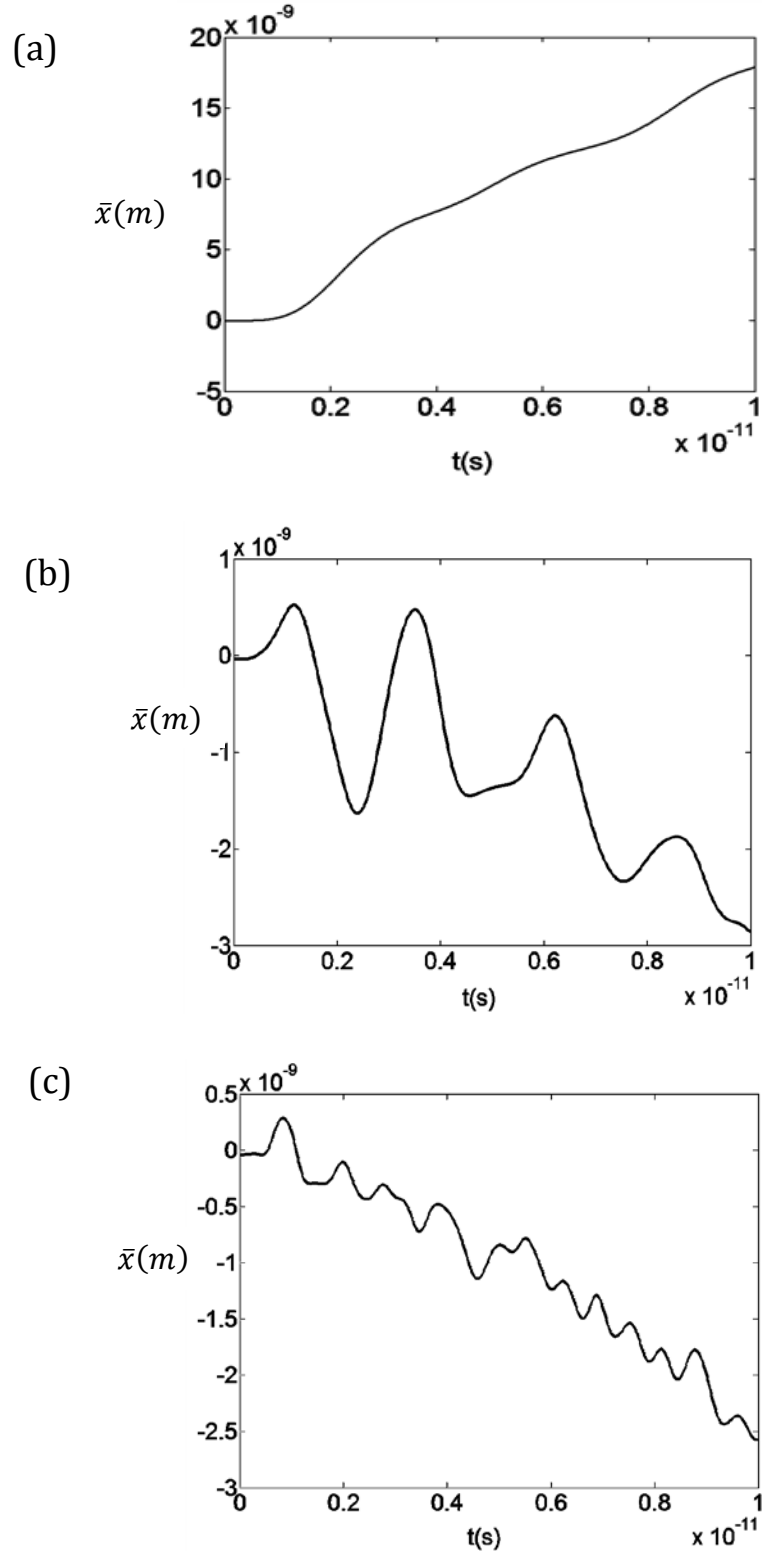
(a)

(b)

(c)

Figure 3.7: (a) The linear curve is the average electron trajectory, $\bar{x}$ calculated for $U = 1meV$ before the peak in Fig. 3.6. Fig. 3.7(b) is average trajectory when $U = 4meV$ and corresponds to the *arrowed* (transition) for average velocity in Fig.3.8. Fig. 3.7(c) represents the calculated average trajectory for $U = 10meV$ far away from the peak.

We classified the trajectory based on the initial conditions; therefore we calculated the electron trajectory by averaging across all the initial conditions. We observed the transformation of the trajectory as the average velocity was changing in Fig. 3.8. Fig. 3.7(a), when $U = 1meV$, shows a monotonically increasing function. When the peak was reached with the increasing drift velocity, the average trajectory calculated for $U = 4meV$ is as represented in Fig. 3.7(b), which is not monotonic but a non-linear function. Far away from the peak, we observed that the average trajectory calculated for $U = 10meV$ which is a non-linear the trajectory of the dynamical system twisting down swiftly as shown in Fig. 3.7(c). By averaging the trajectory we could see the changes in the trajectory on the phase space. This suggests that there may be transition between the dynamical systems. This is associated with the change in the drift velocity and whether the transitions depend on the scattering.

The average velocity can be calculated to achieve a more detailed overview of the dynamics of electrons in SLs. This was done by taking the electron trajectory over many periods of oscillation, and we assumed that there were no scattering events. An example of such an assumption is in the dynamics of cold atoms in the moving optical lattices [33]. It is irrelevant to determine the drift velocity since the scattering effect in the transport of atoms in the optical lattices is negligible.
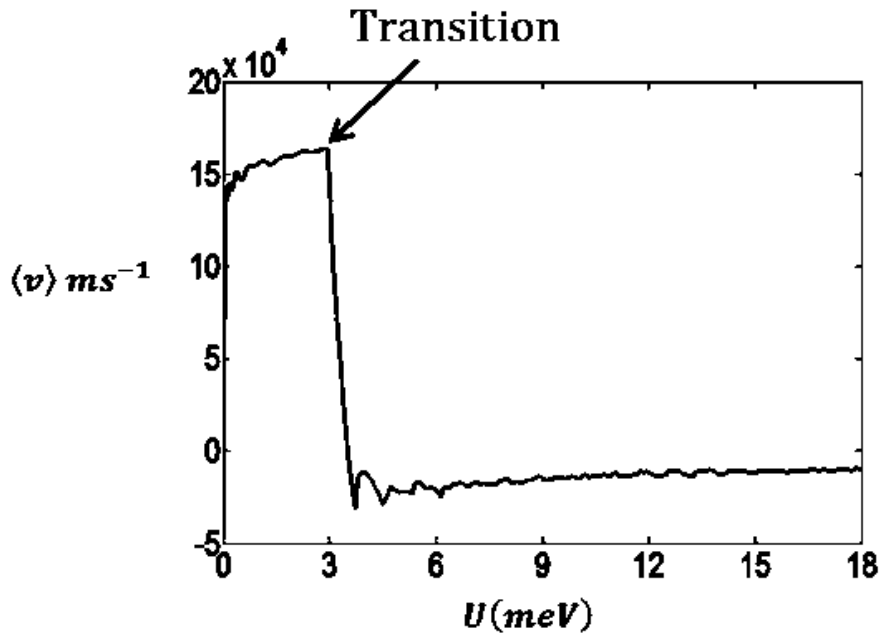
Figure 3.8: The relation between the average velocities, $\langle v \rangle$ of electrons and the wave amplitude, U. In the graph, the average velocity grows steadily at low wave amplitude and afterwards reaches a drastic maximum and drop to negative value.

Fig. 3.8 shows the average velocity, $\langle v \rangle$ against the applied wave amplitude, U. At low wave amplitude the average velocity increases steadily and mainatains a constant at the peak. Thereafter it drops drastically at a certain wave amplitude and maintains a negative average velocity for high values of wave amplitude. In Fig. 3.8, there are basically three regions:- before the peak, at the peak and far beyond the peak. In the first region, before the peak, the average velocity is positive and steadily increases as the wave amplitude increases. When the wave amplitude is increased further, the average velocity reaches a maximum (marked) transition. At this peak of the average velocity, the wave amplitude is about $3meV$. Afterward the average velocity drops drastically to below zero and we have a steady negative value for the increasing value of the wave amplitude. This shows that we have transition before the peak and after the peak.

3.3.2   Phase portraits

We analyse the phase portraits of the electron motion, which enabled us to understand the electron behaviour in the SL. Phase portraits provide information about the number of different trajectories from different initial conditions. This helps to characterise the transition, which is the dynamical regimes we observed depending on the different values of wave amplitudes applied. We used different initial conditions to build the phase portrait, since we obtained the average drift velocity by averaging the velocity of all trajectories. Therefore the phase portrait characterises the electron trajectory at each phase transition for the different values of wave amplitude applied. This enables us to qualitatively understand the equation of motion in the SL. The phase space of the system gives more detailed insight into the system's dynamics.

In order to do this, we considered the motion of electrons in the SL in the reference frame of the acoustic wave. The motion of electrons in a moving reference frame can be described if we rewrite the dynamical system [103-106]. In the moving reference frame of an acoustic wave, the electrons have the velocity of the acoustic wave, and this is almost constant inside the SL since the SL is homogenous. Therefore, we transform from the lab (x, p) frame to the rest (x', p) frame of the acoustic wave. The transformation into the moving frame of the acoustic wave helps us to understand the electron's trajectory. For this, we create the co-ordinate transformation of $x(t)$ into the moving frame of the acoustic wave $x'(t)$ by using the following substitution

$$x'(t) = x(t) - v_s t \tag{3.12}$$

and differentiating *equation* (3.12) gives

$$\therefore \quad \dot{x}'(t) = \dot{x}(t) - v_s \tag{3.13}$$

So, the equation of motion of the electron in the SL will become

$$\dot{x}' = \frac{\Delta d}{2\hbar} \sin \frac{p_x d}{\hbar} - v_s \tag{3.14}$$

$$p = kU \cos kx' \tag{3.15}$$

46

We solved *equations* (3.14) and (3.15) numerically and analytically to identify the phase portrait for different wave amplitudes by taking many initial values (x', p) for momentum and position. We considered the wave amplitude values before the peak transition, at the peak and faraway from the peak. The phase portrait can be obtained analytically by integrating the equation of motion of the electron in the SL. Let *equations* (3.14) and (3.15) be described as

$$f(x,p) = \frac{dx'}{dt} = \frac{\Delta d}{2\hbar}\sin\frac{p_x d}{\hbar} - v_s \tag{3.16}$$

$$g(x,p) = \frac{dp}{dt} = kU\cos kx' \tag{3.17}$$

The entire notations have the usual meaning, Δ is the miniband. d is the lattice constant, p_x is the momentum in the x-direction, and the wave vector is k. Therefore, if we differentiate *equations* (3.16) and (3.17) w.r.t. τ and define $\tau = \omega t \therefore d\tau = \omega dt$ to transform into dimensionless equations as :

$$\frac{dx'}{dt} = \frac{dx'}{d\tau}\frac{d\tau}{dt} \qquad\qquad \therefore \qquad\qquad \frac{dx'}{d\tau} = \frac{dx'}{dt}\frac{dt}{d\tau}$$

and $\qquad\qquad \frac{dp}{dt} = \frac{dp}{dt}\frac{d\tau}{dt} \qquad\qquad \therefore \qquad\qquad \frac{dp}{d\tau} = \frac{dp}{dt}\frac{dt}{d\tau}$

we obtain dimensionless differential equations as follows

$$\frac{dx'}{d\tau} = \left(\frac{\Delta d}{2\hbar}\sin\frac{p_x d}{\hbar} - v_s\right)\frac{dt}{d\tau} \qquad \therefore \qquad k\frac{dx'}{d\tau} = \frac{\Delta d}{2\hbar v}\sin\frac{p_x d}{\hbar} - 1$$

$$\frac{dp}{d\tau} = (kU\cos kx')\frac{dt}{d\tau} \qquad\qquad \therefore \qquad \frac{dp}{d\tau} = \frac{kU}{w}\cos kx'$$

If, we let $\quad \frac{\Delta d}{2\hbar v} = A$, $\quad \frac{d}{\hbar}\frac{kU}{w} = B$, $\quad P = p_x d/\hbar \quad$ and $\quad X = kx'$

then,

$$\frac{dX}{d\tau} = A\sin P - 1 \tag{3.18}$$

$$\frac{dP}{d\tau} = B\cos X \tag{3.19}$$

The general solution of these two equations can be determined if we divide *equation* (3.19) by *equation* (3.18) and we obtain

$$\frac{dP}{dX} = \frac{B\cos X}{A\sin P - 1}$$

$$(A\sin P - 1)dP = (B\cos X)\,dX \tag{3.20}$$

and integrating *equation* (3.20) gives

$$\sin X = \frac{C - A\cos P - P}{B}$$

where C is an arbitrary constant that can be obtained from the initial value of (X, P)

$$\therefore \qquad X = (-1)^n \sin^{-1}\frac{C - A\cos P - P}{B} + \pi n \tag{3.21}$$

$$n = 0, \pm 1, \pm 2 \dots \dots \dots \dots$$

Therefore, the phase portrait can be determined analytically by taking initial values for X and P; these coordinates describe the state at any instant. The dynamical rule specifies the immediate future of all state variables, given only the present values of those same state variables.

To determine the fixed points of the dynamical systems, we equate to zero *equations* (3.14) and (3.15), which are equations of motion of the electron in the SL [105],

$$f(x, p) = \frac{\Delta d}{2\hbar}\sin\frac{p_x d}{\hbar} - v_s = 0 \tag{3.22}$$

$$g(x, p) = kU\cos kx' = 0 \tag{3.23}$$

$$\therefore \qquad \sin\frac{p_x d}{\hbar} = \frac{2\hbar v_s}{\Delta d} \qquad \text{and} \qquad \cos kx' = 0$$

$$\text{let} \qquad \frac{p_x d}{\hbar} = p \qquad \text{and} \qquad kx' = x$$

Therefore fixed points, p and x will be described as

$$p = (-1)^n \sin^{-1}\frac{2\hbar v_s}{\Delta d} + \pi n \tag{3.24}$$

$$n = 0, \pm 1, \pm 2 \dots \dots \dots \dots$$

$$x = \pm \frac{\pi}{2} + 2\pi a \qquad\qquad (3.25)$$

$$a = 0, \pm 1, \pm 2 \,... \,... \,... \,.......$$

The fixed points can be classified according to their stability property: there are stable nodes, unstable nodes, centre and saddle. In this work, we obtained two types of fixed point, the centres and saddles shown in Fig.3.9.
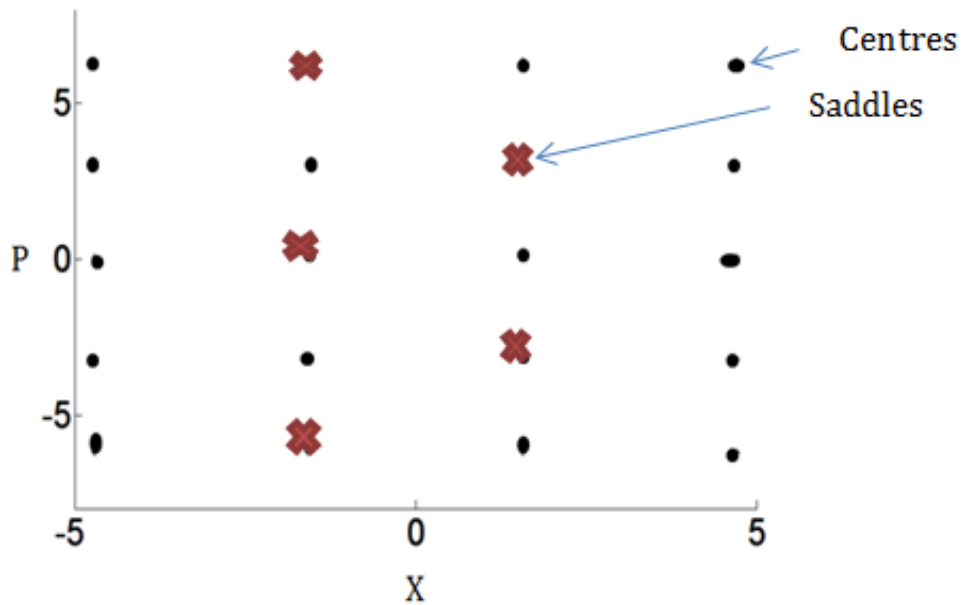

Figure 3.9: A typical phase portrait in the locality of an equilibrium state showing the fixed points: centres and saddles. The fixed points for the system under consideration are as shown. It does not depend on U but on miniband, lattice constant and velocity of the acoustic wave.

It is impossible to derive an explicit formula to obtain the solution of nonlinear *equations* (3.14) and (3.15), therefore analysis of the phase portraits provides a useful means of visualizing and understanding the qualitative features of the solution of a nonlinear equation.

3.4   Phase portrait for small U

Different initial states result in different trajectories, and these sets of trajectories form the phase portrait of a dynamical system. Before the peak of the average drift velocity in Fig. 3.6, we have a linear curve where the wave amplitude, U has values between $1meV$ and $3meV$. For $U = 1meV$, we illustrate the phase portrait in Fig. 3.10. There are two types of the phase trajectories here: the localised trajectory, *marked* (a) and the unlocalised or unbounded trajectory which is parallel to the horizontal axis, *marked* (b). The trajectories that connect the saddle point which separates these two phase trajectories from each other are called separatrix, *marked* (c). The separatrix marks the boundary between two phase curves with different properties. The equilibrium or fixed point in Fig. 3.10 is the simplest form of the orbit that is not moved by any transformation and is marked as a fixed point.
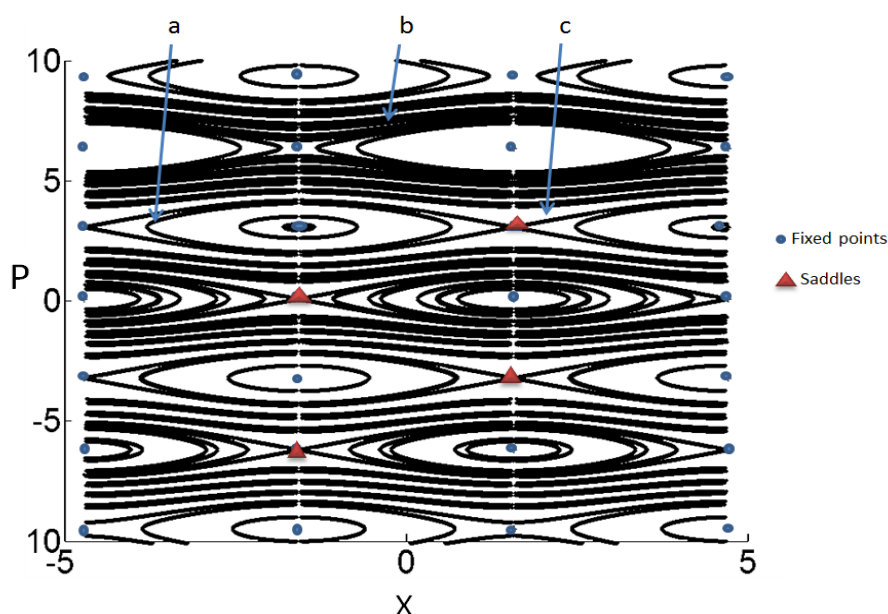
Figure 3.10*:   Momentum of the electron against the position describing the phase portrait of the system before the peak transition when $U = 1meV$. Shown in the figure are the localised trajectory or central *marked* (a) and the unbounded trajectory which is parallel to the horizontal axis, *marked* (b). The separatrix, which connects the fixed points passing through the saddle, is *marked* (c).

In this work, the phase trajectory can be classified into three different trajectories. We have the phase trajectory that rotates, we named it localised and m*arked* it (a) in Fig. 3.10. Note that it could encircle several centres. We called the unbounded trajectory parallel to the horizontal axis the unlocalised trajectory, *marked* (b) in Fig. 3.10. The third phase trajectory, which usually meanders up and down, encircles several "ellipses" and "centres" is *marked* (d) in Fig. 3.23. Another important trajectory is the separatrix, *marked* (c). It separates the localised from unlocalised trajectory and connects the saddle point. We described the dimensionless position as $X = kx'$ for the horizontal axis and for vertical axis the dimensionless momentum was defined as $P = pd/\hbar$.

In real space, the localised trajectory corresponds to regular sinusoidal oscillations, and the amplitude of these oscillations is equal to half the wavelength, λ_s of the acoustic wave. The trajectory is moving in the positive $x-$direction and the motion is periodic in real space. This is seen in the real-space trajectory for single electron dynamics as shown in Fig. 3.2. To describe the path of electron in the SL; we take different points in the phase portrait as the initial value to observe the electron path in the phase space. Therefore in Fig. 3.10, we take equilibrium points to explain the path of electron. The arrow indicates the direction in which the electron is moving. The blue curve (*on line*) indicates that the electron is moving in the clockwise (positive) direction and whenever we have the red curve (*on line*) it means that the electron is moving in an anticlockwise (negative) direction.

Fig. 3.11 shows the path of the electron, the equilibrium point taken in the phase portrait (Fig. 3.10) is (2.0, 6.2). The position-time and momentum-time curves are sinusoidal, so the momentum-position graph at this point on the phase portrait showed that the electron path is localised. The electrons are moving in the clockwise direction. In real space, the electron trajectory shows an almost linear curve in the positive direction. At another equilibrium point on the phase portrait in Fig. 3.10, (-2.0, 2.0), the electron path is localised but the electrons are moving in an anticlockwise direction. This shows that electron is moving in both positive and negative direction in the SL.
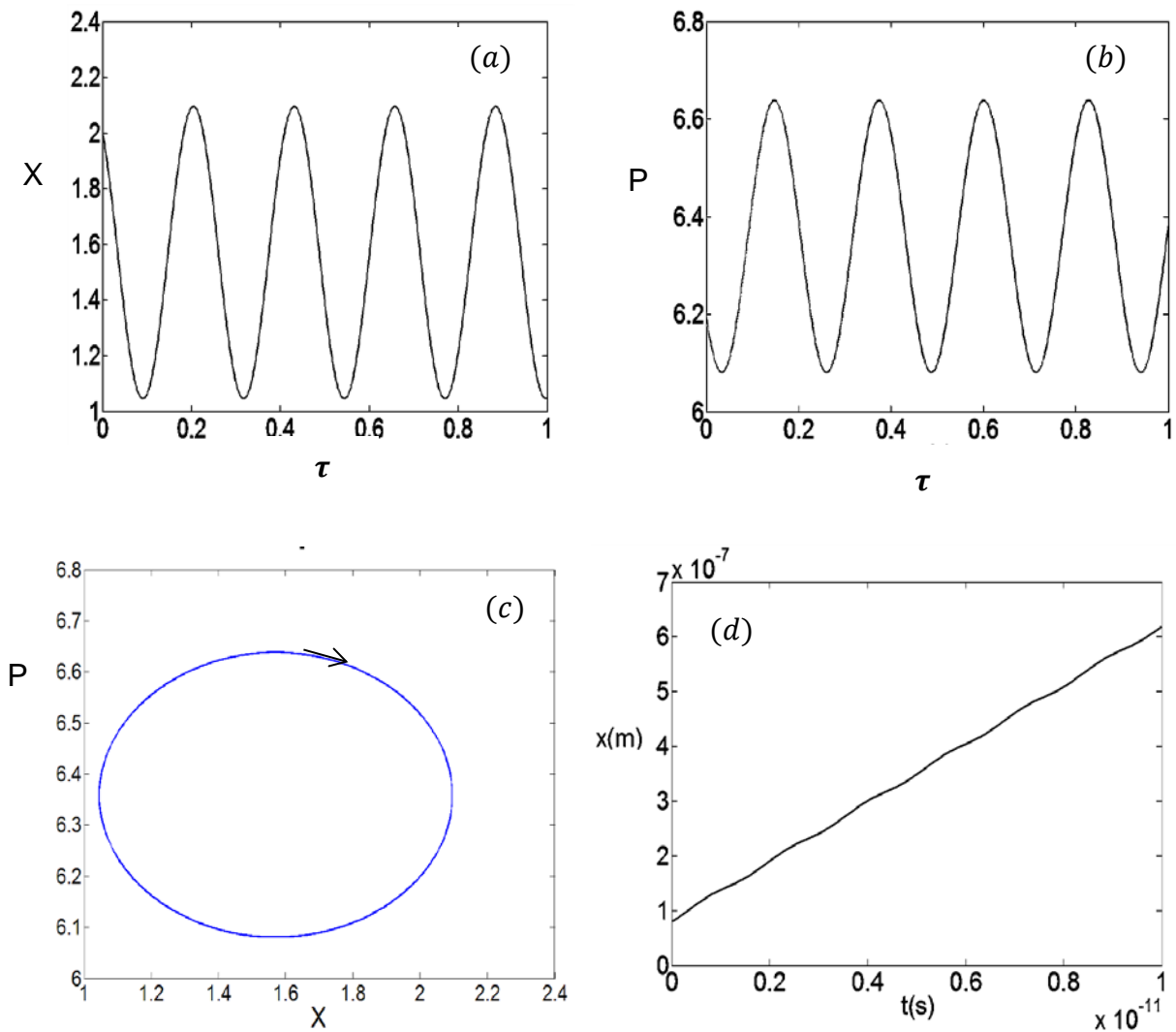
Figure 3.11: Paths of the electron from an initial point on the phase portrait. (a) is the position, X against the time, τ; (b) describes the momentum, P against the time, τ; and (c) is the momentum, P versus the position, X. The initial point (X, P) is $(2, 6.2)$ and the paths of the electron in the SL for the localised trajectory indicates the electron is moving in the positive direction. (d) electron trajectory $x(t)$ for $U = 1meV$ is almost linear curve in the positive direction.

Fig. 3.11 shows that the path of the electron: (a) is the position against the time where we have a sinusoidal curve. (b) shows the momentum against the time, which is also a sinusoidal curve. (c) is the momentum-position curve showing that the electron path is localised and that the electron is moving in a clockwise, positive direction. The electron in this region, when the wave amplitude is minimal, is localised and moves with the

52

velocity of the acoustic wave. Fig. 3.11 (d) shows that the $x(t)$ electron trajectory is regular, and the electron is moving in the positive direction.
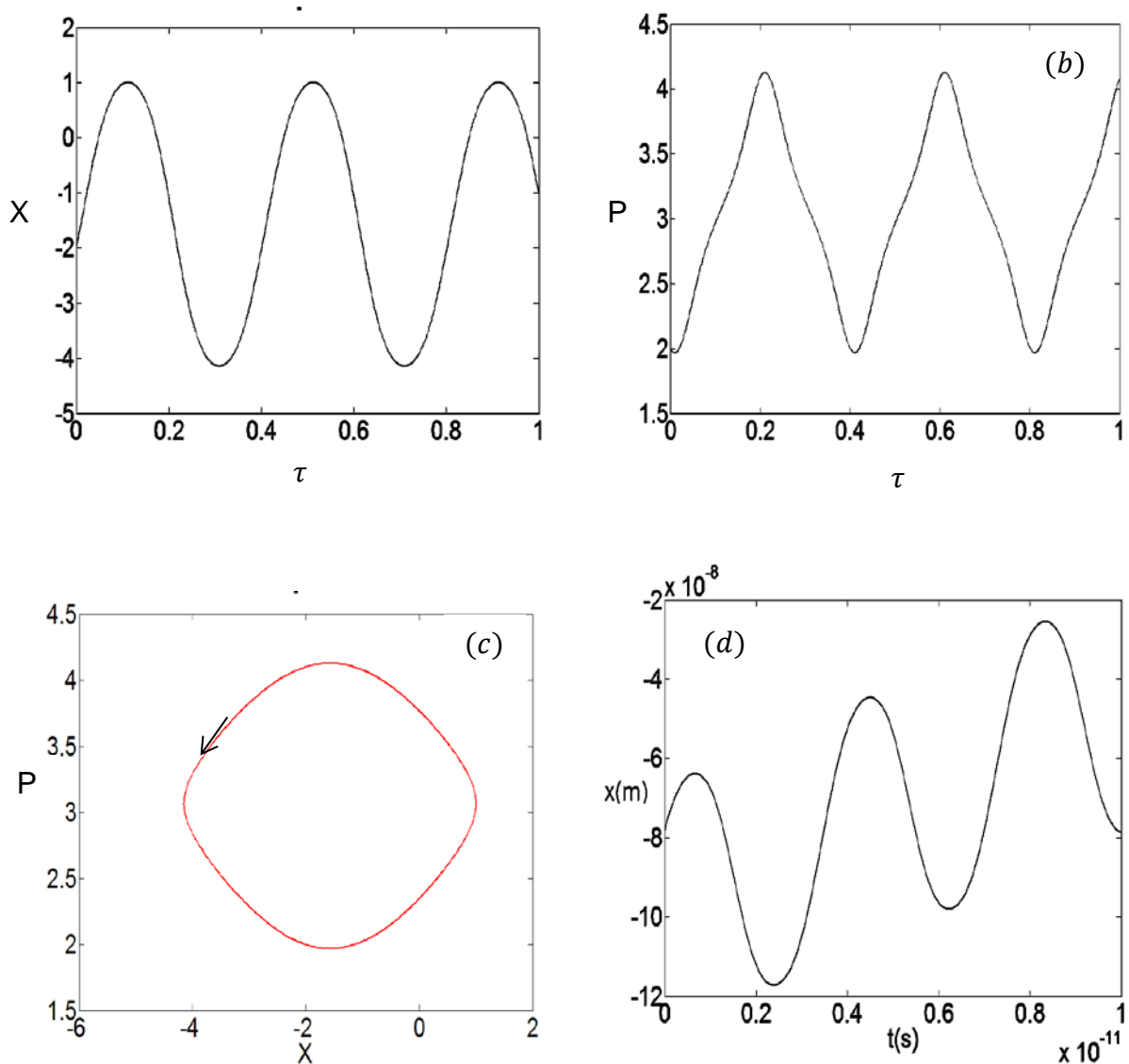
Figure 3.12: Paths of electron in the phase portrait. (a) is the position, X against the time, τ; (b) is the momentum, P against the time, τ; and (c) is the momentum, P against position, X. The paths of the electron in the SL, the localised trajectory indicate that the electron is moving in the negative direction (red). The initial point (X, P) is (-2.0, 2.0) and (d) is the electron trajectory $x(t)$.

We take another equilibrium point $(-2.0, 2.0)$ in Fig. 3.12, where (a) shows the position against the time; (b) the momentum against the time, (c) describes the momentum against the position; and (d) is the electron trajectory $x(t)$. The initial value is $(-2.0, 2.0)$. The momentum-position curve in Fig. 3.12 (c) shows that the

localised trajectory is in an anticlockwise direction, and the electron trajectory $x(t)$ in Fig. 3.12 (d) is localised in the negative direction. Both the position-time and momentum–time curves are almost sinusoidal.
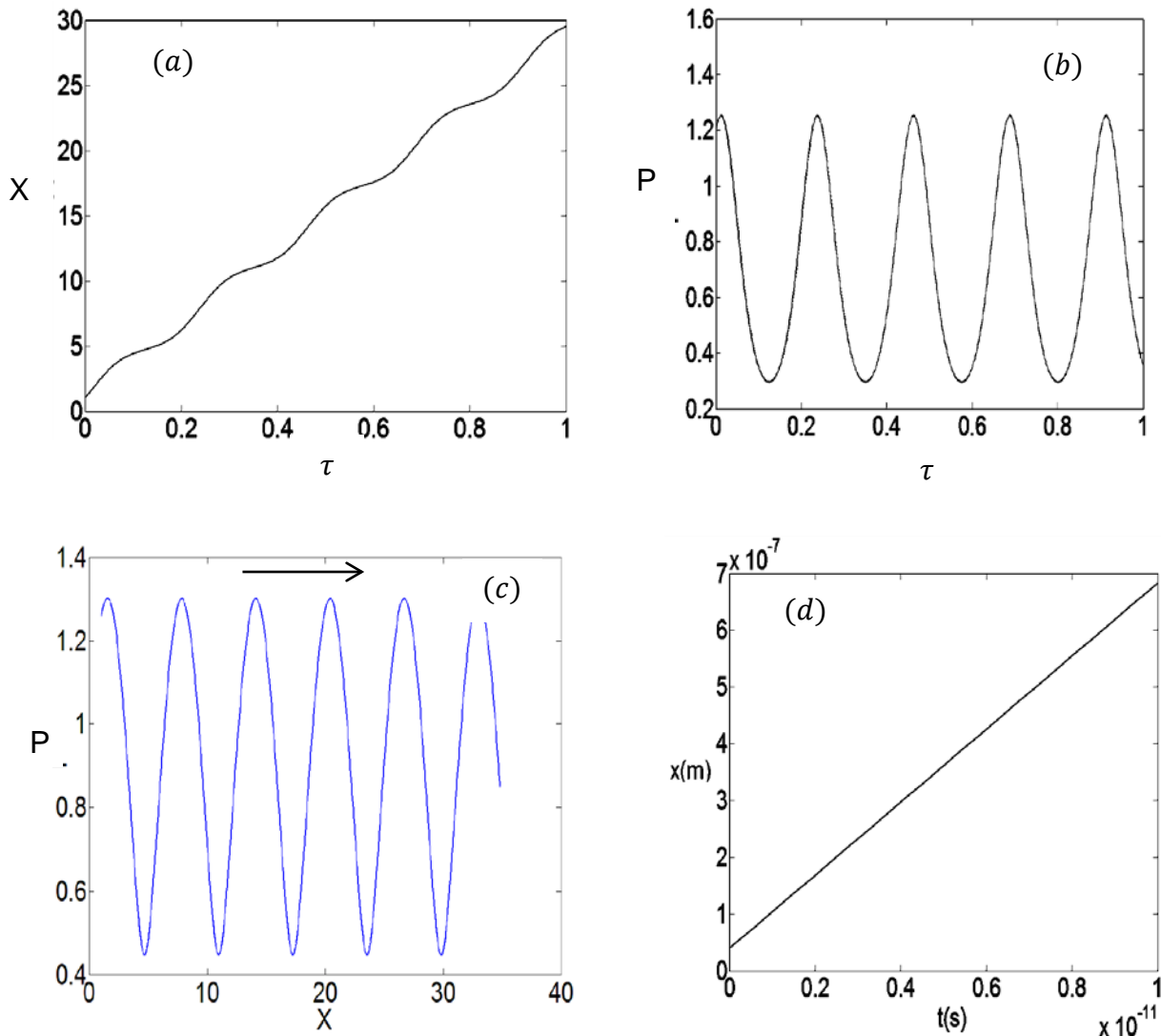
Figure 3.13: Paths of electron by choosing an initial value from the phase portrait. (a) is the position, X against the time, τ which is almost a linear curve in the positive direction. (b) is momentum, P against time, τ (c) is the momentum, P against position, X. The paths of electron in the SL for this unbounded trajectory show that the electron is moving in the positive direction (blue) and initial value (X, P) is (1.00,1.25). (d) is the electron trajectory $x(t)$.

The initial point, in Fig. 3.13 is (1.00,1.25), (a) is the position against the time which is a linear curve. (b) shows a sinusoidal curve for momentum against time. (c), which is momentum against position, is a sinusoidal curve moving in the positive

54

direction. The paths of the electron in the SL for this unbounded trajectory show that the electron is moving in the positive direction, and the $x(t)$ trajectory in (d) is a linear curve moving in the positive direction.
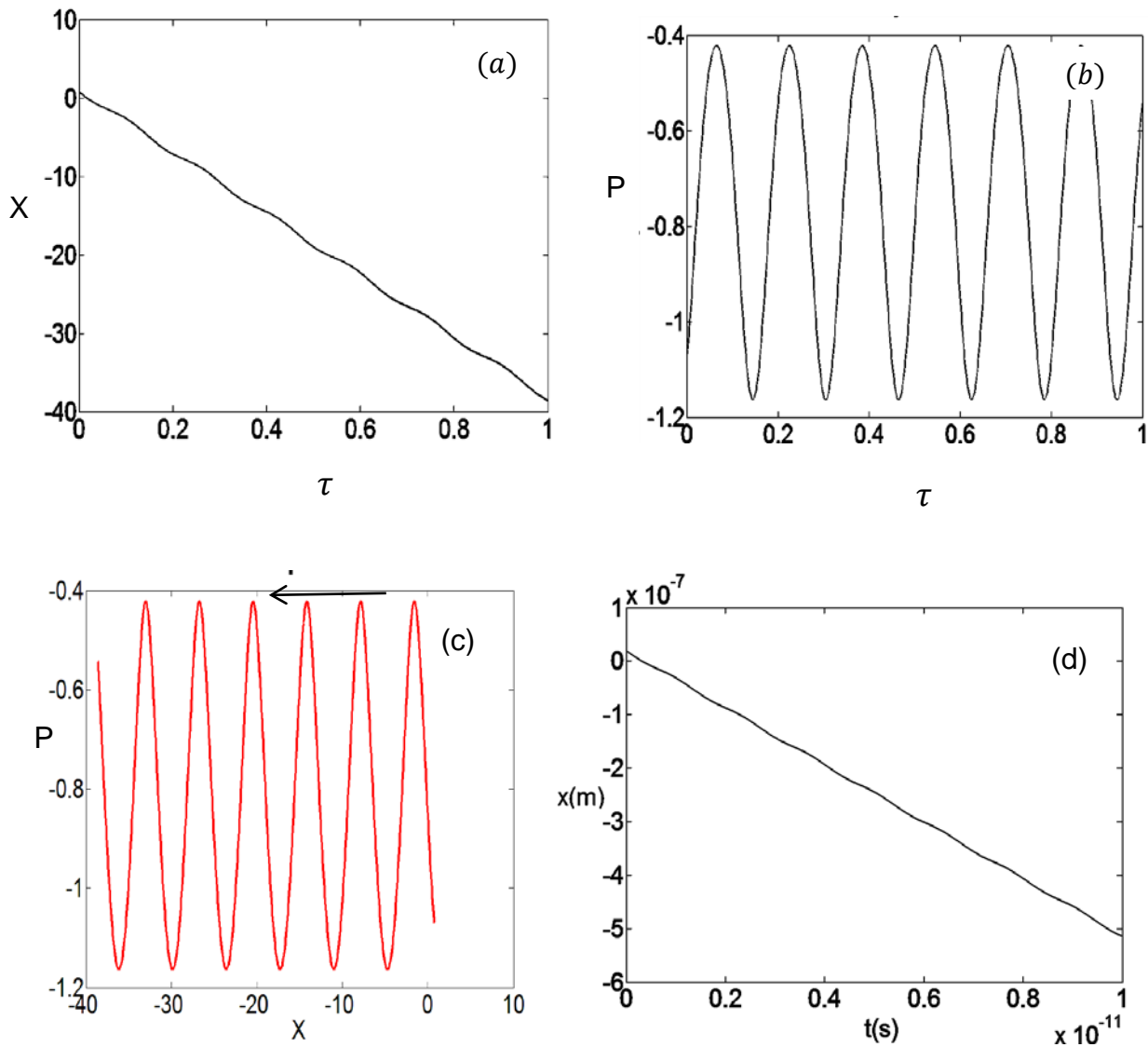

Figure 3.14: Paths of electron by choosing an initial value from the phase portrait. (a) is the position, X against the time, τ (b) is the momentum, P against the time, τ; and (c) is the momentum, P in relation to the position, X. The paths of the electron in the SL indicate that the electron is moving in the negative direction, and the initial value (X, P) is (0.5, 1.10). (d) is the $x(t)$ trajectory.

When the initial value, in the Fig. 3.14 is (0.5,1.10), (a) the position against the time is a linear curve in the negative x-direction. (b) shows a sinusoidal curve for the

momentum against the time while (c) is the momentum versus position whose unlocalised trajectory is moving in the opposite direction. The paths of the electron in the SLs for this unbounded trajectory show that the electron is moving in the negative direction and the $x(t)$ trajectory in (d) shows a linear curve in the negative direction.

We were able to show that we have the localised electron and the unlocalised (unbounded) trajectories moving in both the positive and the negative directions. For different initial values on the phase portrait, we observed the path of the electron as it moved in both the positive and the negative directions. The separatrix separates the types of phase trajectories, so we could distinctly see the electron trajectory characterised the spreading of the charge transport in the SL. In this region, the electron is trapped in the well, and is moving to and fro in the well with the velocity of acoustic wave. The phase trajectories are moving in both the positive and negative directions, as shown in Figs. 3.11 - 3.14, for the different initial states in the phase portrait.

3.5 Phase portrait for *U* close to maximum drift velocity

As the wave amplitude of acoustic wave , U increases and the peak is approached in the Fig. 3.6, the unbounded trajectories begin to disappear. The phase trajectories that are close to the transition are localised, all unbounded trajectories shrink away, and we have localised trajectories embracing several centres. At this transition, we obtain a trajectory that encircles several closed ellipses and the unbounded trajectory disappears completely.
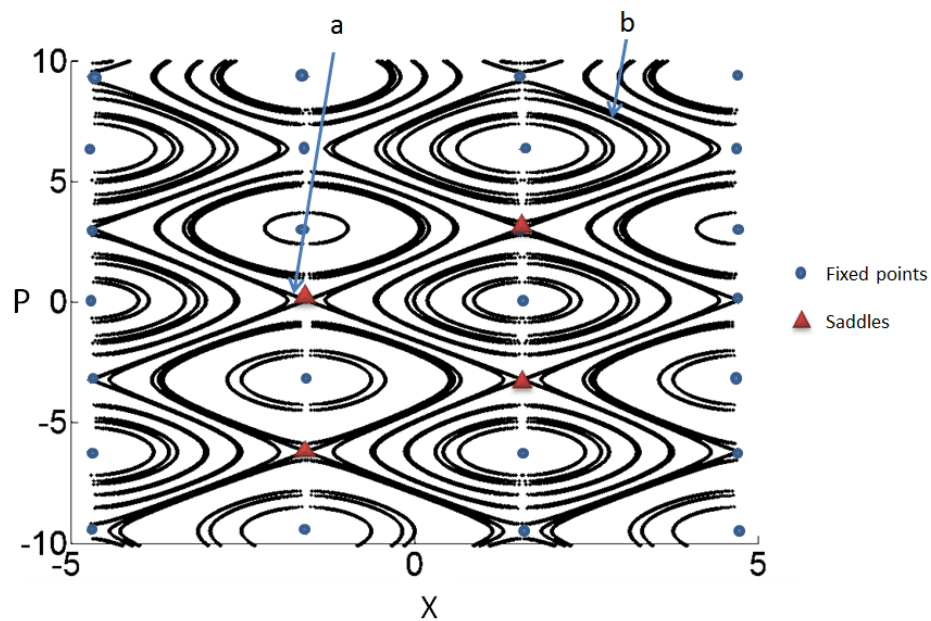
Figure 3.15: Relation of momentum of the electron against the position, the phase portrait of the system close to the transition when wave amplitude, $U = 4meV$.

Fig. 3.15 shows the phase portrait when $U = 4meV$, the unbounded trajectories are disappearing and the few that remain are spiralling down. The separatrix *arrowed* (a) connects the saddle, and the localised trajectory encircling several centres is *arrowed* (b). Also, we looked at the path of the electron by taking some initial points in the phase portrait for U very close to the maximum drift velocity. The electron path when the initial value is $(-3.8, 3.0)$ is shown in Fig. 3.16.
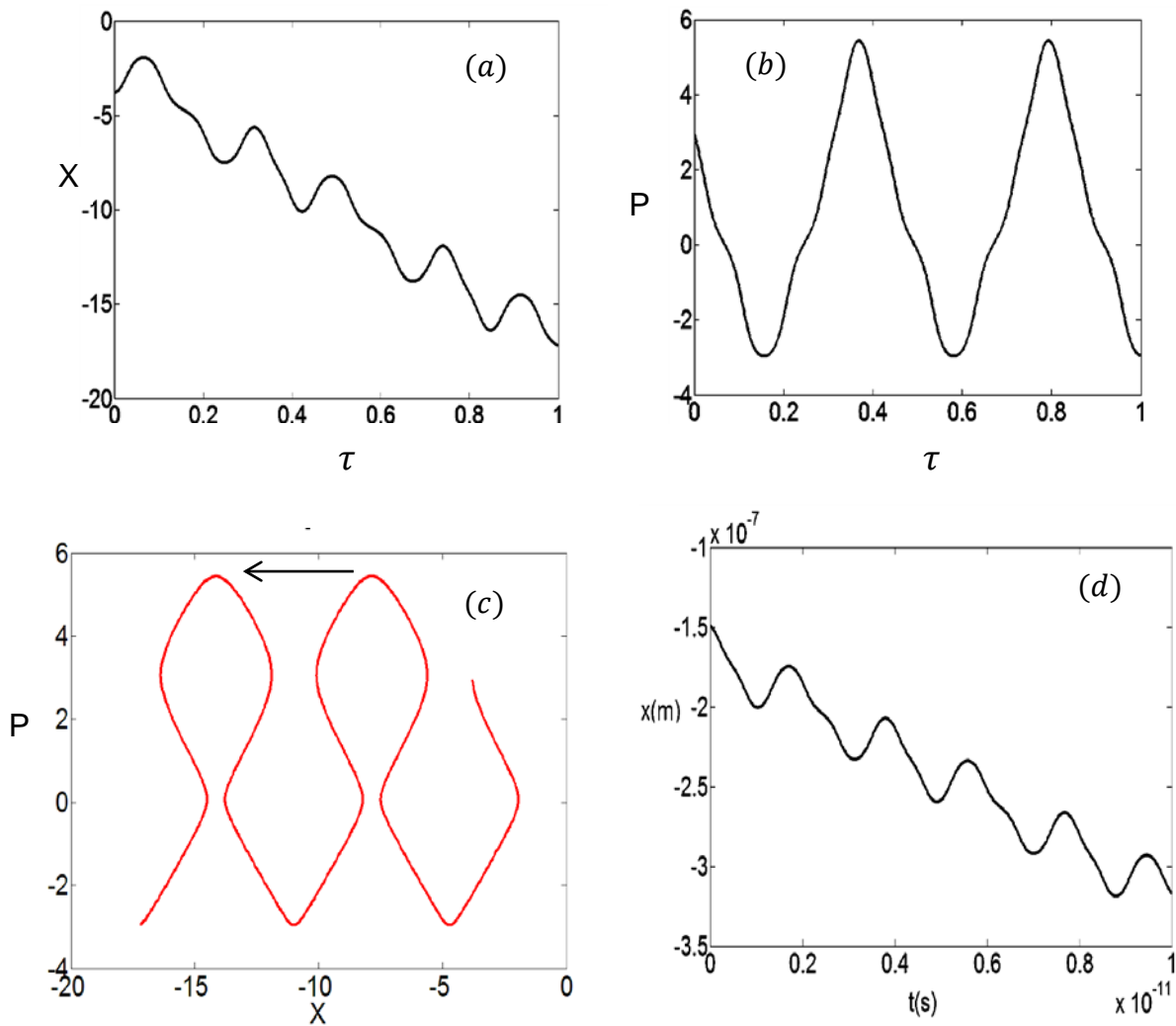
Figure 3.16: Paths of the electron in phase space. (a) is the position, X against the time, τ the graph is meandering down. (b) is the momentum, P against the time, τ (c) is the momentum, P against the position, X the twisting trajectory is towards the negative direction. The paths of the electron in the SL show that the electron is moving in an opposite direction (*red online*). (d) is the electron trajectory when $U = 4meV$ at the initial value of $(-3.8, 3.0)$.

In Fig. 3.16, (a) is the position against the time, and where the curve is meandering down in the negative direction. (b) is the momentum against the time, and the curve is sinusoidal. (c) relates the momentum with the position as the phase trajectory is moving toward the opposite direction. The trajectory is moving in an opposite direction in the phase space. The electron trajectory, $x(t)$, in (d) shows that the electron is moving in the negative direction as the curve meanders down the slope.

With the increase in the wave amplitude applied, the electron is no longer trapped in the potential well.
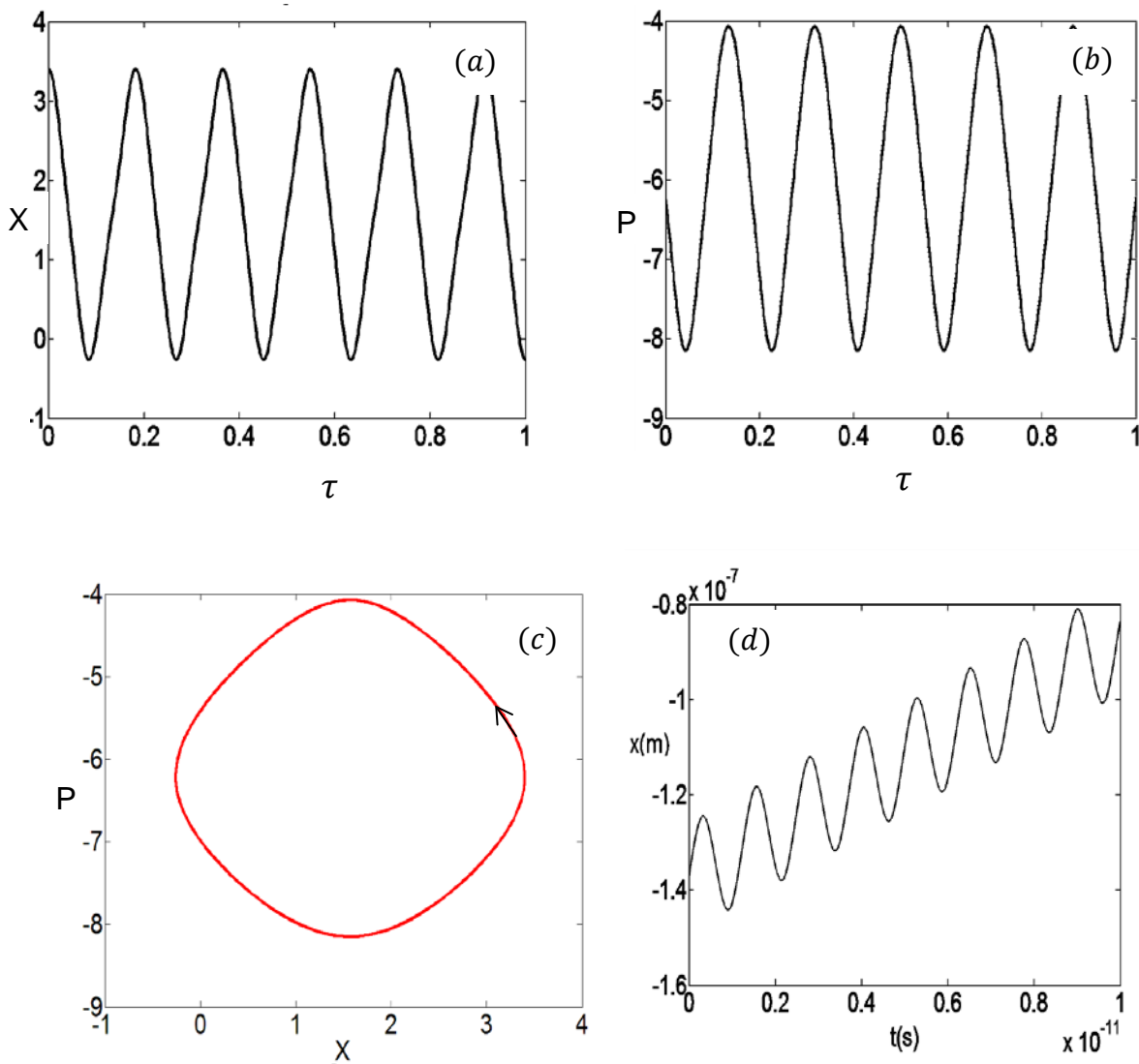

Figure 3.17: Paths of the electron when the initial value (X, P) of the phase plane is (3.5,-6.2) on the phase portrait. (a) is the position, X against the time, τ (in seconds) (b) is the momentum, P against the time, τ (c) is the momentum, P against the position X .The electron path in this region indicates that some of the localised electrons moves in the negative direction about the transition region.

In Fig. 3.17, the initial point is (3.5,-6.2) from Fig.3.15, and the electron paths are localised and move in an anticlockwise direction. In this region, the electron no longer dragged in the SL. (a) is the position against the time, and the curve is sinusoidal. (b) gives the momentum-time depedence which is also sinusoidal. (c) shows the localised

59

trajectory moving in an anticlockwise direction for the momentum-position curve. The electron trajectory, $x(t)$ in Fig.3.17(d) shows a sinusoidal curve in the negative region.
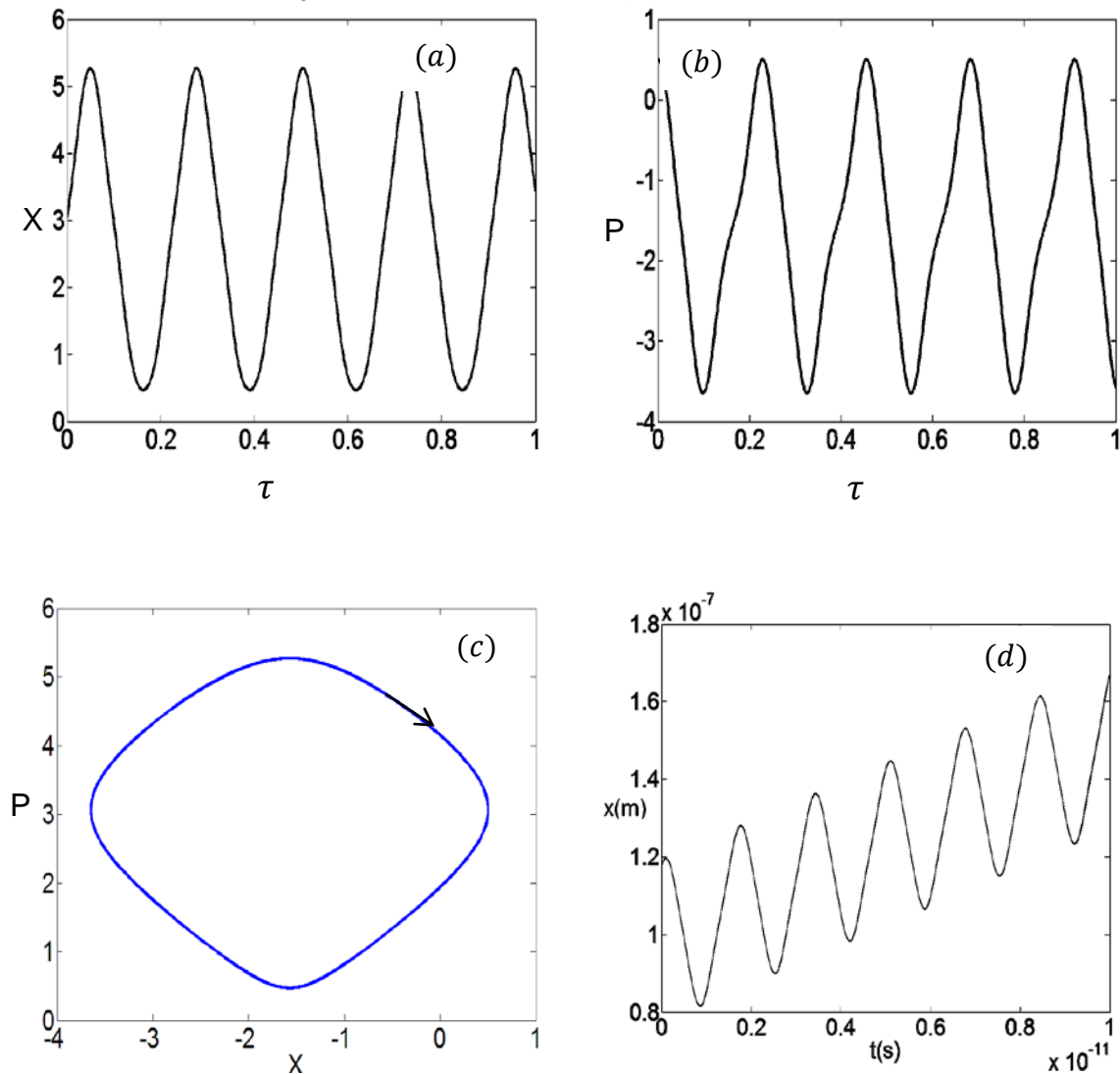

Figure 3.18: Paths of the electron for the phase plane initial value (X, P) of $(3.0,0.5)$ on the phase portrait. (a) is the position, X against the time, τ (b) is the momentum, P against the time, τ, and (c) is the momentum, P against the position X. The electron path indicates that the electron is moving in the positive direction and is localised.

The figure shows the paths of electron for the phase space with the initial value (X, P) of $(3.0,0.5)$ on the phase portrait of Fig. 3.15. Fig. 3.18 (a) is the position against the time, and is sinusoidal. (b) describes a sinusoidal curve for the momentum against the time, (c) is the momentum versus the position, and the electron path indicates that

the curve is localised and is moving in the clockwise direction. (d) is the electron trajectory , $x(t)$. The phase trajectory of the electron is localised and is moving in the clockwise direction.

In this region, which corresponds to the maximum of the drift velocity as shown in Fig. 3.6, the phase portrait showed that the spiral trajectory observed encircles several closed ellipses that are localized trajectories. In real space, the electron is no longer trapped within the acoustic wave; it can reach the edge of the first minizone, and the trajectories can traverse several minizones. When the drift velocity is at maximum, the electron reaches the Brillouin zone edge and the electron Bragg reflects, and then Bloch oscillates. The localised electron undergoes Bloch-like oscillations; this suppresses transport, and the region of negative differential velocity exists, thus inducing charge in the system.

3.6 Phase portrait for large U

After the peak, when $U \geq 7meV$, there are localised phase trajectories that encompass several centres and unlocalised ones that meander down, as shown in Fig. 3.18. This is the phase portrait when $U = 7meV$. The separatrix, *arrowed (a)*, connects the saddle. The localised phase trajectory is *marked (b)*

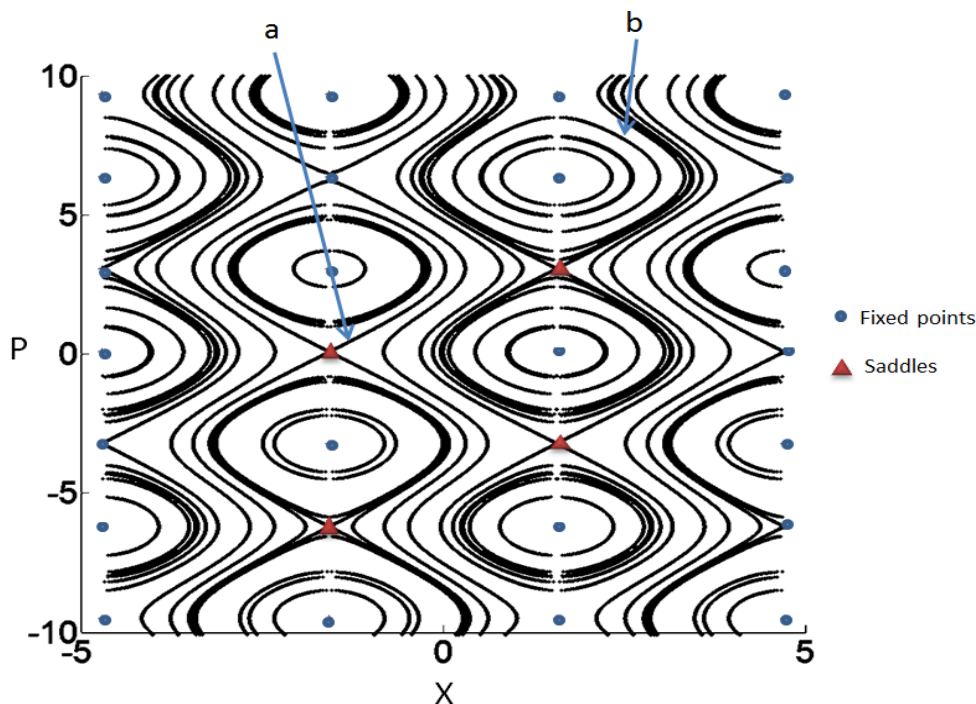Figure 3.19: Momentum of the electron against its position to describe the phase trajectory of the system after the peak when wave amplitude, $U = 7meV$. Shown in the figure is the separatrix (*arrowed (a)*) that connects the saddle. The localised trajectory is *arrowed (b)*.

Shown in Fig.3.19 are the fixed points, and the separatrix connects the saddle. In real space the electron trajectories are moving toward the negative direction, which means that the electron moves in the negative direction. To understand the paths of the electron we find the phase trajectory at some initial points in the phase portrait. In Fig. 3.20, the initial point taken on the phase portrait of Fig. 3.19 is $(-4.0,10.0)$.
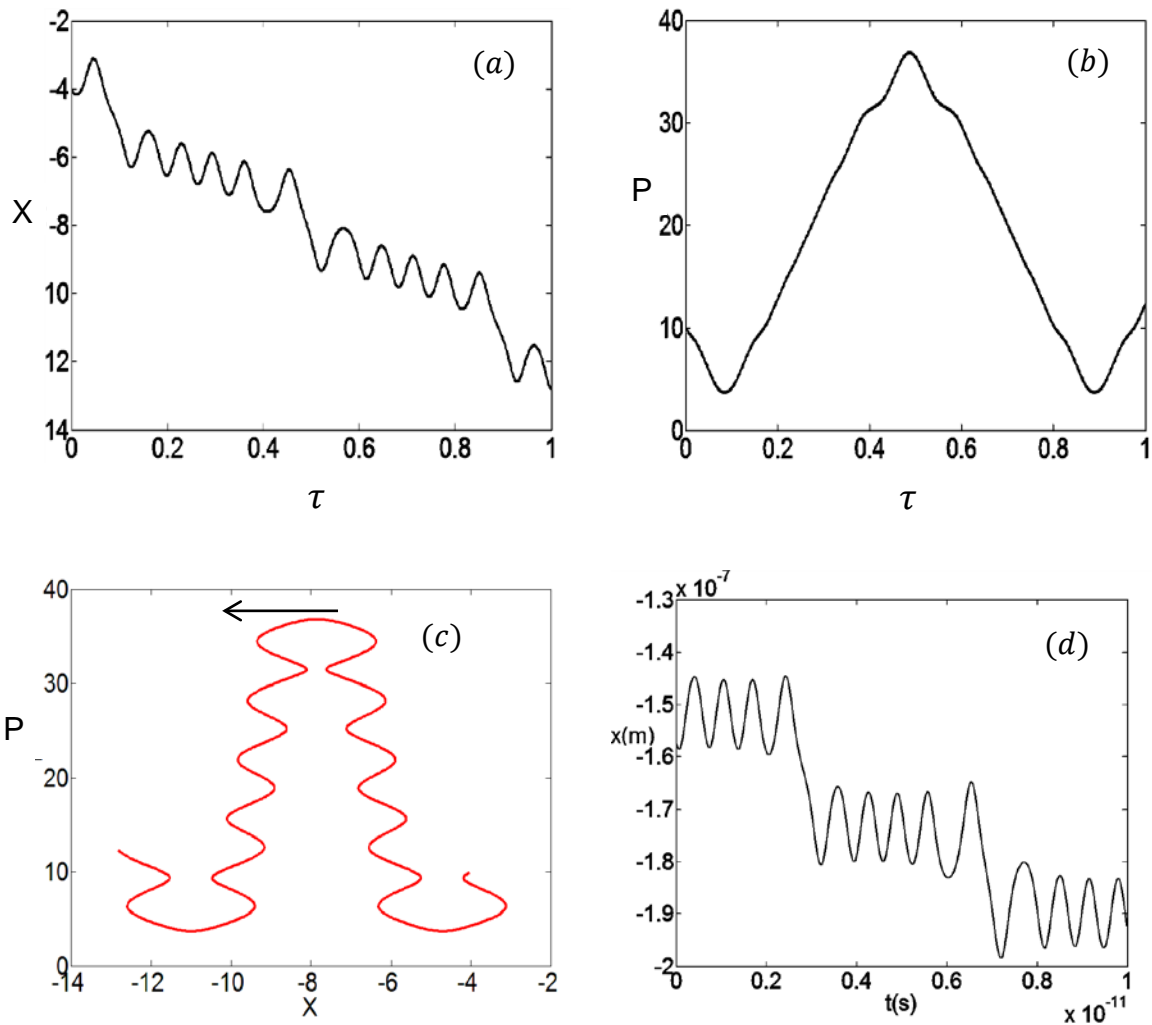
Figure 3.20: Paths of the electron when the initial value (X, P) on the phase portrait is $(-4.0, 10.0)$. (a) is the position, X against the time, τ (b) is the momentum, P against the time, τ while (c) is the momentum, P against the position X. The electron is moving in the negative direction. (d) is the electron trajectory, $x(t)$ initially at (-4.0, 10.0).

The initial value, in Fig. 3.20 is $(-4.0, 10.0)$, (a) is the position, X against the time, τ and the graph is spiralling down. (b) is the momentum against time, the curve is sinusoidal but the period is quite large. (c) is the momentum versus the position, and the phase trajectory is meandering up and down towards the negative direction. The path of the electron is in the negative direction, and the $x(t)$ trajectory in (d) shows that the electron trajectory is in the negative direction as well.
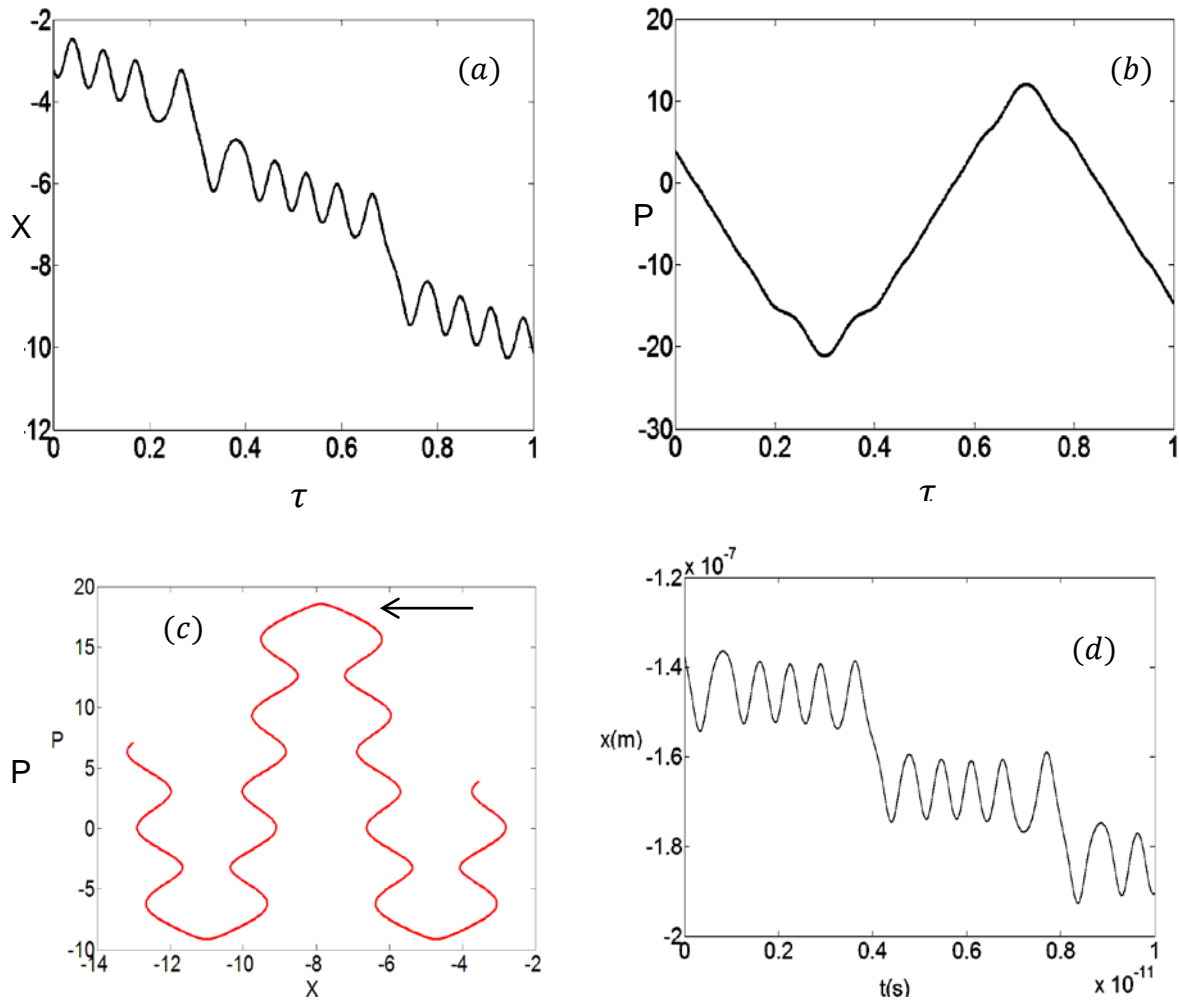
Figure 3.21: Paths of the electron with initial value (X, P) on the phase portrait of $(-3.5, 4.0)$. (a) is the position, X against the time, τ (b) is the momentum, P against the time, τ (c) is the momentum, P against the position, X. The phase trajectory is in the negative direction. *(d)* is the electron trajectory, which is spiralling down.

The initial point in Fig. 3.21 is $(-3.5, 4.0)$. (a) describes the position against the time, and the curve is meandering down. (b) is the momentum versus the time, and the period of the sinusoidal curve is very large. (c) gives the momentum in relation to the position, and the path of the electron in the phase space is a spiral trajectory moving in the (opposite) negative direction. The $x(t)$ trajectory at (d) shows that the electron trajectory is spiralling down in the negative region.
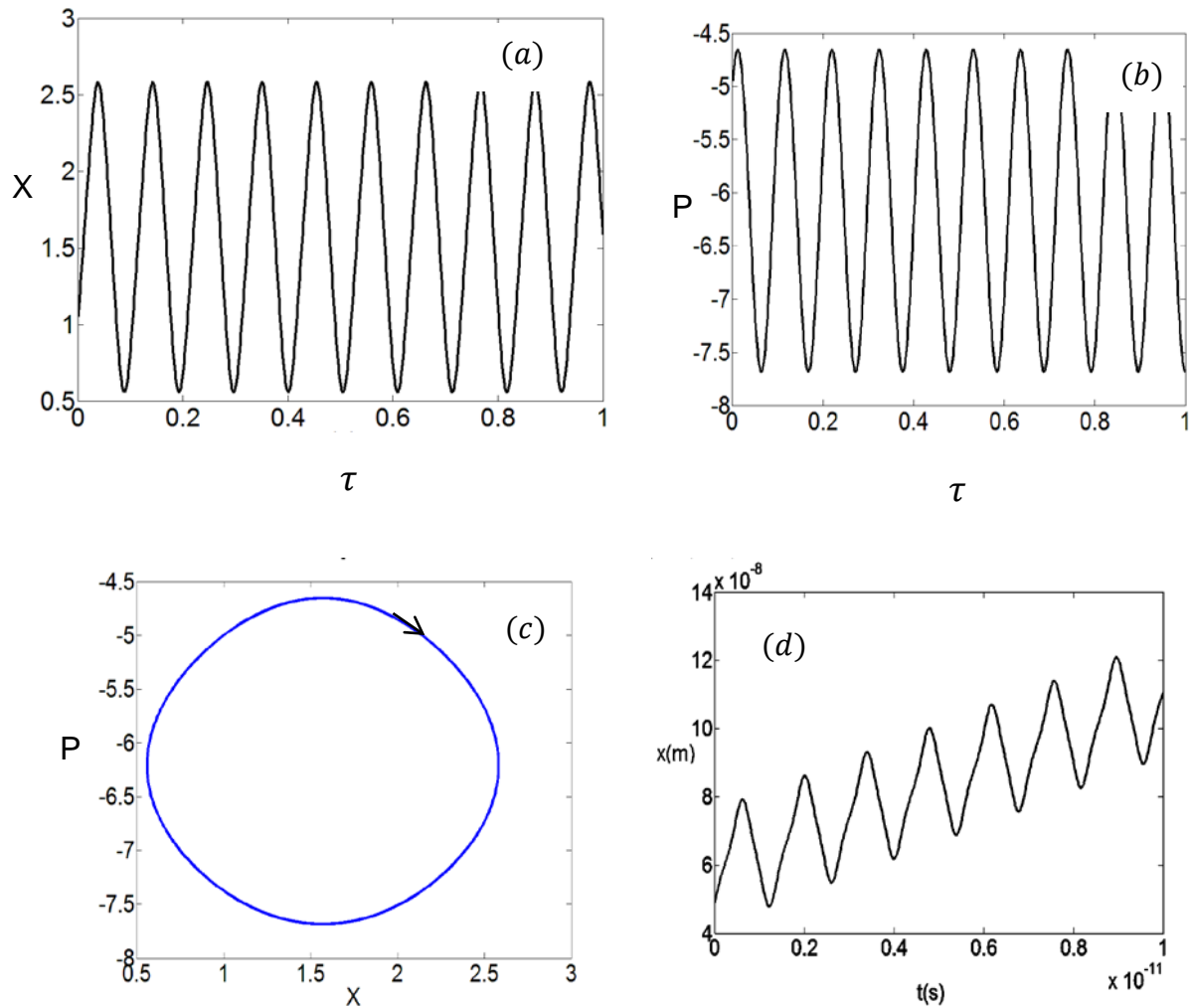
Figure 3.22: Paths of the electron for initial value (X, P) on the phase portrait at (1.2,-5.2). (a) is the position X against the time τ. (b) is the momentum P against the time τ, and (c) is the momentum P against the position X. The electron path in this region indicates that some of the phase trajectory is localised in the clockwise direction.

The initial point taken in Fig. 3.22 is $(1.2, -5.2)$. (a) is the position against the time, and the curve is sinusoidal. (b) is the sinusoidal curve for momentum versus time. (c) describes the curve of the momentum against the position; the phase trajectory is localised and moving in the clockwise direction. The $x(t)$ trajectory at (d), shows that the electron trajectory is sinusoidal with a small period. In real space, this corresponds to the sinusoidal oscillations; but moving in the positive x −direction, it actually means that the electron trajectory is in the positive direction. The oscillations are caused by the instability of the space charge in the SL due to the Bragg reflection of electrons in the lowest wide miniband.

3.7 Phase portrait far beyond the peak

Fig.3.23 shows the phase portrait for an acoustically driven SL where $U = 10meV$ far beyond the peak. The separatix connects the saddles and the localised trajectories encompass several ellipses and centres.
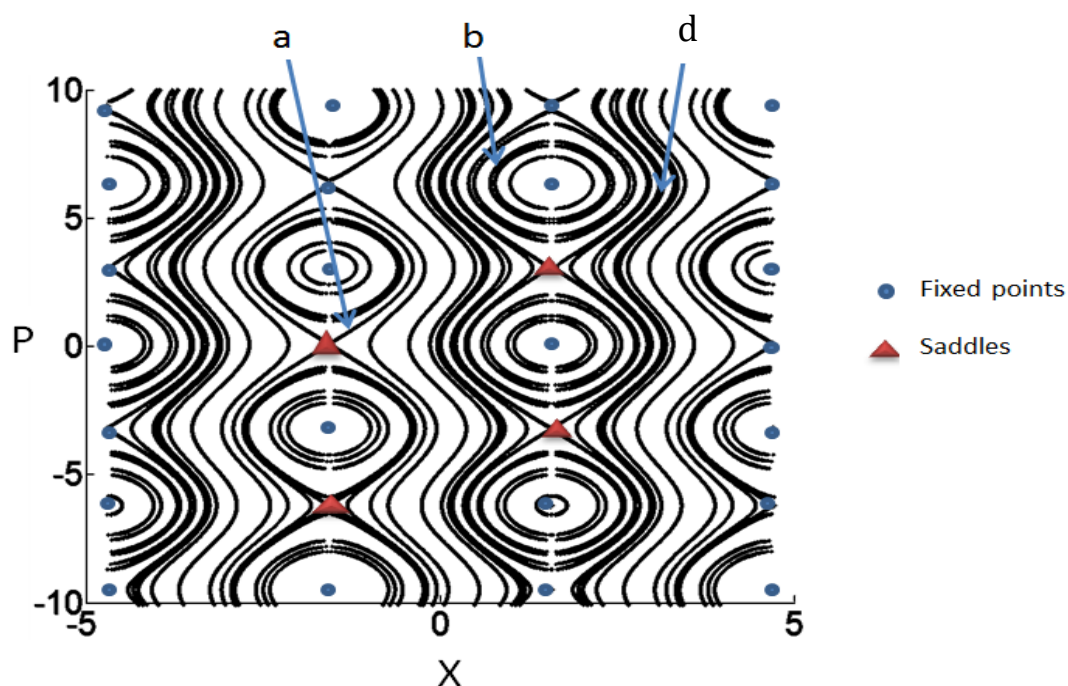

Figure 3.23: Momentum of the electron against the position describing the phase portrait of the system far beyond the peak when wave amplitude $U = 10meV$. The separatrix, *arrowed* (a), connects the saddle. The localised phase trajectory is *arrowed* (b), and the unbounded trajectory is *marked* (d) which is parallel to the vertical axis.

To explain the phase trajectory, we take some points as the initial points on the phase portrait to examine the electron's path.
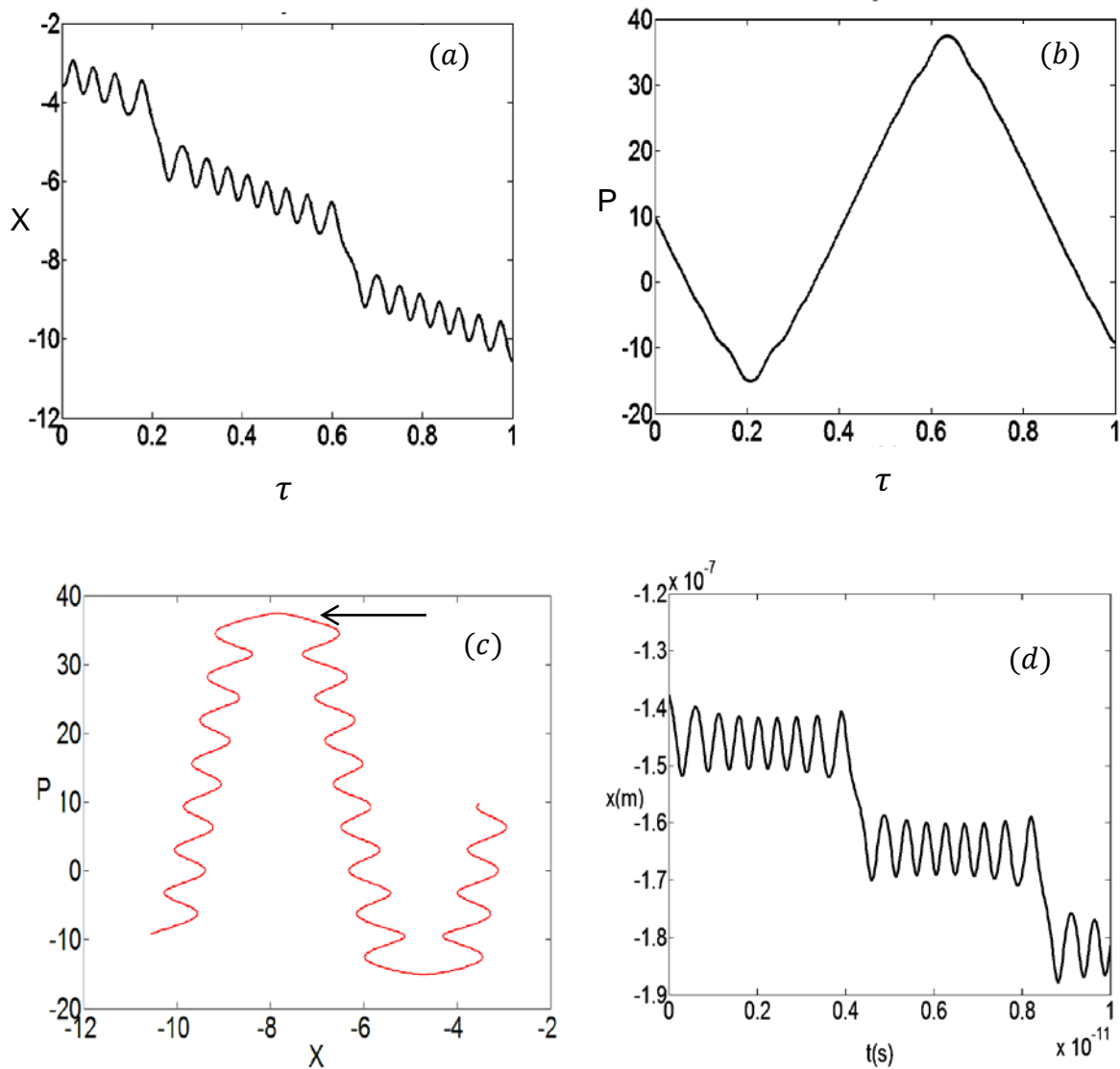
Figure 3.24: Paths of the electron for an initial value (X, P) on the phase portrait of (-3.5,10.0). (a) is the position, X against the time, τ (b) is the momentum, P against the time,τ (c) is the momentum, P against the position X showing that the phase trajectory is moving in the opposite direction. This show that the electron is moving in the negative direction in the SL. (d) is electron trajectory for the intial point.

In Fig. 3.24, the initial point is $(-3.5,10.0)$. *(a)* is the position relating to the time, and the curve is meandering down into the negative position. (b) describes the momentum versus time curve with very large period for the sinusoidal-like curve. (c) is the momentum against the position, and the phase trajectory is meandering up and down toward the (opposite) negative direction. The paths of the electron in the SL for this spiral trajectory show a trajectory moving in the negative direction and, the $x(t)$ trajectory at *(d)* shows the sinusoidal curve in the negative region.
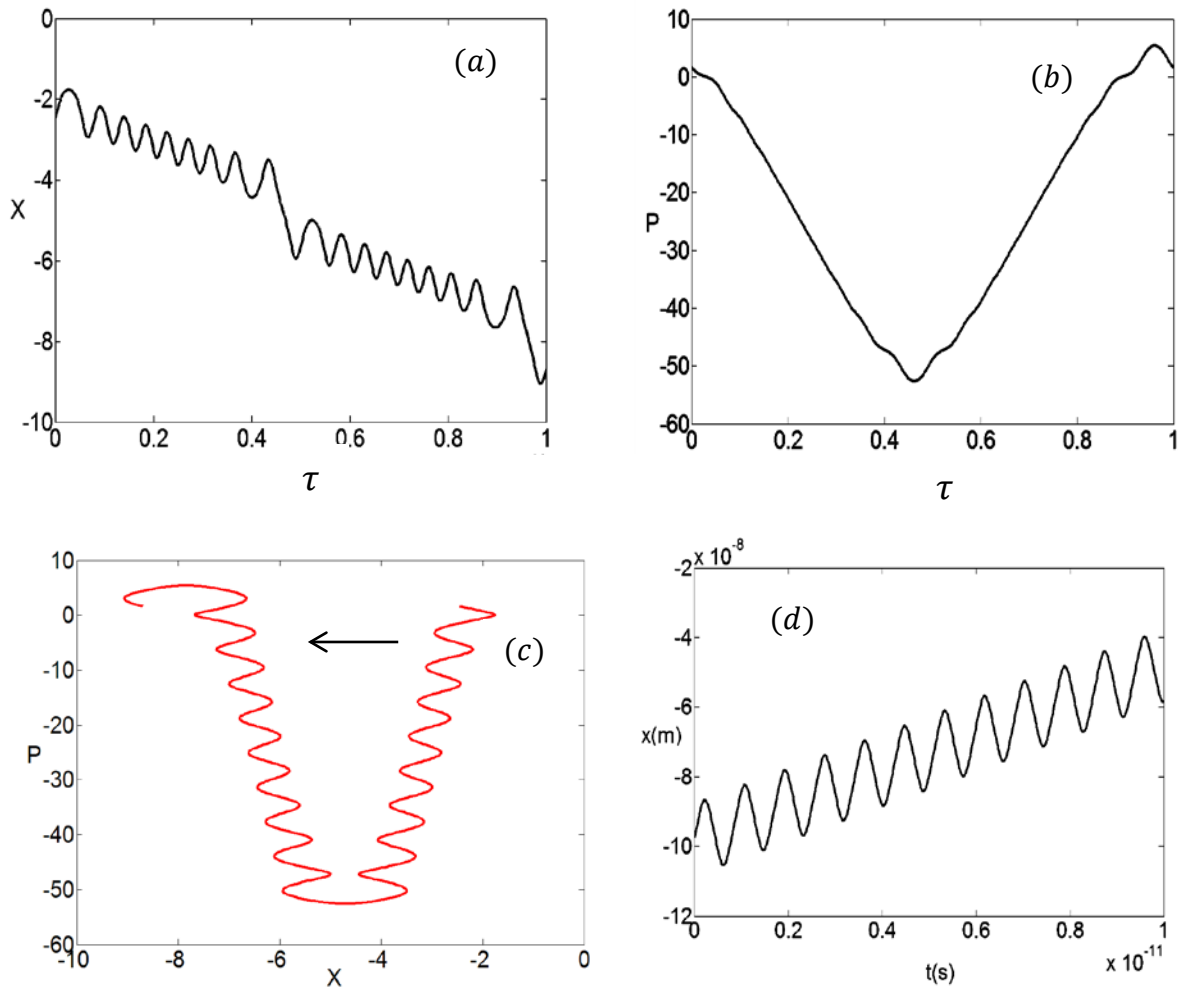
Figure 3.25: Paths of the electron, when the initial value (X, P) on the phase portrait is (-2.5,1.52). (a) is the position, X against the time, τ (b) is the momentum, P against the time, τ (c) is the momentum, P against the position X. The phase trajectory is in the negative direction. The paths of the electron in the superlattices indicate that the electron is moving in the opposite direction.

In Fig. 3.25 the initial point was chosen to be ($-2.5,1.52$). (a) is the position against the time curve, which is twisting down. (b) describes the momentum against the time, producing a sinusiodal curve of a large period. (c) is the momentum against the position, which gives the phase trajectory maendering up and down in the negative direction. The paths of the electron in the SL for this spiral trajectory are moving in the negative direction. The $x(t)$ trajectory in Fig. 3.25 (d) shows that the electron is moving in the negative direction.
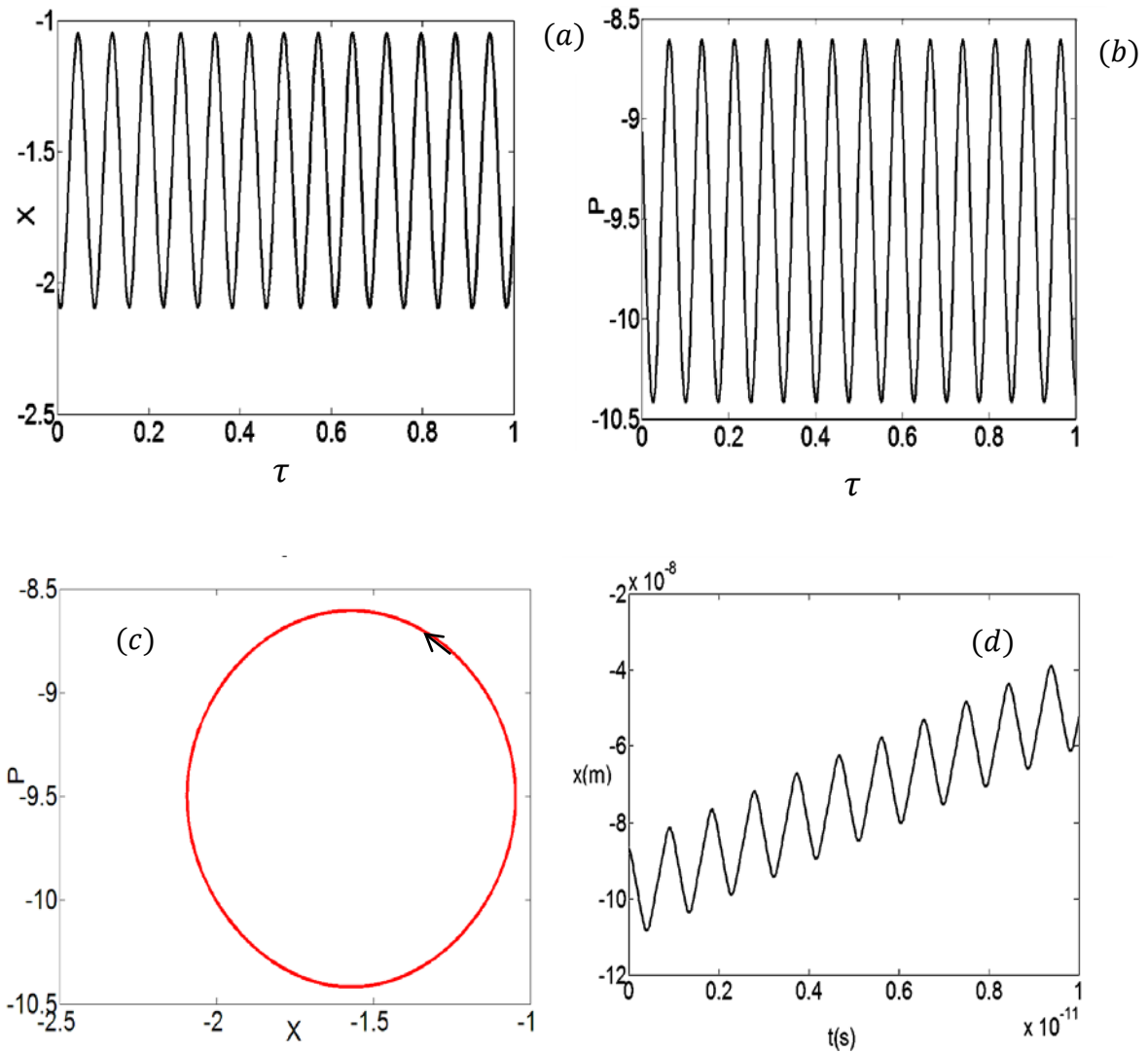
Figure 3.26: Paths of the electron with an initial value (X, P) on the phase portrait of (-2.2,-9.1). (a) is the position X against the time τ. (b) is the momentum P against the time τ, and (c) is the momentum P against the position X. The localized trajectory is moving in the anticlockwise direction, and the $x(t)$ trajectory in Fig. 3.26 (d) shows that the electron is moving in the negative direction.

In Fig. 3.26, the initial point is $(-2.2, -9.1)$. (a) gives the position against the time, which is a sinusoidal curve. (b) describes the momentum versus the time, which is also a sinusiodal curve. (c) is the momentum against the position, which produces a localised trajectory that moves in the anticlowise direction. (d) is the electron trajectory $x(t)$, showing Bloch-like oscillations with jumps in the negative direction. The paths of the electron in the SL for this localised trajectory are moving in the negative direction.

Conclusion

The trajectory of the electron in a SL driven by an acoustic wave depends on the value of the wave amplitude. We observed a sharp transition from the graph of average drift velocity against wave amplitude in Fig. 3.2. This transition is at the peak of the average drift velocity for a certain value of wave amplitude. The wave amplitude was minimal before the peak. The $\langle v_d \rangle - U$ curve was linear; and thereafter at the peak and after the peak, the average drift dropped as we increased the value of the wave amplitude. We characterised these transitions by building a phase portrait. The motion was observed by attaching a frame of reference to the system and measuring its change in position relative to the reference frame.

There are three distinct types of phase trajectories: the localized and unlocalised (unbounded) trajectories, and the trajectory that meanders up and down and encircles several ellipses and centres. For a small acoustic wave amplitude, before the transition two of the types of trajectories were observed, the localised and the unbounded trajectories. The electron trajectory in this region in real space is regular sinusoidal oscillations, the motion is periodic, and the electron moves with the velocity of the acoustic wave applied. As the wave amplitude is increased, the unbounded trajectory shirks away. We observed only the localized trajectories that encircle several closed ellipses. The electrons have more energy to propagate in the SL. When the wave amplitude is increased further, far beyond the transition the trajectories meander up and down and encircle the localised trajectories. The electron trajectory moves in the negative $x - direction$. There is a velocity drop due to motion in the opposite direction. This phenomenon is negative differential velocity, which is observed in a SL. The acoustic wave force induces Bloch-like oscillations, and we have high-frequency oscillations interrupted by jumps, as shown in Fig. 3.24 (d).

The momentum-position curve shows the localisation of the electron. We observed that the paths of the electron are localized in all the transitions, and the electrons are moving in positive and negative directions. These trajectories depend on the value of the wave amplitude. There is a qualitative change in the dynamics that occurs when the system parameter varies. The phase trajectory is different for the varied value of the wave amplitude; therefore transitions exist between the distinct dynamical regimes.

Chapter 4

Effect of static electric field on acoustically driven semiconductor superlattices

4.1 Introduction

In this chapter, we consider the effect of applying an electric field to an acoustically driven SL. In the previous chapter we demonstrated that when an acoustic wave alone is applied along the axis of SL, it induces charge current. The acoustic wave induces high-frequency single electron dynamics in the SL [33, 40]. When a high electric field is applied along the axis of SL, the wavefunction will be localised in each quantum well. This is called Wannier-Stark (WS) localization and the interband transitions are restricted to these regions [107-109]. The electron is subjected to a periodic potential proportional to the strength of the electric field. The constant electric applied to SL induces an oscillatory electronic motion in k space which is called Bloch oscillation [21,110]. In order for Bloch oscillations to occur, the field must be strong and the crystal should have a large period, which we found in the SL. The larger lattice period in the SL will allow the electron to traverse a whole minizone even if scattering occurs [26]. In ordinary crystals, electrons cannot get to the boundary zone because of the limited time of electron collisions, which is about 10^{-14} seconds.

In the following section we shall consider a system where we jointly apply static electric field and acoustic wave along the axis of SL. In particular, we will theoretically analysis the dynamics of electron, when electric field and acoustic wave are jointly applied to the SL. We will examine the phase portrait to understand the effect of the electric field on the trajectories of an electron in an acoustically driven SL.

4.2   Model of electron dynamics

Within the tight-binding approximation, the dispersion, that is the relation between the kinetic energy and the crystal momentum for an electron along the x-axis for the miniband as given by *equation* (3.2). For this system, when the acoustic wave and electric field are applied along the axis of the SL with potential energy eFx for the static electric field, the Hamiltonian is

$$H(x, p_x) = \frac{\Delta}{2}\left[1 - \cos\frac{p_x d}{\hbar}\right] - U \sin[k_s(x) - w_s t] + eFx .\qquad(4.1)$$

The semi-classical equations of electron motion for this system will then be Hamilton's equation described as

$$v_x = \frac{dx}{dt} = \frac{\partial H}{\partial p_x} = \frac{\Delta d}{2\hbar}\sin\frac{p_x d}{\hbar}\qquad(4.2)$$

$$\frac{dp_x}{dx} = -\frac{\partial H}{\partial x} = k_s U \cos[k_s(x) - w_s t] + eF\qquad(4.3)$$

The electron trajectories can be calculated by solving *equations* (4.2) and (4.3) numerically using 4th order Runge-Kutta algorithms. For simplicity we use the initial conditions $x = 0$ at $t = 0$, so that $p = 0$ and assume that there is no scattering.

4.3   Electron trajectory

Minibands in the SL allow electrons to perform terahertz-frequency Bloch-like oscillations when a high electric field is applied along the axis of the SL. In order to understand the effect of the electric field on the electron dynamics in the acoustically

driven SL, we considered the change of electron trajectories in the SL. To do this, we solved *equations* (4.2) and (4.3) numerically for different wave amplitudes and electric field values. The frequency of the acoustic wave was taken to be $w_s = v_s k_s = 4 \times 10^{11}$ rad s^{-1}. Since v_s, the speed of sound in GaAs, and is 5000 ms^{-1}, [33], $k_s = 8 \times 10^7 m^{-1}$. We will consider two extremes, low and high wave amplitudes, since these value correspond to the different dynamical regions in the previous chapter.
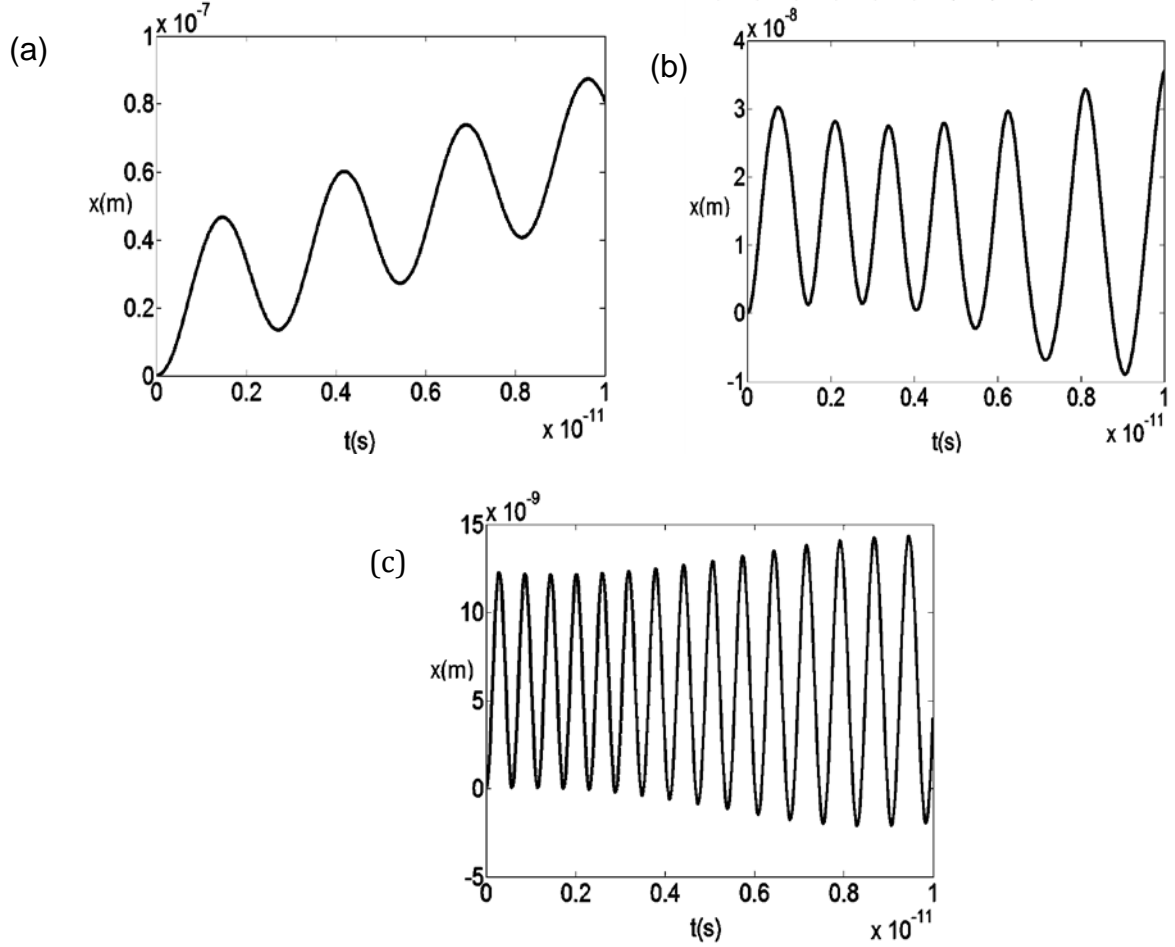

Figure 4.1: The electron trajectories $x(t)$ corresponding to $U = 1meV$ with (a) $F = 1 \times 10^2 Vm^{-1}$, (b) $F = 2 \times 10^5 Vm^{-1}$, (c) $F = 5 \times 10^5 Vm^{-1}$. Both the electric field and wave amplitude were applied together along the axis of the SL at the initial condition $x = 0, p = 0$.

Fig. 4.1 shows the electron trajectories starting from rest ($p_x(0) = x(0) = 0$) for wave amplitude $U = 1meV$. We consider the SL described in section 2.4 with parameters $\Delta = 7meV \ and \ d_{SL} = 12.5nm$. Fig.4.1 (a) shows the electron trajectory when the electric field is $F = 1 \times 10^2 Vm^{-1}$. In this case, we have the usual dragging

regime when the acoustic wave alone was applied along the axis of the SL. This is compared to Fig.3.2 in the previous chapter. Figure 4.1 (b) and (c) illustrate the electron trajectories when the electric field is increased to $2 \times 10^5 Vm^{-1}$ and $5 \times 10^5 Vm^{-1}$ respectively, showing that the drift decreases and the oscillations become more frequent.

Figs. 4.2 show the electron trajectories calculated for $U = 10meV$ and (a) is the electric field of $F = 1 \times 10^2 Vm^{-1}$. (b) is the electric field of $F = 2 \times 10^5 Vm^{-1}$ (c) is the electric field of $F = 5 \times 10^5 Vm^{-1}$.
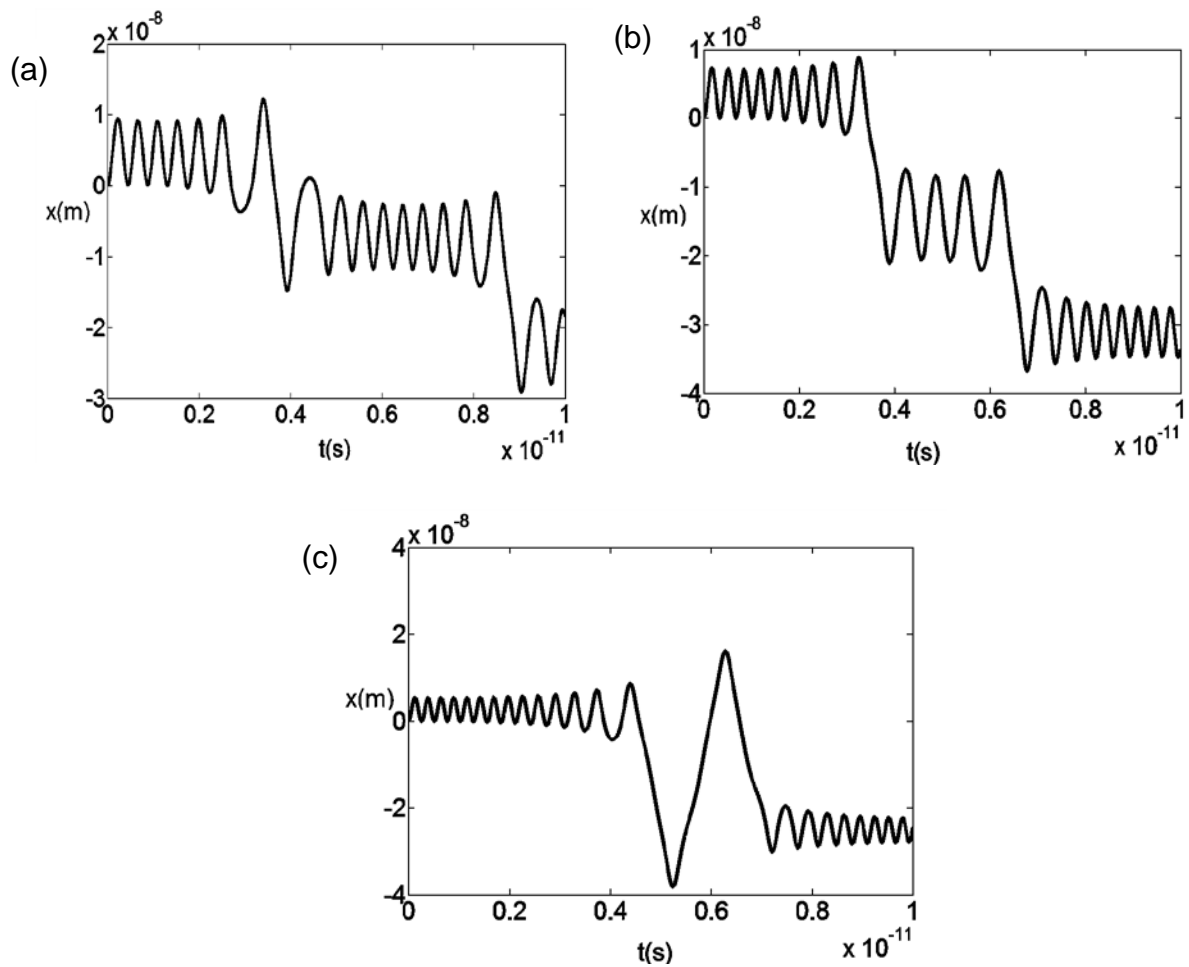

Figure 4.2: The electron trajectories $x(t)$ corresponding to $U = 10meV$ with (a) $F = 1 \times 10^2 Vm^{-1}$, (b) $F = 2 \times 10^5 Vm^{-1}$, (c) $F = 5 \times 10^5 Vm^{-1}$. Both the electric field and wave amplitude were applied together along the axis of the SL and the initial condition was taken as $x = 0, p = 0$. The Bloch oscillation bursts are separated by big jumps.

The trajectory shows high-frequency oscillations interrupted by jumps in the negative x direction as compared to Fig.3.4 in chapter three. These high-frequency fluctuations are Bloch-like oscillations driven by both the electric field and acoustic wave , and the jumps are due to the period when the force of the applied fields are too weak to cause the Bloch oscillations [33]. At very high electric field, the electron trajectory shows very high frequency of oscillations but with interrupted big jumps in the negative $x-$ direction. Therefore high-frequency oscillations are obtained when an electric field is applied to an acoustically driven SL. To gain insight into the electron's trajectory we use the phase portrait which will be discuss in section 4.5.

4.4   Drift velocity with colour map

To characterize the electron transport, we calculate the drift velocity of the electron using the Esaki-Tsu formula, *equation* (2.25). Fig. 4.3 shows the function $v_d(U)$ for different strength of electric fields, F.
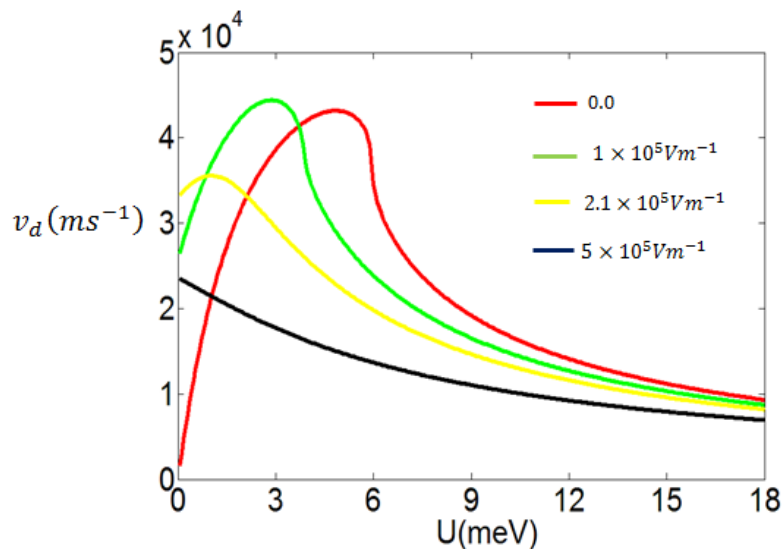

Figure 4.3: The dependence drift velocity on wave amplitude at different values of the static electric field. The red and green curves show the drift velocity calculated when the applied electric field is $F = 0.0$ and $F = 1 \times 10^5 Vm^{-1}$ respectively. The yellow and black curves are when $F = 2 \times 10^5 Vm^{-1}$ and $F = 5 \times 10^5 Vm^{-1}$ respectively. The initial condition is $x = 0$ and $p = 0$.

The red and green $v_d(U)$ curves, corresponding to $F = 0$ and $F = 1 \times 10^5 Vm^{-1}$ respectively, have similar peaks. When the electric field was increased to $F = 2 \times 10^5 Vm^{-1}$ (yellow curves), the drift velocity increases slightly before it falls with increasing U. The falls in drift velocity is due to the Bloch-like oscillations induced that caused the drift velocity to decrease. The black curves correspond to an electric field, $F = 5 \times 10^5 Vm^{-1}$. The drift velocity did not increase with increasing wave amplitude, but rather decreased. This is because there is localisation of the electron due to Bloch oscillation which has suppressed the transport.

To get deeper insight into the joint effect of electric field and acoustic wave we consider the colour map of v_d *(U, F)* in Fig. 4.4. The dashed line gives the maximum v_d *(U)* for different F.
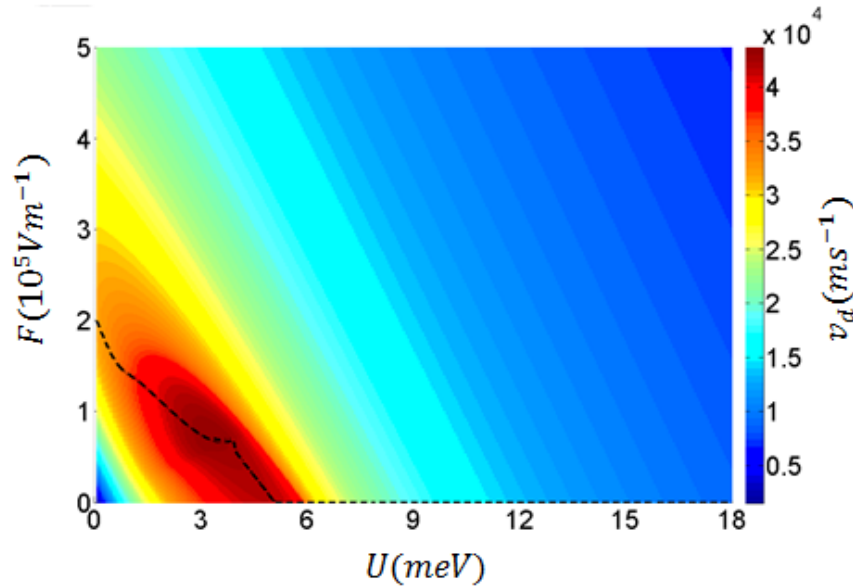

Figure 4.4: Colour map of v_d *(U, F)*: the dependence of the drift velocity on the combination of the applied electric field, F and wave amplitude, U with the initial condition of $x = 0$ and $p = 0$. The dashed line shows F_c against U.

The dash line shows the critical value of electric field F_c, the value of the field when the dynamical change occurred against the wave amplitude, U in Fig. 4.4. This can be calculated by finding the value of electric field when the drift velocity reaches its maximum. A critical value is the value of the field when the dynamical change occurred. In the previous chapter we find the critical value of the wave amplitude to equal approximately to the modified energy dispersion $E'(p_x)$ that is $E'(p_x) \approx U_c$.

The static electric field and acoustic wave jointly applied along the axis of SL produced an interesting result; the high drift velocity obtained implies a higher fundamental frequency of the current self-oscillations. Therefore the electric field and acoustic wave combined produced much higher frequencies. The red colour indicates high drift velocity and the blue colour shows the drop in the value of drift velocity in Fig.4.4. The minibands allow the electron to perform terahertz frequency Bloch oscillation when a strong electric field is applied to the axis of SLs. The Bloch oscillations cause the electron drift velocity to decrease as the electric field increases, and trigger frequency oscillations accompanied by the emission of electromagnetic radiation [111]. The acoustic wave controls miniband electron transport by creating complex terahertz electron dynamics in superlattices which produce high-frequency current oscillations. When an electric field and acoustic wave are applied together along the axis of a SL, the electron behaviour depends on the wave amplitude of the acoustic wave and the strength of the electric field. Increasing the wave amplitude and electric field generate a high-frequency current oscillation.

4.5 Phase portrait of electric field effect on acoustically driven superlattices

Knowing the equations of motion for the electron dynamics of the acoustically driven SL in the electric field, we analytically calculate and built the phase portrait to characterise the electron trajectory at each dynamical regime for different strength of wave amplitude and electric field applied along the axis of the SL.

$$\frac{dx'}{dt} \quad = \quad \frac{\Delta d}{2\hbar}\sin\frac{p_x d}{\hbar} - v_s \qquad\qquad (4.4)$$

$$\frac{dp}{dt} \quad = \quad kU\cos kx' + eF \qquad\qquad (4.5)$$

All the notations have the usual meaning, namely Δ is the miniband, d is the lattice constant, p_x is the momentum and the wave vector is k. To make the analysis more convenient we write the equations (4.4) and (4.5) in dimensionless form, using the following substitution and expressing $\tau = wt$, $\therefore d\tau = wdt$. Therefore, we have

$$\frac{dx'}{dt} = \frac{dx'}{d\tau}\frac{d\tau}{dt} \qquad\qquad \therefore \qquad\qquad \frac{dx'}{d\tau} = \frac{dx'}{dt}\frac{dt}{d\tau}$$

and

$$\frac{dp}{dt} = \frac{dp}{d\tau}\frac{d\tau}{dt} \qquad\qquad \therefore \qquad\qquad \frac{dp}{d\tau} = \frac{dp}{dt}\frac{dt}{d\tau}$$

We obtain dimensionless differential equations as follows

$$\frac{dx'}{d\tau} = \left(\frac{\Delta d}{2\hbar}\sin\frac{p_x d}{\hbar} - v_s\right)\frac{dt}{d\tau} \qquad \therefore \qquad k\frac{dx'}{d\tau} = \frac{\Delta d}{2\hbar v}\sin\frac{p_x d}{\hbar} - 1$$

$$\frac{dp}{d\tau} = (kU\cos kx' + eF)\frac{dt}{d\tau} \qquad \therefore \qquad \frac{dp}{d\tau} = \frac{kU}{\omega}\cos kx' + \frac{eF}{w}$$

if, we let $\quad \frac{\Delta d}{2\hbar v} = A$, $\qquad \frac{d}{\hbar}\frac{kU}{\omega} = B$, $\qquad P = \frac{p_x d}{\hbar} \qquad$ and $\qquad X = kx'$.

$$\frac{dX}{d\tau} = A\sin P - 1 \tag{4.6}$$

and

$$\frac{dP}{d\tau} = B\cos X + \frac{\omega_B}{\omega} \tag{4.7}$$

where

$$\omega_B = \frac{eFd}{\hbar} \qquad\text{and taking}\qquad \frac{\omega_B}{\omega} = c_2$$

To find the equations describing the phase trajectories we divide *equation* (4.7) by *equation* (4.6) and obtain

$$\frac{dP}{dX} = \frac{B\cos X + c_2}{A\sin P - 1}$$

$$(A \sin P - 1)dP = (B \cos X + c_2)\, dX \tag{4.8}$$

and integrating *equation* (4.8) gives

$$B \sin X + X c_2 = c_1 - A \cos P - P \tag{4.9}$$

Equation (4.9) is a transcendental equation and the solution can only be found numerically and the constant c_1 can be found from the initial condition.

To determine the fixed points, we equate the equations of motion of the electron in the SL to zero,

$$\frac{\Delta d}{2\hbar} \sin \frac{p_x d}{\hbar} - v_s = 0 \tag{4.10}$$

$$kU \cos kx' + eF = 0 \tag{4.11}$$

$$\therefore \qquad \sin \frac{p_x d}{\hbar} = \frac{2\hbar v_s}{\Delta d} \qquad \text{and} \qquad \cos kx' = -\frac{eF}{kU}$$

$$\text{Let} \quad \frac{p_x d}{\hbar} = p \quad \text{and} \quad kx' = x$$

Therefore, the fixed points are

$$p = (-1)^n \sin^{-1} \left(\frac{2\hbar v_s}{\Delta d} \right) + \pi n \tag{4.12}$$

$$n = 0, \pm 1, \pm 2.$$

$$x = \pm \cos^{-1} \left(-\frac{eF}{kU} \right) + 2\pi a \tag{4.13}$$

$$a = 0, \pm 1, \pm 2.$$

The fixed points (x, p) is classify according to the stability; in this system there are two types of fixed points: the centres and saddles as shown in Fig.4.5 where we take $U = 10 meV$ and $F = 5 \times 10^5 Vm^{-1}$. The fixed points will exist only when $B > c_2$.
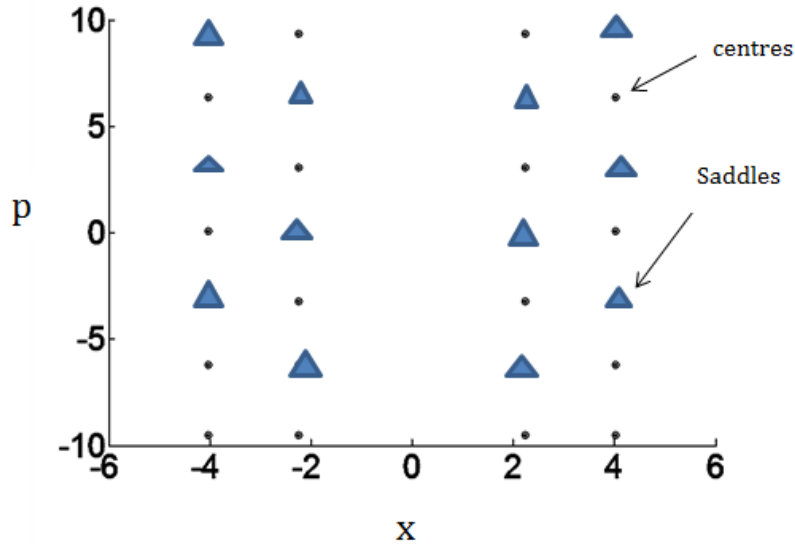
Figure 4.5: A typical phase portrait showing the fixed points: centres and saddles. The fixed points depend on miniband, lattice constant and velocity of the acoustic wave. It also depends on the values of the wave amplitude and the electric field.

Whenever $c_2 > B$, the system collapsed, all the fixed points disappeared - this corresponds to global bifurcation. This indicates that the global bifurcation exists and the value of the static electric field when $c_2 > B$ can be calculated. That is $\frac{\omega_B}{\omega} = B$

$$\therefore \qquad F = F^* = \frac{kU}{e}$$

Therefore, the electric field is a function of the wave amplitude, $F^* = f(U)$. The value of electric field when global bifurcation occurs. To understand how bifurcation affects the electron trajectory , we analysis the phase portrait of the acoustically driven SLs in the electric field, we varied electric field strength to observe the change in the shape of phase trajectories and see what happened with the fixed points as the electric field, F approaches F^* and when $F \gg F^*$. We examined the phase portraits for small U , the wave amplitude close to transitions and faraway from transition (large U). We consider how changes in electric field affect phase trajectory instigating the symmetry breaking in the phase portrait.
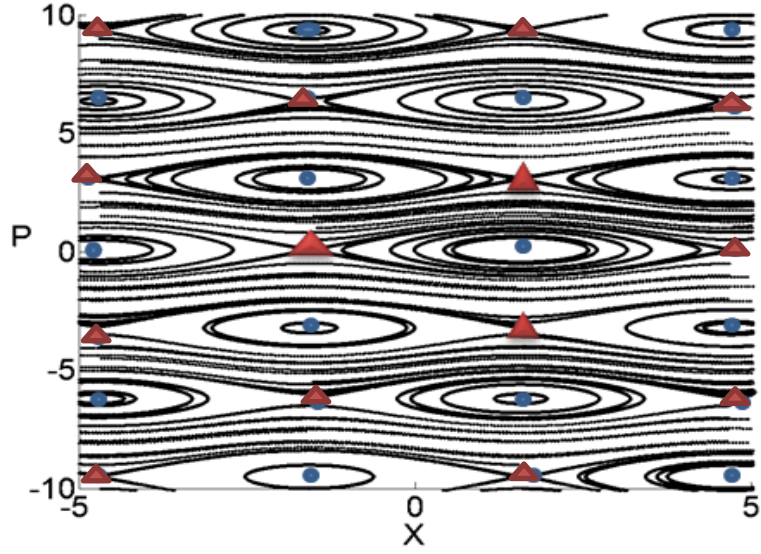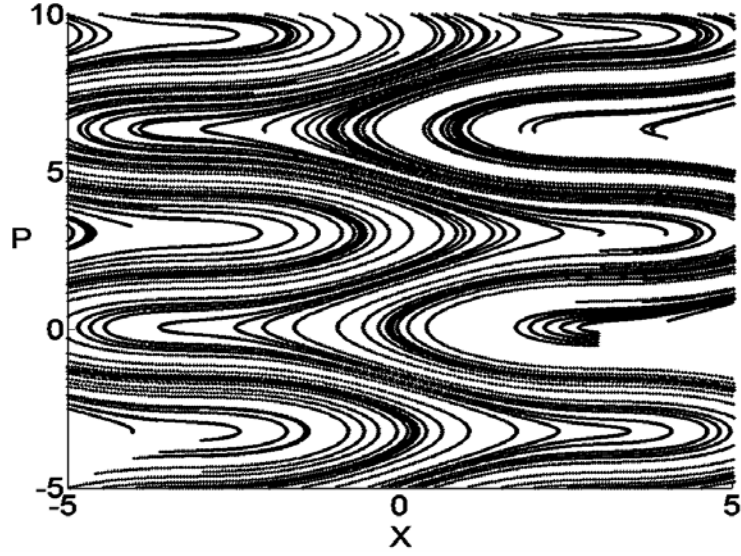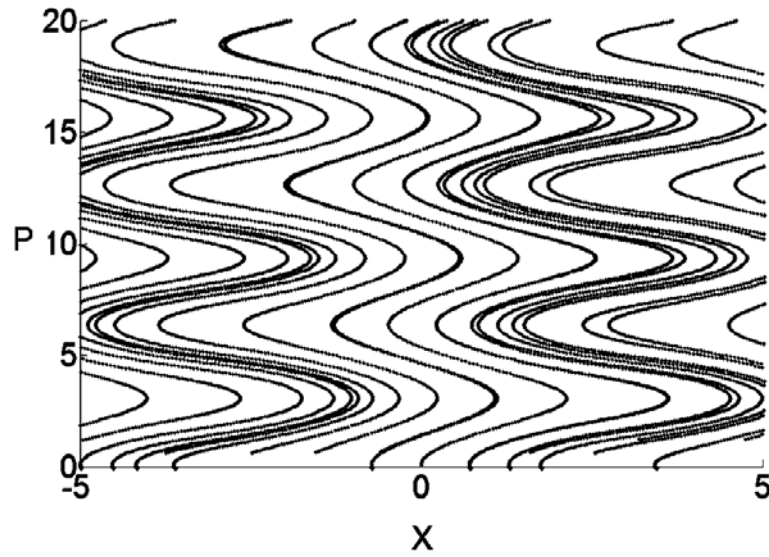
(a) $U = 1meV$, $F = 1 \times 10^2 Vm^{-1}$
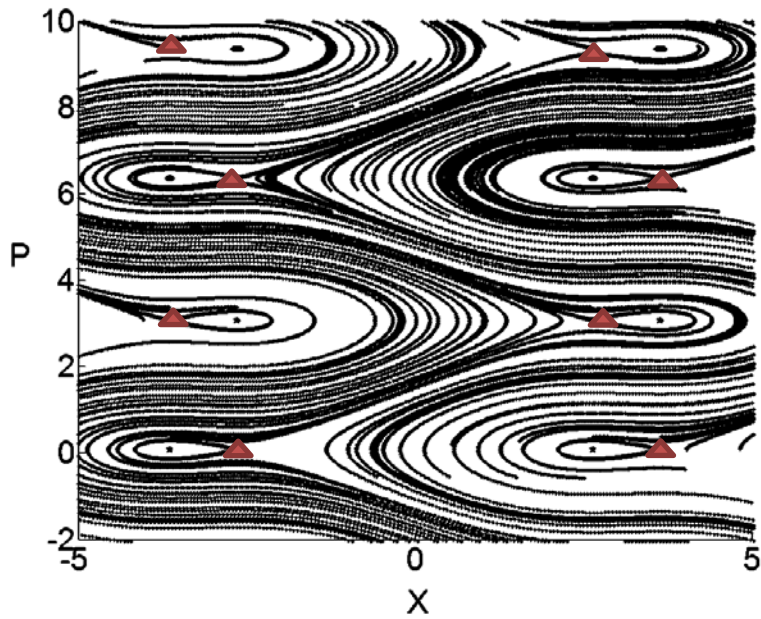
(b) $U = 1meV$, $F = 7 \times 10^4 Vm^{-1}$

Figure 4.6: (a) - (b) Here, we are presenting the electron trajectories in the phase space. The phase portrait of the electron trajectories is the plot of the momentum against the position when $U = 1meV$ for different electric fields values applied (a) $F = 1 \times 10^2 Vm^{-1}$ and (b) $F = 7 \times 10^4 Vm^{-1}$ For low electric field we observed trajectories that are separated by the separatrix; there are fixed points and saddles,▲.

(c) $U = 1meV$, $F = 9 \times 10^4 Vm^{-1}$
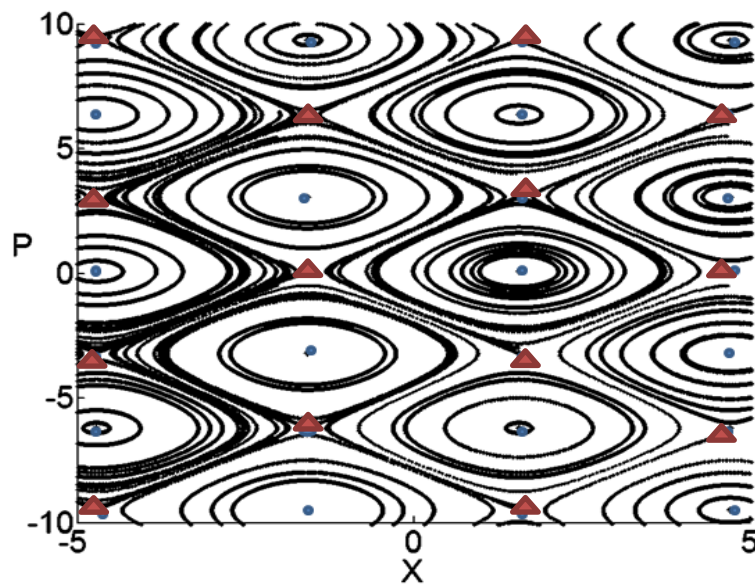

(d) $U = 1meV$, $F = 2 \times 10^5 Vm^{-1}$

Figure 4.6: (c) - (d) Here, we are presenting the electron trajectories in the phase space, the phase portrait of the electron trajectories is the plot of the momentum against the position when $U = 1meV$ for different electric fields values applied (c) $F = 9 \times 10^4 Vm^{-1}$ and (d) $F = 2 \times 10^5 Vm^{-1}$. When the electric field is increased, we observed that the fixed points collide with each other and there is evolution of phase trajectories.

The phase portraits for the different electric field applied are showed in Fig. 4.6 when $U = 1meV$. At low electric field of $F = 1 \times 10^2 Vm^{-1}$, $F \ll F^*$, we observed two types of trajectories: the localised and the unlocalised (unbounded) trajectories, which are separated by the separatrix, the separatrix connect the saddles in (a). The phase portrait is the same if we compared to Fig.3.10 in the previous chapter for low wave amplitude applied to the SL. But when we increase the electric field close to F^*, $F = 7 \times 10^4 Vm^{-1}$ in (b), $F \le F^*$ the fixed points move toward each other and the shape of the electron trajectory changes and some saddles also exists. When $F \ge F^*$ in (c), all the fixed points disappeared completely. The fixed points collide with each other. In Fig.4.6 (d) for electric field of $2 \times 10^5 Vm^{-1}$ which is $F \gg F^*$ the trajectories are meandering down and there are no fixed points. We have a change in momentum, but there is no change in the position over time. The value of electric field when global bifurcation can occur is approximately, $F^* \approx 8 \times 10^4 Vm^{-1}$ when $U = 1meV$.

Increasing U to $4meV$, the wave amplitude close to the transition, Fig.4.7 showed the phase portrait of electron motion. The strength of electric field when the global bifurcation may occur is approximately, $F^* \approx 3 \times 10^5 Vm^{-1}$.

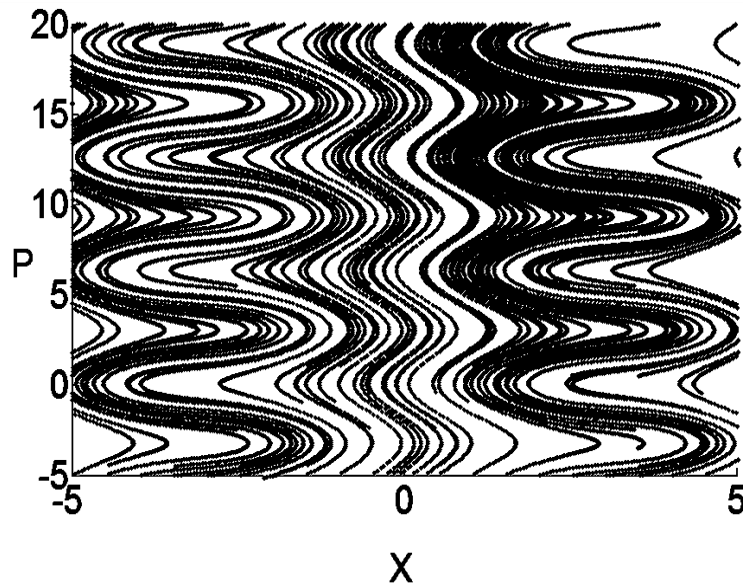(a) $U = 4meV, F = 1 \times 10^2 Vm^{-1}$

Figure 4.7: (a) The phase portrait of electron trajectories when $U = 4meV$ and the electric field is $F = 1 \times 10^2 Vm^{-1}$ .There is more localised trajectories encircle several closed centres and ellipses.
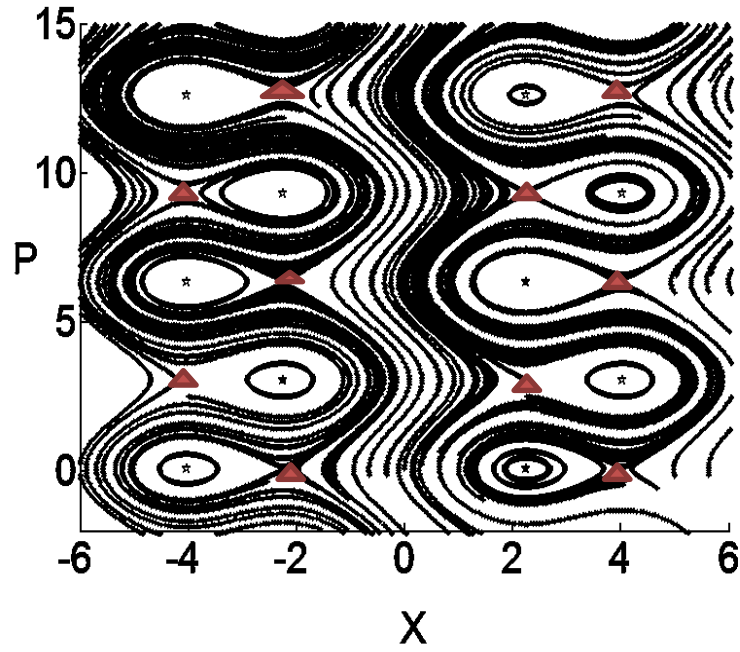
(b) $U = 4meV, F = 2 \times 10^5 Vm^{-1}$

(c) $U = 4meV, F = 4 \times 10^5 Vm^{-1}$

Figure 4.7 (c) and (d): The phase portrait of electron trajectories (the momentum plotted against the position) for $U = 4meV$ with applied electric field strengths of (b) $F = 2 \times 10^5 Vm^{-1}$ and (c) $F = 4 \times 10^5 Vm^{-1}$. As we increase the electric field strength, the fixed points collide with one another.
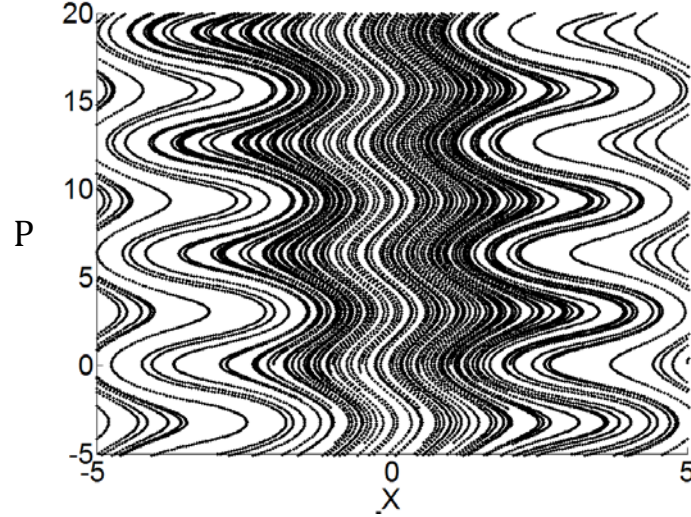
(d) $U = 4meV$, $F = 5 \times 10^5 Vm^{-1}$

Figure 4.7(d): The phase portrait of electron trajectories (the momentum plotted against the position) for $U = 4meV$ with the applied electric field strengths of $F = 5 \times 10^5 Vm^{-1}$. As we increase the electric field strength, the fixed points disappear completely and the shape of phase trajectory changes.

At very low electric field when $F \ll F^*$, $F = 1 \times 10^2 Vm^{-1}$ in (a), the phase portrait showed many localised central trajectories encompass many centres and ellipses as it occurred in Fig.3.15 in the previous chapter, with some saddles existing. Increasing the electric field, very close to F^*, $F \leq F^*$ in (b), the phase portrait tends toward a sort of symmetry breaking with localised trajectories in each form. We observed more central localised trajectories and the fixed points approach each other as shown in(b) , some saddles were also observed. When the electric field, $F \geq F^*$ that is $F = 4 \times 10^5 Vm^{-1}$ in (c), the fixed points collide with each other and vanished totally. The phase trajectories' shape changes and there are no localised trajectories. The symmetry breaking is more obvious with twisting trajectories in-between. When we increased the electric field further in (d), $F = 5 \times 10^5 Vm^{-1}$ such that $F \gg F^*$, the shape of trajectories change. The areas engaged by the twisting trajectories in-between the split increased.

In Fig. 4.8, $U = 10meV$ which is far away from the transition we applied varied value of the electric field, (a) is when $F \ll F^*$, (b) is very close to F^* and (c) & (d) are when the electric field is more than F^* .
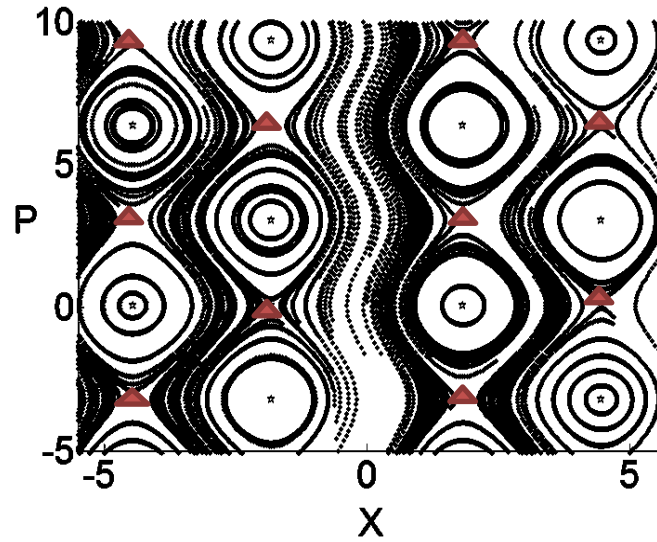
(a) $U = 10meV$, $F = 2 \times 10^5 Vm^{-1}$
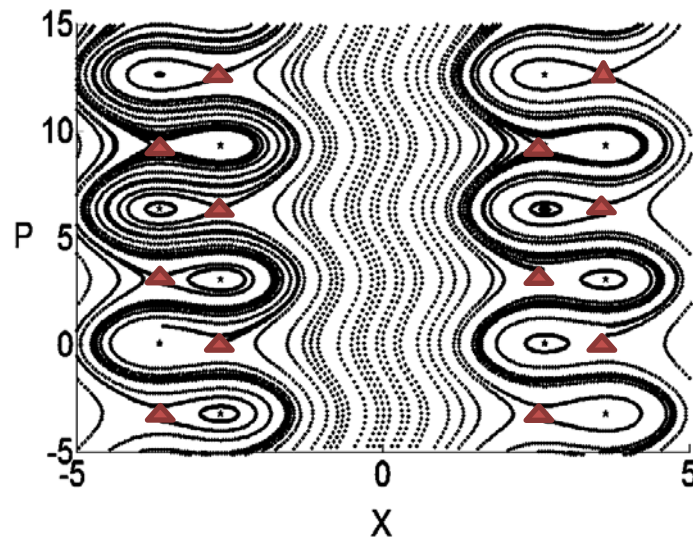
(b) $U = 10meV$, $F = 7 \times 10^5 Vm^{-1}$

Figure 4.8(a) and (b): The phase portrait of the electron trajectory present in the phase space consisting of the momentum against the position when $U = 10meV$ in (a) - (b) for different electric field strengths applied (a) $F = 2 \times 10^5 Vm^{-1}$ and (b) $F = 7 \times 10^5 Vm^{-1}$.
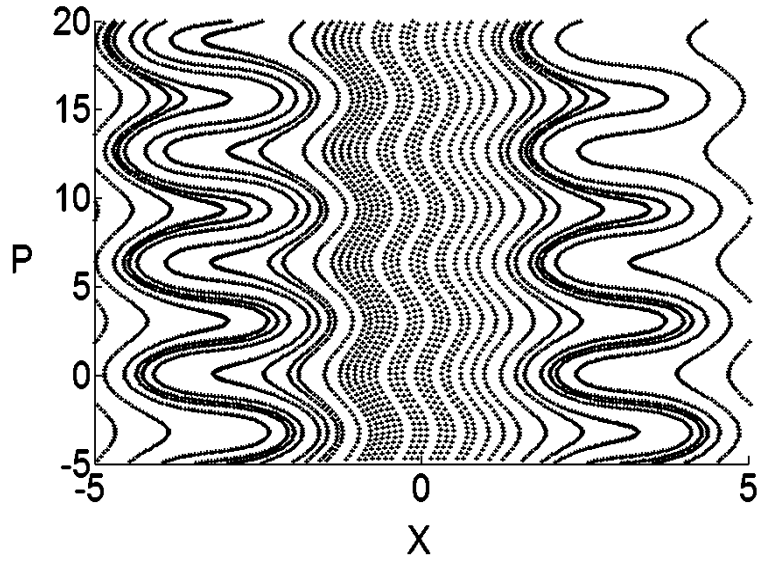
(c) $U = 10meV, F = 9 \times 10^5 Vm^{-1}$
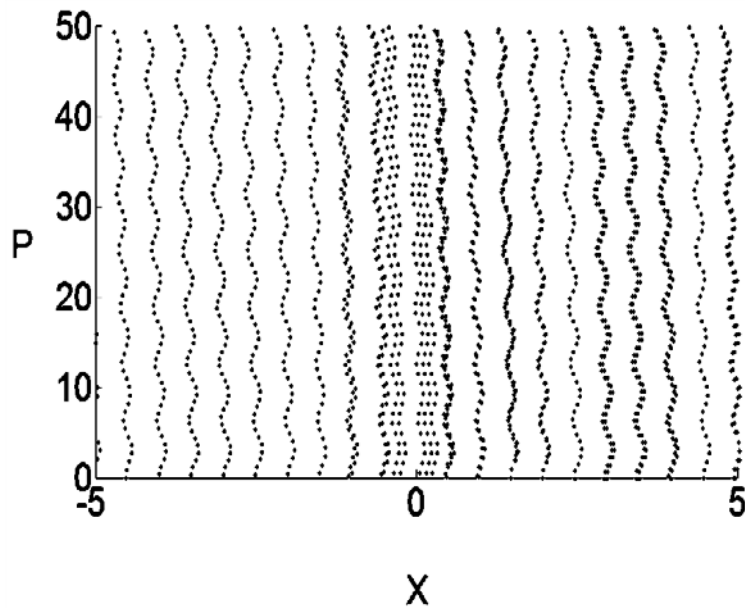
(d) $U = 10meV, F = 5 \times 10^6 Vm^{-1}$

Figure 4.8 (c) and (d): The phase portrait of the electron trajectory present in the phase space consisting of the momentum against the position when $U = 10meV$ in (a) - (d) for different electric field strengths applied (a) $F = 2 \times 10^5 Vm^{-1}$ (b) $F = 7 \times 10^5 Vm^{-1}$, (c) $F = 9 \times 10^5 Vm^{-1}$, and (d) $F = 1 \times 10^6 Vm^{-1}$. For the high value of the wave amplitude and electric field, the shape of localised trajectory changed and the fixed points collide with one another.

When $F \ll F^*$, $F = 2 \times 10^5 Vm^{-1}$ there are localised trajecrories which encompasses several centres and saddles. The trajectories inclines into splitting into equal areas in (a), and a twisty trajectroies in-between and there are many central trajectories in each form. In (b), $F = 7 \times 10^5 Vm^{-1}$, the electric field is very close to F^*, the shape of phase trajectories change and the fixed points tend to bump into each other and the saddles still exist. The trajectories bifurcate into two equal forms and the area in-between the form increased with more twisting trajectories. As we increased the electric field, $F = 9 \times 10^5 Vm^{-1}$ $F \geq F^*$ in (c), the twisting trajectories in-between the forms engaged more areas. The fixed points collide with each other and disappeared completely, changing the shape of phase trajectory. There are no more localised trajectories. And when we increased the electric field further as shown in (d), the trajectories drift down; the electric field is $1 \times 10^6 Vm^{-1}$ such that $F \gg F^*$. The value of electric field when global bifurcation can occur at $U = 10 meV$ is approximately, $F^* = 8 \times 10^5 Vm^{-1}$.

Conclusion

When a static electric field was applied to the acoustically driven electron in the SL, a much higher drift velocity was obtained as illustrated in Fig 4.5. The peak of drift velocity is reached at the critical values of both the static electric field and the wave amplitude. This is the value when dynamical change occurred.

We use phase portraits to explain the path of the electron. This gives an insight into the electron trajectory when both electric field and wave amplitude are applied. The electric field introduces another type of phase portrait which is different from the phase portrait when the acoustic wave alone was applied along the axis of SL. There is evolution of phase trajectories in the phase space that caused the stability of equilibrium (fixed points) to change. The fixed points collide with one another as the electric field increases. When $U = 1 meV$ and $F^* \approx 8 \times 10^4 Vm^{-1}$, the phase trajectories cross through the fixed points and the fixed points disappeared. When the wave amplitude, U increased to $4 meV$ and electric field is approximately, $F^* \approx 3 \times 10^5 Vm^{-1}$

the shape of the phase trajectory changes and the fixed points collide with each other. The same thing happens at high value of wave amplitude,$U = 10meV$, and the electric field is approximately, $F^* \approx 8 \times 10^5 Vm^{-1}$. When the fixed points disappear and the shape of phase trajectories changed completely global bifurcation occurs. Therefore, the value of electric field when global bifurcation occurs depends on the strength of wave amplitude. The electric field applied to the acoustically driven SL affect the electron trajectory in the SL.

Chapter 5

Summary and conclusions

In this work, we investigated systems which control and enhance the dynamics of electrons in the SL. This thesis has investigated a SL that is driven by an acoustic wave alone, to ascertain how a propagating acoustic wave will affect the electron dynamics in the SL. An acoustic wave propagating through a SL is an example of a moving lattice propagating through a static lattice. The dynamics of the electron are affected by the magnitude of the wave amplitude applied along the axis of the SL. We also examined the effect of an electric field on an acoustically driven SL when simultaneously applying to the axis of the SL both an acoustic wave and static electric field.

Chapters One and Two reviewed some of the fundamental theories of electron conduction in a crystal. The electron was considered in a periodic potential and cold atom in optical lattices. Chapter Three explored the dynamics of the electron in a SL when an acoustic wave is applied. A phase portrait was built to characterize the transition observed in the system for different wave amplitudes. The phase space gives a detailed insight into the system's dynamics. From the momentum and position curves, the paths of the electron are localized in all the transitions and the electrons move in

both positive and negative directions. This shows that there is a qualitative change in the dynamics. The dynamics of the electron in a SL depend on the wave amplitude. We observed different phase trajectories for varied values of wave amplitude; therefore transitions exist between the distinct dynamical regimes.

Chapter Four investigated the effect of a static electric field on an acoustically driven SL. The static electric field and acoustic wave jointly applied to the axis of SL produce high-frequency current oscillations. The phase portrait shows that the path of the electron when an electric field and acoustic wave are applied together along the axis of a SL is different to when the acoustic wave alone is applied. More localized trajectories were observed, but the saddles were lost as we increase the wave amplitude and the electric field. When fixed points and saddles cannot be determined, the system collapsed. This happens whenever $c_2 > B$, the fixed points disappeared as $F \rightarrow F^*$, the value of electric field when the bifurcation occurred and it depends on the value of wave amplitude applied. Therefore, when $F = F^*$, the fixed points collide with each other. The fixed point disappeared and there are no more localised trajectories. When the electric field is very high, far away from F^*, $F \gg F^*$ the meandering trajectories are straighten up as we have in Fig.4.8 (d). This suggests that at very high electric fields and acoustic wave, global catastrophes may occur: this could be another interesting work to consider in the future. Therefore, an acoustic wave can be used to control electron transport in a SL when an electric field is applied; since $F^* = f(U)$, applying moderate value of the wave amplitude will impede the occurrence of global catastrophe. When static electric field and acoustic wave are applied to the SL high frequency oscillations are obtained. The high frequency has applications in medical imaging, wireless data transfer, security scanning, water quality monitoring and so on.

The colour map of v_d (U, F), in Fig.4.4 shows a monotonic increase in the drift velocity. When the electric field is $F = 2 \times 10^5 Vm^{-1}$, the maximum of drift velocity was reached. The origin of this maximum required further investigation. What is the effect of increasing the drift velocity, and how a large drift velocity will affect the phase portrait? The evolution of electron trajectory, the shape and frequency of electron trajectory are topics for further studies. Also, the analysis in this work is based on the single electron transport, and then an extension will be to consider the effect of applying electric field and acoustic wave jointly on the collective transport, for example, the charge domain dynamics.

References

[1]   Andreas Wacker Semiconductor *Superlattices: a model for nonlinear Transport.* Physics Reports 357 1 -111 2002.

[2]   E. Ott. *Chaos in Dynamical Systems.* Cambridge University Press, 2nd edition, 2002.

[3]   A. Amann, K. Peters, U. Parlitz, A. Wacker, and E. Sch¨ oll: *A hybrid model for chaotic front dynamics: From semiconductors to water tanks*, Phys. Rev. Lett. 91: 066601 2003.

[4]   J.H. Denschlag, J.E. Simsarian, H. Haffner, C. McKenzie, A. Browaeys, D. Cho, K. Helmerson, S. L. Rolston and W. D. Phillips *A Bose-Einstein condensate in an optical lattice.* J. Phys. B: At. Mol. Opt. Phys. 35 3095-3110 2002.

[5]   J.F. Palmier, H. Le Person, C. Minot, A. Chomette, A. Regreny, D. Calecki *Hopping mobility in semiconductor superlattices* Superlattices and Microstructures Volume 1, Issue 1, Pages 67 -72, 1985.

[6]   J. Bleuse, G. Bastard, and P. Voisin *Electric-Field-Induced Localization and Oscillatory Electro-optical Properties of Semiconductor Superlattices Phys.* Rev. Lett. 60, 220 – Published 18 January 1988.

[7]   H. T. Grahn, K. von Klitzing, K. Ploog, and G. H. Döhler *Electrical transport in narrow-miniband semiconductor superlattices* Phys. Rev. B 43, 12094 (R) – Published 15 May 1991.

[8]   L. Esaki and R. Tsu. *Superlattice and Negative Differential Conductivity in semiconductors.* IBM J. Res. Dev., 14:61 1970.

[9]   L. Esaki. *Advances in Semiconductor Superlattices, Quantum Wells and Heterostructures.* Journal de Physique Colloque C5, supplément au n 4, Tome 45, avril 1984.

[10]   M.A.Herman *semiconductor superlattices* Akademie Verlag berlin 1986.

[11]   B.F. Levine: J. Appl. Phys. 74 (8) R1 1993.

[12]   Meimei Z. Tidrow *Device physics and state-of-the-art of quantum well infrared photodetectors and arrays* Materials Science and Engineering: B Volume 74, Issues 1–3, Pages 45–51, 1 May 2000.

[13]   J. M. Slaughter, D. W. Schulze, C. R. Hills, A. Mirone, R. Stalio, R. N. Watts, C. Tarrio, T. B. Lucatorto, M. Krumrey, P. Mueller, C. M. Falco: J. Appl. Phys. **76** (4) 2144 1994.

[14]   R. Mazurczyk. *Semiconductor Superlattices.* Chaos, Solitons & Fractals Vol. 10, No. 12, pp. 1971 – 1982 1999.

[15]   Oliver Morsch, Markus Oberthaler *Dynamics of Bose-Einstein condensates in optical lattices* Reviews of Modern Physics, Volume 78, January 2006.

[16]   O. Mandel, M. Greiner, A. Widen, T. Rom, T. W. Hanseh and I. Bloch *Coherent Transport of Neutral Atoms in Spin-Dependent Optical Lattice Potentials* Phys. Rev. Lett. 91:10407 2003.

[17]   Yu. Bomze, R. Hey, H. T. Grahn and S. W. Teitsworth. *Noise-Induced Current Switching in Semiconductor Superlattices: Observation of Nonexponential Kinetics in a High-Dimensional System.* Physical Review Letters 109, 026801 2012.

[18]   Phillip L. Gould, George A. R, and David E. Pritchard, Phys. Rev. Lett. 56, 827 1986.

[19]   P. J. Martin, Bruce G. Oldaker, Andrew H. Miklich, and David E. Pritchard, Phys. Rev. Lett. 60, 515 1988.

[20]   C.S. Adams, M. Sigel and J. Mlynek, Phys. Rep 240, 143 1994.

[21]   K. Leo, P. H. Bolivar, F. Bruggemann and F. Schwedler   *Observation of Bloch Oscillations in Semiconductor Superlattices* Solid state Communications, Vol. 84, No.10, pp. 943-946, 1992.

[22] H. T. Grahn *Negative Differential Resistance and Domain formation in Semiconductor superlattices*   Proceedings of a workshop held in IL Ciocco, Lucca, Italy, September 1992.

[23]   Albert C., J. Luo and Valentin Afraimovich   *Hamiltonian Chaos Beyond The KAM Theory* Springer Link.

[24]   Tsu *and* G*.* Dohler*.*   *Hopping conduction in a superlattice.*   Phys**.** Rev**.** B 12 1975**.**

[25]   M.T. Greenaway, A.G. Balanov, D.Fowler, A.J. Kent, and T.M. Fromhold, *Using sound to generate ultra-high-frequency electron dynamics in Superlattices*, *Microelectronics Journal* 40*,* 725-727 2009*.*

[26]   J. Hizanidis, A.G. Balanov, A. Amann, E. Schöll, *Noise-induced Oscillations and their control in semiconductor superlattices*, Int. Journal of Bifurcation and Chaos 16, 1701–1710 2006.

[27]   L. Esaki and L. L. Chang,   *New Transport Phenomenon in a Semiconductor Superlattice* Phys. Rev. Lett. 33, 495 1974.

[28]   H.C.Liu J. Appl. Phys. 63 p. 2856 1988.

[29]   Miriam Paton, H.C. Liu *A novel asymmetrically coupled quantum well infrared modulator* Superlattices and Microstructures Volume 4, Issue 6, Pages 737–739, 1988.

[30]   B. A. Vojak, W. D. Laidig, N. Holonyak, Jr., M. D. Camras, J. J. Coleman, P. D. Dapkus: J. Appl. Phys. 52 (2) 621 1981.

[31]   S. P. Stapleton, S. Bujkiewicz, T. M. Fromhold, P. B. Wilkinson, A. Patane, L. Eaves, A. A. Krokhin, M. Henini, N. S. Sankeshwar, and F. W. Sheard. *Use of stochastic web patterns to control electron transport in semiconductor superlattices*. Physica D, 199(1-2):166{172}, Dec 1 2004. Workshop on Trends in Pattern Formation, Dresden, Aug 25-Sep 19, 2003.

[32]   Formhold et al Chaotic *electron diffusion through stochastic webs enhances current flow in superlattices* Nature, Volume 428 Issues 6984 pages 726 – 730, 2004.

[33]   M.T. Greenaway. *Single particle and collective dynamics in periodic Potentials*. PhD thesis. School of Physics and Astronomy, University of Nottingham 2010.

[34]   D.R. Fowler, A.V. Akimov, A.G. Balanov, M.T. Greenaway, M. Henini, T.M.Fromhold, and A.J. Kent, Semiconductor *charge transport driven by a picosecond strain pulse*, *Appl. Phys. Lett.* 92, 232104 2008.

[35]   A. Huynb, B. Perrin, B. Jusserand and A. Lemaitre. *Terahertz Coherent acoustic experiments with semiconductor superlattices*. Applied Physics   Letters 99, 191908 2011.

95

[36] D.Fowler, D.P.A. Hardwick, A.Patane, M.T.Greenaway, A.G. Balanov. M. Fromhold, L. Eaves, M. Henini, N. Kozlova, J. Freudenberger and N.Mori. *Magnetic-field-induced miniband conduction in Semiconductor Superlattices.* Phys. Rev. B, 76(24):245303 2007.

[37] L. Esaki and L.L. Chang. *Semiconductor superlattices in High magnetic fields.* Journal of Magnetism and Magnetic Materials 11 208 -215 1979.

[38] Wang, C., Cao, J. and Zhang, C. *Noise temperature spectrum of hot electrons in semiconductor superlattices.* Journal of Applied Physics, 105 (1), 013717-1-013717-5 2009.

[39] S. Winnerl et al *Ultrafast detection and autocorrelation of picosecond THz radiation pulses with a GaAs/AlAs superlattice* Appl. Phys. Lett. 73, 2983 1998.

[40] M.T. Greenaway, A. G. Balanov, D. Fowler, A. J. Kent and T.M. Fromhold. *Using acoustic waves to induce high-frequency current oscillations in superlattices.* Physical Review B 81, 235313 2010.

[41] Tobias K, Koichiro Tanaka, and Keith A. Nelson *Resonant and nonresonant control over matter and light by intense terahertz transients.* Nature Photonics 680–690 2013.

[42] Pallab Bhattacharya *Semiconductor Optoelectronic Devices* 2nd edition Prentice Hall, 1997.

[43] Timo Hyart. *Tunable Superlattice Amplifiers Based on Dynamics of Miniband Electrons in Electric and Magnetic Fields*. Dissertation, University of Oulu, Finland 2009.

[44] F. Aristone, B. Goutiers, J. L. Gauffier and L. Dmowski *Effect of DX Centers in the Vertical Transport Properties of Semiconductor Superlattices* Brazilian Journal of Physics, vol. 30, no. 1, Marco 2000.

[45]   H. Kroemer *Large-amplitude oscillation dynamics and domain Suppression in a superlattice Bloch oscillator*. Mesoscale and Nanoscale Physics 2000.

[46]   M. Jaros *Electronic Properties of Semiconductor alloy systems.* Rep. Prog. Phys 48 1091 -1154 1985.

[47]   S. Peil, J. V. Porto, B. L. Tolra et. al, Phys. Rev. A 67, 051603 2003.

[48]   P. Blair Blakie and Charles W. Clark, J. Phys. B: At. Mol. Opt. Phys. 37 1391 2004.

[49]   Prasanta Misra *Physics of Condensed Matter* Elsevier Science, 2010.

[50]   R. Smoluchowski and J. S. Koehler Band *Theory and Crystal Structure* Annual. Rev. Phys. Chem.2:187-216 1951.

[51]   Charles Kittel. *Introduction to Solid State Physics.* Wiley, 2005.

[52]   F. Duan, J. Guojun *Introduction to Condensed Matter Physics*, Singapore: World Scientific, cop. Volume 1 2005.

[53]   G. Aruldhas and P. Rajagopal. *Modern Physics* Phi learning 2nd Edition 2006.

[54]   Clarence Zener *A Theory of the Electrical Breakdown of Solid Dielectrics* Proceedings of the Royal Society of London. Series A, Containing Papers of a Mathematical and Physical Characte*r* Vol. 145, No. 855, pp. 523-529 Jul. 2, 1934.

[55]   Alexander J. Cowan and James R. Durrant *Long-lived charge separated states in nanostructured semiconductor photoelectrodes for the production of solar fuels* Chem. Soc. Rev., 2013, 42, 2281-2293.

[56]   R Chen, T Ma, LG Wang, HQ Lin**.** *Electronic Bloch oscillation in a pristine monolayer graphene*. Mesoscale and Nanoscale Physics 2013.

[57] H. T. Grahn. *Semiconductor Superlattices: Artificial Crystals with Unique Electronic and Transport Properties.* Brazilian Journal of Physics, vol.32, no.2A, June, 2002.

[58] P. J. Mohr and B. N. Taylor, *The fundamental physical constants*, Phys. Today 55, August BG 6-16 2002.

[59] M. Abramowitz and L. A. Stegun, Eds., *Handbook of Mathematical Functions*, New York: Dover Publications, 1964.

[60] E. Merzbacher, *Quantum Mechanics.* Wiley, New York, 2nd edition, 1970.

[61] Mário G. Silveirinha and Nader Engheta *Transformation electronics: Tailoring the effective mass of electrons Phys.* Rev. B 86, 161104(R) – Published 8 October 2012.

[62] Timo Hyart, Alexey V. Shorokhov and Kirill N. Alekseev. *Theory of Parametric Amplification in Superlattices* Physical Review Letters 98, 220404 2007.

[63] Timo Hyart, Natalia V. Alexeeva, Jussi Mattas and Kirill N. Alekseev. *Terahertz Bloch Oscillator with a Modulated Bias.* Physical Review Letters 102, 140405 2009.

[64] K. F. Renk, E. Schomburg, A. A. Ignatov, J.Grenzer, S.Winnerl, K.Hofbeck. *Bloch oscillations and nonlinear transport in Semiconductor superlattices.* Physica B 244 196 -200 1998.

[65] K. F. Renk, A. Meier, B. I. Stahl, A. Glukhovskoy, M. Jain, H. Appel, and W. Wegscheider *Operation of a Bloch oscillator* Institut für Angewandte Physik, Universität Regensburg, 93040 Regensburg, Germany.

[66] B. Maxime, P. Ekkehard, R. Jakob, C. Yvan and S. Christophe *Bloch Oscillations of Atoms in an Optical Potential* Phys.Rev.Lett.76.4508 1996.

[67]   N.W. Ashcroft and N.D. Mermin. *Solid State Physics*. W. B. Saunders Company, 1 edition, 1976.

[68]   H. Aoki… [et. al.] *New Horizons in Low-Dimensional Electron Systems: A Festschrift* in Honour of Professor H. Kamimura. Kluwer Academic Publishers 1991.

[69]   M.T. Greenaway, A.G. Balanov, E. Schöll, and T.M. Fromhold, *Controlling and enhancing terahertz collective electron dynamics in superlattices by chaos-assisted miniband transport*, Phys. Rev *B* 80, 205318 2009.

[70]   Bernhard Rieder. *Semiclassical Transport in Semiconductor Superlattices with Boundaries.* Dissertation, Universität Regensburg 2004.

[71]   L. L. Chang and L. Esaki. *Semiconductor Superlattices by MBE and Their Characterization*. Prog. Crystal Growth Charact. Vol. 2, pp.3-14 1979.

[72]   A. C. Tselis and J. J. Quinn *Theory of collective excitations in semiconductor superlattice structures* Phys. Rev. B 29, 3318 – Published 15 March 1984.

[73]   Holger T. Grahn. *Semiconductor Superlattices: Growth and Electronic Properties.* World Scientific 1995.

[74]   Safa Kasap, Peter Capper Springer *Handbook of Electronic and Photonic Material*, 2007 – Springer

[75]   P. Giannozzi *Numerical Methods in Quantum Mechanics* Lecture Notes Anno accademico 2012/2013

[76]   C. Weisbuch and B. Vinter *Quantum Semiconductor Structures* Academic Press, INC. 1991.

[77] B. K Ridley *Quantum Process in Semiconductors* 3rd Edition Clarendon Press. Oxford 1993.

[78] Timo Hyart, Kirill N. Alekseev and Erkki V. Thuneberg. *Bloch gain in dc - ac driven semiconductor superlattices in the absence of electric domains.* Physical Review B 77. 165330, 2008.

[79] A. J. Kent, R. N. Kini, N. M. Stanton, M. Henini, B. A. Glavin, V. A. Kochelap, and T. L. Linnik *Acoustic Phonon Emission from a Weakly Coupled Superlattice under Vertical Electron Transport: Observation of Phonon Resonance* Phys. Rev. Lett. 96, 215504 – Published 2 June 2006.

[80] J. W. Morris, Jr. *A Survey of Materials Science IV. Mechanical Properties* Dept. of Materials Science and Engineering University of California, Berkeley Fall, 2008.

[81] Mário G. Silveirinha and Nader Engheta *Transformation electronics: Tailoring the effective mass of electrons Phys.* Rev. B 86, 161104(R) – Published 8 October 2012.

[82] R. G. Scott, S. Bujkiewicz, T. M. Fromhold, P. B. Wilkinson, and F. W. Sheard *Effects of chaotic energy-band transport on the quantized states of ultracold sodium atoms in an optical lattice with a tilted harmonic trap* Phys. Rev. A 66, 023407 – Published 20 August 2002.

[83] C. J. Pethick and H. Smith. *Bose-Einstein Condensation in Dilute Gases.* Cambridge University Press, 2nd edition, 2008.

[84] K. J. Ahn, F. Milde, and A. Knorr. *Phonon-wave-induced resonance fluorescence in semiconductor nanostructures: Acoustoluminescence in the terahertz range.* Phys. Rev. Lett., 98(2):027401, 2007.

[85] Bloch I. Nature Phys. 1, 23-30 2005.

[86] Ben Dahan, E. Peik, J. Reichel, Y. Castin and C. Salomon. *Bloch oscillations of atoms in an optical potential*. *Phys.Rev.Lett.* 76(24):4508 4511, 1996.

[87] Markus Greiner & Simon Fölling Condensed-matter physics: Optical lattices *Nature* 453, 736-738 5 June 2008.

[88] P Blair Blakie And Charles W Clark *Wannier States And Bose–Hubbard Parameters For2D Optical Lattices* Institute Of Physics Publishing Journal Of Physics B: Atomic, Molecular and Optical Physics J. Phys. B: At. Mol. Opt. Phys. 371391–1404 2004.

[89] Greenaway, M.T. Balanov, A.G. Fromhold, T.M. *Resonant control of cold-atom transport through two optical lattices with a constant relative speed* American Physical Society 2013.

[90] O. Morsch, .J.H. Muller, M, Cristiani, D. Carnpini, and E. Arimondo. *Bloch oscillations and mean-field effects of Bose-Einstein condensates in 1D optical lattice. Phys. Rev. Lett.* 87(14):140402, 2001.

[91] D. Lohse, Nature (London) 434, 33 2005.

[92] James P. Wolfe *Propagation of large-wavevector acoustic phonons new perspectives from phonon imaging* Advances in Solid State Physics Volume 29, pp 75-105 1989.

[93] Maznev, A. A. et al *Lifetime of sub-THz coherent acoustic phonons in a GaAs-AlAs superlattice* Follow Journal Applied Physics Letters , Volume 102 (4) Jan 28, 2013.

[94] S. P. Stapleton, S. Bujkiewicz, T. M. Fromhold, P. B. Wilkinson, A. Patane, L. Eaves, A. A. Krokhin, M. Henini, N. S. Sankeshwar, and F. W. Sheard. *Use of stochastic web patterns to control electron transport in semiconductor superlattices*. Physica D, 199(1-2):166{172}, Dec 1 2004. Workshop on Trends in Pattern Formation, Dresden, Aug 25-Sep 19, 2003.

[95] G. Romano, G. Mantini, A. Di Carlo, A. D'Amico, C. Falconi and Z. Lin Wang. *Piezoelectric potential in vertically aligned nanowires for high output nanogenerators.* Nanotechnology 22 465401, 2011.

[96] Wang Zhi-Gang *et al Effect of electron–phonon interactions on the dynamical localization of semiconductor superlattices Chinese Phys. 14 1232* 2005.

[97] Takuma Tsuchiyat and Tsuneya Ando *Electron-phonon interaction in Semiconductor superlattices*   Semicond. Sci. Technol. *7* 873-876 1992.

[98] J. Bardeen and W. Shockley. *Deformation potentials and mobilities in non-polar crystals.* Phys. Rev., 80(1):72{80}, Oct 1950.

[99] O Madelung. *Introduction to Solid-State Theory*. Springer-Verlag, 1978.

[100] M. Cardona and N. E. Christensen.   *Acoustic deformation potentials and heterostructure band offsets in semiconductors.* Phys. Rev. B 35, 6182 – Published 15 April 1987.

[101] S. Salleh, A.Y. Zomaya S. Abu Bakar   *Computing For Numerical Methods Using Visual C++* John Wiley & Sons, Inc., Hoboken, New Jersey 2007.

[102] M. Gunz *Differential Equations and Numerical Approximation using C++* Project Paper 2007.

[103] D. W. Jordan and P. Smith, *Nonlinear Ordinary Differential Equations*, Oxford 1995.

[104] Scheinerman E. R. *Invitation to Dynamical Systems* Dover Books. 2012.

[105] L. Perko. *Differential Equations and Dynamical Systems*. Springer-Verlag, 2nd edition, 1996.

[106] F. Verhulst. *Nonlinear Differential Equations and Dynamical Systems*. Springer-Verlag, Berlin, 2nd edition, 1996.

[107] Agulló-Rueda. F, Mendez E.E , Brum J.A, Hong J.M. *Coherence and localization in superlattices under electric fields* Surface Science Volume 228, Issues 1–3, Pages 80–83, 1 April 1990.

[108] Morifuji M., et al. *Electronic band structure of superlattices under a uniform electric field and Wannier-Stark effect* Semiconductor science and technology 7 no.8: 1047-1051 1992.

[109] E.E. Mendez, F. Agulló-Rueda *Optical properties of quantum wells and superlattices under electric fields* Journal of Luminescence, Volume 44, Issues 4–6, Pages 223–31, December 1989.

[110] Feldmann, J., K. Leo, J. Shah, D. A. Miller, J. E. Cunningham, T. Meier, G. von Plessen, A. Schulze, P. Thomas, and S. Schmitt-Rink. *Optical investigation of Bloch oscillations in a semiconductor superlattice. Physical review. B, Condensed matter* 46, no. 11 7252. 1992.

[111] Waschke, C., Roskos, H. G., Schwedler, R., Leo, K., Kurz, H., & Köhler, K. *Coherent submillimeter-wave emission from Bloch oscillations in a semiconductor superlattice.* Physical review letters, 70(21), 3319 1993.